1994

A Study of The Electrical And Optical Properties of Zno Thin Films Spray Pyrol Ysed From Zn(C2H302)2 2H20

Ambia, Md. Ghulam

University of Rajshahi

A STUDY OF THE ELECTRICAL AND OPTICAL PROPERTIES OF ZnO THIN FILMS SPRAY PYROLYSED FROM $Zn(C_2H_3O_2)_2\ 2H_2O$

MD. GHULAM AMBIA

A Thesis is Submitted for the Degree of Ph.D. in the
Department of Applied Physics and Electronics.
Rajshahi University, Rajshahi
1994

Dedicated to
my
parents

ACKNOWLEDGEMENT

I wish to express my heartfelt appreciation and deep respect to my ex-supervisor, Late Professor, M.N. Islam (Department of Applied Physics and Electronics, Rajshahi University, Rajshahi.) for his guidance, advice and encouragement while he was alive.

I would like to offer my deepest sense of gratitude and respect to my present supervisor, Professor, M. Azizar Rahman Sarker, Department of Applied Physics and Electronics, Rajshahi University, Rajshahi, for his valuable suggestions, delivering inspiration and help during the preparation of this thesis.

I also appreciate with deep respect my co-supervisor, Professor, M. Obaidul Hakim, Department of Physics, Rajshahi University, Rajshahi, for his constant guidance, encouragement and every possible active help throughout the whole of my work and preparation of the thesis.

I am highly grateful to my teacher, Professor, Sayeedur Rahman Khan, Department of Applied Physics and Electronics, Rajshahi University, Rajshahi, for his kind help in doing the electron microscopic work for the samples.

I am grateful to the chairmans of the department of Applied Physics and Electronics for providing me the facilities to carry out the experimental work.

I offer my thank to Mr. M. Shahidul Islam, Instrument Engineer, Mr. A. Latif Talukder, Instrument Engineer and Mr. M. Mozammel Haque, Store Keeper in the Department of Applied Physics and Electronics for rendering their service during the course of the experimental work.

I am indebted to Mr. M. Moksed Ali, Glass Blower in the Department of Chemistry for his kind help in blowing different sizes of glass tubes suitable for the work.

I gratefully acknowledged my sponsor U.G.C. for awarding me a junior research fellowship to carry out this research programme.

I like to thank the Ministry of Education for granting me study leave during the period of my experimental work.

Finally, I thank my wife Mrs. Dil-Afroza for her encouragement and sacrifices during the period of research work.

ABSTRACT

Investigations have been carried out on spray pyrolysed undoped and indium doped ZnO thin films for the thickness range 700-4000 Å. The undoped ZnO thin films were found to be non-stoichiometric but homogeneous and polycrystaline in structure as confirmed by the structural studies. The virgin films were highly resistive whereas vacuum annealed films are good transparent conductors. Aging effect has been observed within the first 15 days of the film fabrication. Size effect has been observed below 1500 Å. The doped film (ZnO : In) showed higher carrier concentration and Hall mobility.

The effect of successive post-deposition heat treatments in air and vacuum has been studied. It has been observed that the heat treatment in different ambients have remarkable effects on the electrical transport properties. Due to the successive heat treatment operation, the carrier concentration changes from 10^{15} – 10^{18} cm^{-3} and mobility changes from 4 - 16 cm^2/VS. Oxygen chemisorption-desorption mechanism were found to play an important role to control the electronic properties. Various grain boundary and energy band parameters have been calculated by using conventional extrinsic semiconductor theory and grain boundary trapping models. The samples were non-degerate at room temperature, and the Hall mobility was found to be modulated by the grain boundary potential barrier height via the samples temperature.

For ZnO thin films two distinct scattering process viz the grain boundary scattering and the piezoelectric scattering are found to play a predominant role in limiting the Hall mobility.

An attempt has also been made to study the electromechanical properties of ZnO thin films. From this study gauge factor was calculated.

Thermoelectric powre (TEP) of the films has been measured from room temperature upto 200°C with reference to pure lead (Pb). The thickness and temperature dependence of its related parameters have been studied. The Fermi levels are determined using non-degenerate semiconducting model. The carrier scattering index, activation energy and temperature co-efficient of the activation energy, have all been obtained at different range of thickness and temperatures. It was interesting to note that the Fermi levels in these films were found to pinned near the conduction bang edge with the increase of temperature.

The optical transmission study was performed between visible to near infrared region in order to establish a tentative energy band picture of the material. The optical transmission was found more than 95% both for doped and undoped films in the visible range of the spectra. It is observed that the optical band gap is similar to that of pure bulk crystal and shows an appreciable Burstien-Moss shift with the increase of carrier concentration.

CONTENTS

CHAPTER 1

INTRODUCTION

Experimental work on thin films has been continued in different parts of the world for successful applications of their properties in scientific, engineering and industrial purposes. The increasing demands for microelectronic and microstructural compounts in different branches of science and technology have greatly expanded the sphere of thin film research. During the last three decades a great deal of research works have been carried out on the thin films of metals, semiconductors, insulators and cermet (granular metal) materials. Sufficient time has also been utilized to search for other new coating materials relevant to electro-optical proterties. These comprise the spectrally selective coating, transparent conducting coating, solar absorbing coating, heating elements, antistatic coating on instrument panels, and electrical contact in liquid crystal, electrochromic and electroluminescent displays, smart window coating, photochromic and thermochromic coating etc. According to design and structure of the devices, these coating may be either a single or multilayer on a suitable neutral substrate or may be a layer forming composite structure with the substrate. Among the above varieties of coatings, transparent conducting oxide thin films have initially figured prominently for their application in solar cells but recently their utility in the different branches of science and

technology has been extended so much that they have become the subject matter of study and research with great interest. The description of appplications of this type of films in different areas are given below.

1. APPLICATIONS OF TRANSPARENT CONDUCTING COATINGS

The usefulness of transparent conducting coatings have recently been increased to different fields of Physics. For example acousto-electrical, acousto-optical and electro-optical applications, some of these applications are described below:

1.1 (i) As solar cell over coat

Both single crystal and polycrystalline silicon have been used to form junction with transparent conducting ZnO over coat yielding high efficiency solar cells[1]. P-type single crystal CdTe is also frequently used for this purpose [2,3]. Beside this, many other binary and ternary compounds such as ZnO/InP[4], ZnO/Zn_3 P_2[5] and ZnO/$CuInSe_2$[6] etc. heterojunctions solar cells have been reported. In fabricating this type of cells, the transparent conducting coating must permit the transmission of solar radiation directly to the active region with little or no attenuation and can serve simultaneously as a low resistance contact to the junction and as an antireflection coating for the active region. The ease of fabrication and greater stability of these films can help to obtain the cells with minimum manufacturing cost.

1.1 (ii) Use as heat reflector

Because of the high luminous or solar transmittance with high infrared reflectance ZnO thin films are spectrally selective and have application to solar thermal energy conversion, solar photovoltaic conversion, heating elements on aircraft window for deicing and defogging. Low emittance coatings and solar control coatings for windows in building and cars, heat reflecting coating for solar collector cover plates and for incandescent and fluorescent light sources. In a conventional incandescent lamp, the tungsten filament emits about 90% heat and 10% visible radiation. Normally both heat and light pass through the glass envelope. The application of a heat reflecting coating inside the glass envelope of the lamp will result in the reflection of the thermal part back to heat the filament and only the visible part will be transmitted. Thus the power consumed to heat the filament is reduced considerably and a cool visible illumination is received.

Thermal balance is necessary for spacecraft instruments. This requires heat retention under cold and heat radiation under hot conditions. This is essential for the performance of its very sensitive and sophisticated electronic equipments. This heat regulation becomes possible by switchable composite coatings of spectrally selective materials.

1.1 (iii) As antistatic coatings

Antistatic coating on flexible substrate such are polyester or polymer are used in electrical contacts in liquid crystal. They are also used to fabricate instrument panels and packaging for delicate integrated circuits during there transport and storage.

In spacecrafts this type of coatings are used for antistatic purposes. Fild intensity fluctuations in the earth's magnetosphere and continuous irradiation of UV and other charged particles may differentially bias spacecraft areas to a dangerously high potential. By using this coating poperly uniformity of potential on the exterior of the craft may, therefore, be brought about.

1.1 (iv) As gas sensors

The increasing interest in areas such as pollution control, detection of hazardous gases and monitoring of combustion processes has lent prominence to gas sensors based on metallic oxide thin films have become attractive owing to their simplicity and portability. Thin films of ZnO[7] has shown promising results in the detection of gases such as CO, CO_2, H_2, H_2S, alcohols and hydrocarbons. The basic principle plays in the gas sensing devices is that the films exhibit a change in electrical conductivity when a change in the ambient occurs. The change in conductivity can be either due to direct transfer of electrons from the absorbed gas to semiconductor or due to a reaction of the absorbed gas with

previously chemisorbed surface oxygen. Other transparent conducting oxides are also important for gas sensing applications. Among them SnO_2 is frequently reported.

1.1 (v) Reflection absorber tandem for photothermal conversion

Semiconductor-metal tandems can give the desired spectral selectivity by absorbing short wavelength radiation in a semiconductor whose bandgap is (≈ 0.6 ev) and having low thermal emittance as a result of the underlying metal. The useful semiconductors have undesirable large refractive indices, which would tend to yield high reflection losses at the semiconductor-air interface and has a somewhat higher emittance than that of pure metal. Hence it is necessary to antireflect the surfaces in the range of solar radiation. This job can be performed by selecting a transparent conductor whose transparency lies between visible and near IR region and possesses low emittance, can be used for a metallic substrate. In addition this layer will also act as antireflecting coating for the semiconductor thus suppressing the reflection loss. Therefore, a coating of a transparent conductor on any semiconductor absorber surface will yield a selective absorber tandem . ZnO: In[8] thin films are used as antireflection coating in the configuration (ZnO: In)/PbS/stainless steel. The emittance of the system is decided by the combined reflection behavior.

1.1 (vi) Other applications

Because of the comparatively high electromechanical coupling co-efficients, piezoelectric ZnO thin films have been used widely in many technical applications, such as bulk surface acoustic wave filters, ultrasonic transducers and microwave sound detector. Other important applications are the production of resistive heating layers, protecting vehicle window glasses and window glasses of residential houses. In order to reduce damaging of glass containers during manufacturing or filling, it is desirable to apply oxide layers that could reduce the co-efficient of friction considerably.

1.2 FUNDAMENTAL AND TECHNICAL PROBLEMS OF OBTAINING TRANSPARENT CONDUCTING FILMS

Highly transparent and good conducting films are needed in the applications of thin film devices and solar cells. The films which possess these properties naturally yield greater figure of merit. But there is a fundamental conflict between the two when photon energy incident on a material it creates electron hole pairs which limits the transparency at short wavelengths. Whereas steep increase of reflectivity due to free carrier absorption limits the transparency at long wavelengths. Since the conductivity of a material is directly proportional to its free carrier content, higher electrical conductivity, therefore, automatically produces opacity in the films. This is why electrical good conductors are

generally opaque which occur in the case of metal films. From some basic considerations it is generalized that materials having long mean free path can produce layers of larger figure of merit. Long free paths are expected in high conductive thick metal films that are opaque. But in the case of semiconductor whose band gap is sufficiently high (≈ 3 eV) different situation may happen. Thicker films with high transmission are passible in order to create long free path, but conductivity would be diminished due to high band gap. The only way to have a good transparent conductor is to create electron degeneracy in a wide band gap semiconductor by introducing non-stoichiometry or by adjusting dopant in a control manner. Oxide semiconductors are of wide band gap materials that can face the above mentioned problem considerably.

Sometimes, substrate materials create problem in obtaining transparent conducting films. This problem is remarkable in the case of cheap soda lime glass substrate from which alkali ions diffuse into the films. These alkali ions produce compensating effect with free electrons, acting as a p-type native doping agent in n-type material and impart high resistivity to the samples.

Another important factor which associated with deposited system is the quality of the spray particles (aerosol) produced at the time of deposition. A very small uniform size of spray particles yield relatively a film of better quality. Therefore, the design and modification are very important. Besides this, many

unwanted opaque suspended foreign dust particles in the deposition environment may be incorporated and would result hazard films. Therefore, clear working liquid and dust free deposition chamber should yield transparent films.

1.3 THE AIM OF THE WORK

Currently more than 85% of the total energy consumption of the world are available from the mineral resources. But when this source will be exhausted world will face the great energy-crisis problem. Considering this aspect, the effort has been continued to explore non-conventional energy sources. As an outcome transparent conducting films appear which are extensively applied as window layers particularly in heterojunction solar cells. In view of this it becomes meaningful to prepare transparent conducting thin films in author's laboratory.

In the light of the previous results and the existing problems it is necessary to select materials that can be deposited by a simple and easy method to yield relatively better transparent conducting films. Furthermore, we have decided that among the various film deposition method, chemical spray pyrolysis method has grown interest owing to its simplicity and inexpensivility. Because of the above mentioned causes the fabrication of ZnO thin films by spraying method has been selected. To utilize these films successfully it is essential to characterise the sample and to study their electrical and optical properties. Some of these studies have been carried out and reported in this work.

1.4 THE STRUCTURE OF THE THESIS

The experimental work carried out on the fabrication and characterization of ZnO thin films presented in this thesis has been divided into six chapters. Chapter-1 includes an introduction to ZnO thin films, some of their applications, the major problems that impede in obtaining transparent conducting films and the aim of the work. In chapter-2 critical review of ZnO and other oxide films have been presented.

The background of experimental techniques and apparatus employed in the present study have been discussed in chapter-3. In chapter-4 the experimental setup and procedures for the various experimental studies have been described. Chapter-5 deals with the effects of different deposition process variables on the ZnO films' properties.

In order to obtain a tentative energy band picture and good figure of merit of the material, a systematic analysis of electrical, optical and structural properties with appropriate interpretation have been discussed. The concluding remarks of the present work and a few suggestions for further work have been given in chapter-6.

REFERENCES

1. D.E. Brodie, R.Singh, J.H. Morgan, J.D. Leslie, C.J. Moore, And A.E. Dixon. Proc. 14th IEEE. photovoltaic specialists conf. San Diego. C.A. 1980. IEEE, New York, (1980) 4468.
2. A.L. Fahrenbruch. J. Aranovich, F. courreges. T.Chynoweth, and R.H. Bube. Proc. 13th IEEE Photovoltaic specialists conf. Washinton DC. 1978. IEEE New York. (1978) 281.
3. Julio A. Aranovich. Dolores Golmayo, Alan L. Fahrenbruch, and Richard H. Bube. J. Appl. Phys. 51(8) (1980) 4260.
4. Chris Eberspacher, Alan, L. Fahrenbruch and Richard H. Bube. Proc. 17th IEEE Photovoltaic specialists conf. Kissimmee F.L. (1984) 459.
5. P.S. Nayar and A. Catalano. Appl. Plys. Lett. 39(1), (1981) 105.
6. M.S. Tomar and F.J. Garcia, Thin Solid Films, 90(1982) 419.
7. T. Seiyama, A.Kato, K. Tujiishi and M. Nagatoni Anal. Chem. 34(1962) 1502.
8. G.B. Reddy. Ph. D. thesis, Indian. Institute of Technology, New Delhi 1982.

CHAPTER 2

A BRIEF REVIEW OF TRANSPARENT CONDUCTING MATERIALS

2.1 THE ZnO MATERIAL

Zinc oxide material can be prepared by several number of techniques but its properties are naturally studied in three different forms. These are (i) single crystal of ZnO, (ii) Sintered specimen of ZnO and (iii) Polycrystallnine and amorphous ZnO meteiral.

2.1 (i) ZnO single crystal

ZnO single crystal has Wurtzite structure. In its lattice the oxygen ions are arranged in close pack hexagonal structure and the Zinc ions occupy half of the tetrahedral interstitial positions and have the same relative arrangement as the oxygen ions as shown in figure 2.1. Actually the environment of each ion does not have exact tetrahedral symmetry. Instead the spacing between nearest neighbours in the direction of the hexagonal or c axes is somewhat smaller than for the other three neighbours. The binding is essentially polar; however, there is a homopolar component[1] of binding between next nearest Zinc and Oxygen ions in the direction of the c-axis. The crystals are usually obtained in the form of hexagonal prisms. The lattice constants are a=3.24 Å, c=5.19 Å and c/a=1.60. The radius for covalent binding of neutral Zn and O are 1.31 Å and 0.66 Å respectively and the radius for ionic binding of

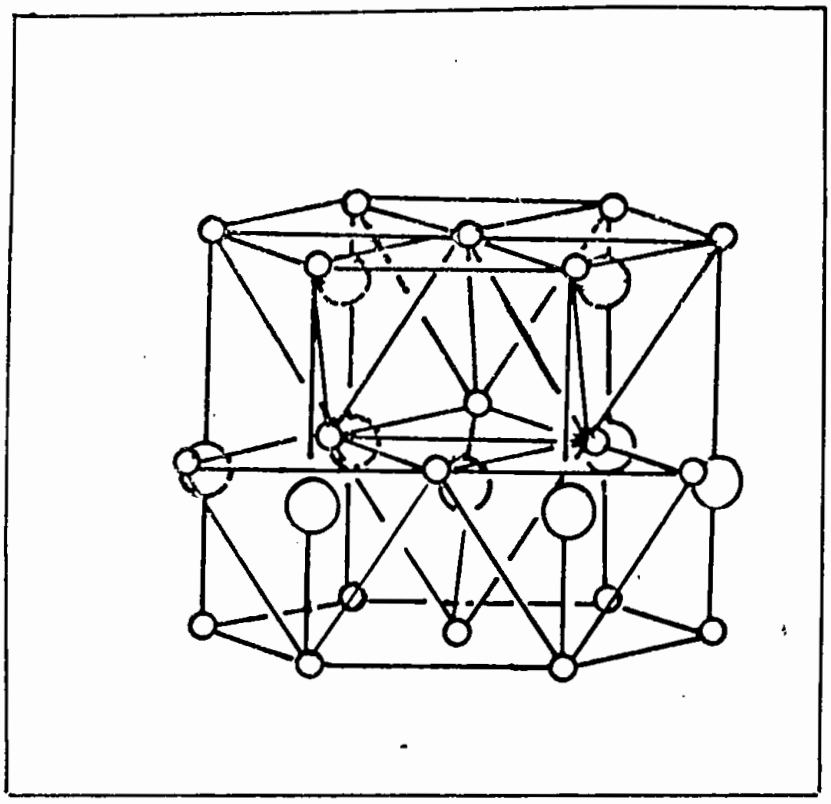

Figure 2.1 The wurtzite lattice of ZnO.
Larger circles indicate zinc atoms
and small circles indicate oxygen atoms.

Z^{++} and O^{--} are 0.70Å and 1.32Å respectively[2].

2.1 (ii) Sintered ZnO material

Mollwo et.al.[3] deseribed the procedure of preparing sintered layers. In this process, metallic Zinc in an appropriate crucible is vaporized in air by heating with a torch. The Zinc vapour is oxidized and is deposited on a glass plate at a high temperature. Another investigator[4,5] produced compact sintered specimens by compacting chemically pure Zinc oxide powder with high pressure. The density of sintered specimen is of the order of 5.5 g/cm^3 relative to a density of 5.6 g/cm^3 for single crystals. The grain size differs from sintered specimen to single crystals. It is 5 to 20μ for sintered specimen and 1μ for single crystal. The studies on sintered ZnO are hardly noticed.

2.1 (iii) Polycrystalline and amorphous ZnO material

The optical and electrical properties of solids can vary greatly from one specimen to another when the structure and purity of the specimens vary. The most reproducible and reasonable results may be expected from chemically well defined single crystal. Such crystals of Zinc oxide are not easily made. Hence many investigations are based on the use of polycrystalline material in the form of sintered specimens or thin layers. On earlier, ZnO thin layer was obtained by evaporating metallic Zinc on quartz glass or ordinary glass in high vaccum and was allowed to oxidize the

coating after formation. Seitz[6] reported the structural study of thin layer prepared in this way. The crystallites were of the order of 3 X 10^{-6} cm in size on the surface in a layer of thickness of about 10^{-5} cm. The orientation of crystallites was found in such a type that the c axis was perpendicular to the support. The informations on polycrystalline thin films of ZnO for both undoped and doped samples are presently available. The study on amorphous ZnO thin films are seldom noticed.

2.2 THIN FILMS OF ZnO TRANSPARENT CONDUCTOR

It is well known that ZnO thin films have been used as a transparent conductor for long time. Some metallic thin films of thickness of the order of 100 Å may be transparent but they are weakly adherent to substrate and are very fragile. On the other hand ZnO films become very hard and stable against chemical attack and decay. However, ZnO thin film is highly adherent to many substrates and under high temperatures. Due to all these unique combinations of properties, ZnO has become an important material for research and technology.

2.3 DEPOSITION TECHNIQUES OF OXIDE SEMICONDUCTORS

A variety of thin film deposition techniques have been employed to deposit transparent conducting oxide films. Some of the commonly used techniques are as follows :

2.3 (i) Evaporation

Vacuum and also reactive evaporation have been employed to deposit various transparent conducting films by using oxide sources as source material. Evaporation rate, substrate temperature, source to substrate distance and oxygen partial pressure are the important controlling parameters.

2.3 (ii) Post oxidation of metal films

Thin metal oxide films have been prepared by the oxidation of respective metal films. Watanabe[1] prepared ZnO thin film by this method. The conductivity and transparency are controlled primarily by the oxidation temperature, which is typically in the range 350-500°C.

2.3 (iii) Reactive evaporation

Reactive evaporation of metallic oxide films have been achieved by the vaccum evaporation of the corresponding metal or alloy in an oxygen atmosphere onto the heated substrate at about 400°C.

2.3 (iv) Activated reactive evaporation

In the activated reactive evaporation technique, the reaction between the evaporated species and the gas is activated by establishing a thermoionically assisted plasma in the reaction zone. The technique has been used to deposit excellent quality

transparent conductors of ZnO[8,9] films. Lau et.al[8] informed that the films deposited at higher temperature (T>300°C) were always inferior to the films deposited below 200°C.

2.3 (v) Direct evaporation

Thin metallic oxide films have been deposited by thermal or electron beam evaporation of oxide sources. Kenigsberg et.al[10] deposited ZnO thin films by electron beam method.

2.3 (vi) Sputtering

Among the deposition techniques sputtering is one of the most extensively used technique for the deposition of transparent conducting oxide films. Both reactive and nonreactive type of d.c and r.f sputtering and recently magnetron and ion beam sputtering have been used. As-sputtered films are usually (not always) amorphous in nature but elevated substrate temperature or post-deposition heat treatment gives polycrystalline films.

2.3 (vii) Reactive sputtering of metallic targets

For thin oxide film deposition reactive sputtering may be used. Ar-O_2, N_2-O_2 or O_2 are generally used as the sputtering gas, although in some cases H_2 has been added to reduce the target and/orfilm. Jim et.al[11] reported the results of ZnO:Al films which had about 1% luminous absorptance, about 85% thermal IR reflectance and a d.c resistivity of about 5 X 10^{-4} Ω cm under optimum condition of 3000 Å thick films.

2.3 (viii) Sputtering from oxide targets

Sputtering from oxide targets has been applied to form transparent conducting oxide films. Excellent transparent conducting films of ZnO[12-16] have been deposited by this method. Hot-pressed, pure or mixed oxide targets are generally used. The target's porosity determines its susceptibility to contamination or reduction.

2.3 (ix) Ion beam sputtering

Ion beam sputtering from oxide targets has been successfully employed to deposit oxide films. This technique involves minimal intrinsic heating and electron bombardment and hence constitutes a low temperature deposition method which can be useful for several application of transparent conduction.

2.3 (x) Chemical vapour deposition (CVD)

Chemical vapor deposition (CVD) consists of a surface reaction, on a solid surface, involving one or more gaseous reacting species. Metallic oxides are generally deposited by the vaporization of a suitable metal bearing compound (which is volatile, thermally stable at a temperature sufficiently high to produce an adequate vapour pressure and thermally unstable at higher temperatures of deposition criteria generally fulfilled by organometallic compounds) and its in situ oxidation with O_2, H_2O or H_2O_2. O_2, N_2 or argon wich are generally used as carrier gases. ZnO

film prepared from the oxidation of diethylzinc[17] on glass substrate exhibit high degree of c-axis orientation. The film growth was carried out over the 200-500°C ttemperature range. Another film of ZnO[18] deposited from the same material have shown conductivity between 10^{-2}—50 Ω^{-1} cm^{-1}. The main control parameters are the gas flow, the gas composition, the substrate temperature and the geometry of the deposition apparatus.

2.3 (xi) Spray pyrolysis (SP)

Spray pyrolysis[19,20] which is the main concern of this work, involves spraying of an ionic solution, usually aqueous, containing soluble salts of the ccnstituent atoms of the desired compounds onto heated substrate. Hydrolysis and pyrolysis are the main chemical reactions normally involved in this technique. There is slight difference between (SP) and (CVD). In spray pyrolysis technique the chemicals vaparize and react on the substrate surface after reaching on it[21] but in chemical vapor deposition vaporization takes place before reaching the substrate surface. The demarcation is obvious but in practice a combination of both the processes may take place in either case of CVD or SP technique. The technique is very simple and is adaptable for mass production of large area coating for industrial applications.

Transparent conducting films of ZnO have been deposited by spraying an aqueous solution of $Zn(C_2H_3O_2)_2$ $2H_2O$[22,23], $ZnCl_2$[22,23,24], $Zn(NO_3)_2$ $4H_2O$[25] and by spraying alcoholic solution also[23]. In-doped

ZnO film was obtained by mere addition of $InCl_3$[26] and Al and Te dopped films were obtained by adding $AlCl_3$ and $TeCl_3$[27] respectively with the spray solution. It was reported that to achieve better film, the optimum substrate temperature to be in the range of 300°C—450°C, the gas flow rate of about 5-10 l/min at a pressure of near about 0.5 kg/cm^2 with a solution flow rate of about 4-20 cm^3/min. The size of spray particles/droplets and their distribution affect the uniformity of the surface and the optical transmission of the films[28].

2.3 (xii) Dip technique

The dip technique[29] consists essentially of inserting the substrate into a solution containing hydrolysable metal compounds and pulling it out at a constant speed into an atmosphere containing water vapour. In this atmosphere, hydrolysis and condensation process take place. Finally, the films are hardened by a high temperature cycle to form transparent metal oxides. The important control parameters are the viscosity of the solution, the pulling speed and the firing temperature. The rate of heating also needs to avoid cracking of the films. This technique has been used commercially to deposit large area coatings.

2.3 (xiii) Other techniques

Other techniques like chemical solution growth[30] and chemical deposition method[31] have been used to deposit ZnO thin films occassionally.

2.4 DOPANTS USED

In most cases, Indium and Aluminium have been used as dopant element in ZnO films[11,26] by different workers. Besides these Terbium[27], Tin[31] and Galium have been used for this purpose. Better result was reported for Indium and Aluminium dopant than the others with respect to conductivity and transparency.

2.5 CHARACTERISTICS OF ZNO

Some characteristics of ZnO are given in table-2.1. Most of the values differ slightly for specimens of different origin. The differences in the lattice constant are of the order of one percent, whereas the differences in the density are of the order of ten percent. In the case of exceedingly structure sensitive properties such as the magnetic susceptibility and the dielectric constant, only the order of magnitude of the values is important[2].

TABLE - 2.1. Characteristics of ZnO[2]

Lattice	Hexagonal, wurtzite (B4-type) Figure-2.1
Lattice constant	a = 3.24Å, C=5.19Å, c/a=1.60
Distance of neighbouring Zn^{++} and O^{--} ions	In the direction of c-axis d=uc=1.96Å of the three remaining neighbours $d = \sqrt{a^2/3 + c^2\left(U - \frac{1}{2}\right)^2} = 1.98Å$ (u=0.378 instead of 0.375 for ideal tetrahedral arrangement)
Molecular weight	Zn : 65.38, O : 16.00, ZnO : 81.38
Ionic radius for tetrahedral coordination	$Zn_{neutral}$: 1.31Å, $O_{neutral}$: 0.66Å, for covalent binding (Pauling). Zn^{++} : 0.70Å, O^{--} : 1.32Å for ionic binding (Pauling). Zn^{++} : 0.78Å, O^{--} : 1.24 for ionic binding (Goldschmidt)
Density	X-ray density 5.62 - 5.78 g/cm^3, corresponding to 4.21 X 10^{22} ZnO - molecule/cm^3, pycnometric : maxima 5.84 g/cm^3, active ZnO : <5 g/cm^3
Enthalpy of formation	Zn (solid) + $\frac{1}{2}$ O_2 (gas) → ZnO (solid) : -83.17 Kcal/mole corresponding to -3.61eV/ZnO - molecules in lattice
Lattice energy	965 Kcal/mole

Specific heat										
	20	30	50	100	150	200	300	500	900	°K
	0.17	0.60	1.98	4.24	6.22	7.20	9.66	11.2	12.3	cal/mole deg.

Vaper pressure	12 torr at 1500°C, 1 torr at 1400°. Sublimation in high vacuum is appreciable at 1000°C.
Melting point	≈ 2000°C only at high pressures.
Dielectric constant	Values in literature for powder and sintered specimens between 10 and 36. Single crystals (2.4 X 10^{10} cps); ϵ = 8.5

Magnetic susceptibility	Temperature	273	196	83°K	
	ZnO (active)	-0.31	-0.20	+0.62	X 10^6
	ZnO (tempered)	-0.25	-0.26	-0.25	
Electron affinity	≈ 4.2 eV.				

2.6 PROPERTIES OF ZnO THIN FILMS AND SINGLE CRYSTAL

2.6 (i) Structural

All types of structural studies were employed for ZnO films including x-ray and electron microscopy by many workers. The deposited films were found to compose of columnar crystallites[22] with the bulk wurtzite structure. The grain sizes as reported by the workers were in the range 50-300Å. In sputtered ZnO films, c-axis was found strongly oriented perpendicular or parallel to the substrate depending mainly on the substrate material. The degree of preferred orientation depends on the deposition parameters[15,16]. Films prepared by CVD[17] and spray Pyrolysis[22] exhibit a preferred c-axis orientation. Takashi Yamamota et.al.[32] reported that the lattice constant along the axis of the ZnO film is 5.14Å while that of the ZnO single crystal was 5.19Å. Hicker Nell[33] described that ZnO films might have a slight lattice strain.

2.6 (ii) Electrical

The electrical properties of ZnO thin films are very much sensitive to their method of preparation. Since the methods of preparation are diverse, a large scatter in the electrical properties were reported. Stoichiometric ZnO thin film is highly resistive. The reported[34] electrical resistivity of ZnO thin films prepared by enhanced reactive evaporation method is found in the range $6X10^{-4}$—$7X10^{8}$ ohms-cm. The resistivity of spray pyrolysed as

deposited ZnO films was found to 10^2 ohm-cm which decreased to 10^{-3} ohm-cm on annealing in vacuum[35] or H_2[22]. A drastic change in resistivity was found when the ZnO films were doped with trivalent indium. The doped film resistivity is $\approx 10^{-3}$ ohm-cm with a high electron concentration $4X10^{20}$ cm^{-3} and an electron Hall mobility of about 15 cm^{-2} v^{-1} s^{-1}[26], This value of Hall mobility is certainly very small in comparison to those of single crystal ZnO sample whose room temperature value of Hall mobility was varied from 100 to 200 cm^2 v^{-1} s^{-1}[36] for carrier concentration of the order 10^{16} cm^{-3}. In thin film the various type of scattering effect plays an important role in reducing Hall mobility. The scattering processes which are dominant in ZnO thin films are grain-boundary scattering[26], lattice scattering[37], ionized impurity scattering[22,37] and piezoelectric scattering[38]. All of these scattering processes in ZnO thin films were considered independently by different workers namely Rupprecht[39] and Hutson[40] on both undoped and doped single crystal of ZnO. According to Hutson, as-grown single crystals showed good conductivity. These as-grown crystals had defect structure although intentional doping was avoided. The room temperature carrier concentration obtained was in the range 1.2 X 10^{15}—3.3 X 17^{17} cm^{-3}. The concentration increased appreciably when they were doped with Li, Zn and H_2. The conductivity and carrier concentration were in the range of 10—10^3 ohm^{-1} cm^{-1} and 10^{18}—10^{20} cm^{-3} respectively in the case of In-doped crystals[39]. The density of state mass was found to be $m^N \approx 0.5m$ and

polaron mass m^0 = 0.27 m. The room temperature lattice scattering mobility fits the data quite well with experiment and was computed from the combination of optical and acoustical mode scattering[40].

2.6 (iii) Optical

The optical properties of ZnO thin films have been studied by different workers. Mollwo[41] measured absorption co-efficient of thin layer of ZnO formed by evaporation. A very steep increase in the absorption constant was found to be about 3.2 eV at the wavelength of 385 x 10^4 Å. ZnO thin films exhibit a direct optical band-gap of 3.3 eV[22], similar to that observed in bulk. High optical transmission (≈ 85%) in the solar spectrum has been obtained in spray deposited films with resistivity about 8 x 10^{-4} ohm-cm. Films with sheet resistance of 85 ohm/□ deposited by magnetron spattering[12] exhibit a transmission of 90% in the spectral range from 4000 to 8000Å. Jin et.al.[11] measured the transmission and reflection co-efficient of ZnO:Al films deposited on caF_2 substrate. The measurement was confined in the 2000 Å ≤ 10^4 ≤ 10^5 Å wavelength interval, for which caF_2 was transparent. In the luminous range the transmittance was high and in the UV films were opaque owing to absorption at the semiconductor band gap. The IR transmittance drop at λ = 10^5 Å for zero Al content and at λ = 0.15 x 10^5 Å for about 2% Al. IR reflectance displayed a concomitant increase. Major et.al.[42] studied the spectral dependence of the specular transmittance in

the wavelength range 3000—25000 Å and of the specular reflectance in the range 3000—100000 Å for films of undoped and In-doped ZnO. The measured transmittance was (about 80—85%) in the visible region and fell sharply in the UV region because of the onset of fundamental absorption. Undoped ZnO films showed nearly constant transmittance up to 25000 Å and a nearly reflectance upto 100000 Å. In In-doped sample both R and T decrease in the near IR region.

Barnes et.al.[43] measured the optical absorption of single crystal. The 3700 Å absorption edge for single crystal corresponds to a band-gap of 3.2 eV. For ZnO crystals, however, Mollwo[44] showed spectra with the absorption edge at 3.5 eV. At this wavelength, although the absorption co-efficient is rising rapidly and reached $500cm^{-1}$, ZnO film shows birefringence, the refractive indices being 2.01 and 2.03. At wavelength near 4000Å the dispersion is very large. The dielectric constant at a wavelength of 1cm is 8.5 (Hufson)[40], which is much larger than (refractive index)^2, indicating strong lattice absorption in the infra-red region.

2.7 OTHER TRANSPARENT CONDUCTORS

Like ZnO, there are several other oxides which are found to show various degree of transparent conductive properties. Among them, SnO_2, In_2O_3, CdO, Cd_2SnO_4, Bi_2O_3 and TiO_2 are remarkable. Of all these oxides, SnO_2 and In_2O_3 have been studied extensively[45,46].

Out of these oxides SnO_2 In_2O_3 thin films can show excellent transparent conducting properties. In_2O_3 films are slightly superior than SnO_2 because of its higher mobility[30]. The cost of preparation of SnO_2, In_2O_3 and Cd_2SnO_4 is very high than that of other oxides films. All of these transparent conductors exhibit n-type conductivity in both doped and undoped conditions.

2.8 FIGURE OF MERIT OF TRANSPARENT CONDUCTING COATING

To compare the performance of different oxides, Fraser et.al.[47] have defined a quantity, called the figure of marit, which relates the optical transmission and sheet resistance. A modified definition, more appropriate for solar cells, has been given by Haacke[48] and is expressed as

Figure of merit $\phi_{TC} = T^{10}/R_{\square}$

where T is the transmittance and R is the electrical sheet resistance.

The reported figure of merit for ZnO film prepared by activated reactive evaporation (ARE) are in the range $3.4X10^{-3}$—$22.6X10^{-3}$ ohm^{-1} for different wavelengths. The heighest value was obtained at 0.55 and 0.75 wavelength. For magnetron sputtered film[12] it is found to be $4.10X10^{-3}$ Ω^{-1} from the data of $R_{\square}$ and T.

REFERENCES

1. K.Lark-Horovitz and C.H. Ehrhardt. Phys. Rev. 57, (1940) 603.
2. G, Heiland, E. Mollwo, and F. Stöckmann. Solid State Physics. Vol-8, Academic Press New York and London (1959).
3. E.Mollwo and F. Stöckmann. Ann. Physik ¦6¦3, (1948) 223.
4. E.E. Hahn, J.Appl. Phys. 22. (1951) 855.
5. S.E. Harrison, Phys. Rev. 93, (1954) 52.
6. G. Seitz. Diplomarbeit, University of Erlangen, 1955.
7. Hideo. Watanabe, Japan. J. Appl. Phys. 9(1970) 418.
8. W.S. Lau and S.J. Fonash. Journal of electronic materials, vol. 16 no 3. (1987) 141.
9. D.E. Brodie, R. Singh. J.H. Morgan. J.D. Leslie. L.J. Moore and A.E. Dixon. Proc. 14th IEEE Photovoltaic specialists conf. san Diego. C.A. 1980, IEEE, New York, (1980) 468.
10. N.L. Kenigsberg and A.N. Chernets Sov. Phys. Solid state, 10(1963) 2235.
11. Z.C.Jin. I. Hamberg and C.G. Granqvist. Thin Solid Films. 164(1988) 381.
12. J.B. Webb. D.F. Williams and M. Buchanan. Appl. Phys. Lett. 39(1981) 640.
13. J.O. Barnes, D.J. Leary and A.G. Jordan. J. Electrochem Soc. 7(1980) 1636.
14. O. Caporaletti, Sol. Energy mater, 7(1982) 65.
15. H.W.Lehmann and R. widmer. Proc. 6th lnt. vacuum congr. kyoto. 1974. in Jpn. J. Appl. Phys. suppl. 2. part 1 (1974) 741.

16. H.W. Lehmann and R. Widmer. J. Appl. Phys. 44(1973) 3868.

17. Sorab K. Ghandhi, Robert J.Field and James R. Sheely. Appl. Phys. Lett 37(5) (1980) 449.

18. A.P. Roth and D.F. Williams. J. Appl. Phys. 52(11) (1981) 6685

19. K.L. Chopra. R.C. Kainthla, D.K. Pandya and A.P. Thakoor. Phys. Thin Films. 12(1982) 167.

20. M.S. Tomar and F.J. Garcia. Prog. Crystal growth charact., 4(1981) 221.

21. J.C. Viguie and J. Spitz. J. Electrochem Soc., 122(1975) 585.

22. Julio Aranovich, Armando Ortiz and Richard H. Bube. J. vac. Sci. Technol. 16(4) (1979) 994.

23. M.S. Tomar and F.J. Garcia. Thin Solid films, 90(1982) 419.

24. Chris Eberspacher, Alan L. Fahrenbruch and Rchard H. Bube. Thin Solid Films 136(1986) 1.

25. L. Bahadur, M. Hamdani, J.F. Koenig and P. chartier, Solar energy materials. 14(1986) 107.

26. S. Major. A. Banerjee and K.L. Chopra. Thin Solid Films 108(1983) 333.

27. A. Ortiz, C. Falcony, M. Garcia and A Sanchez J. Phys. D. Appl. Phys. 20(1987) 670.

28. G. Blandenet, M. Court and Y. Lagarde, Jhin Solid Films, 77, (1981) 81.

29. H. Dislich E. Hussmann, Thin Solid Films, 77(1981)129.

30. K.L. Chopra, S.Major and D.K. Pandya, Thin Solid Films 102(1983) 1.

31. M. Ristov. G. J. Sinadinovski. I. Grozdanov and M. Mitriski. Thin Solid Films. 149(1987) 65.

32. Takashi Yamamota, Takashi Shiosaki and Akira Kawabata. J. Appl. Phys. 51(6) (1980) 3113.

33. F.J. Hickernell. Proc. IEEE ultrasonics Symp. (1977) 1264.

34. D.E. Brodie, R. Singh, J.H. Morgan, J.D. Leslie, C.J. Moore, and A.E. Dixon, Ch 1508-1/80/0000-0468500.75 (c) 1980 IEEE.

35. E.Shanthi Ph.D. Thesis. Indian Institute of Technology. Delhi (1981).

36. J.Schoenes, K. Kanazawa and E. Kay. J. Appl. Phys. 48(1977) 2537.

37. Masanobu Kasuga and Shinzi Ogawa. Japanese Journal of Applied Physics, Vol 22, No.5 (1983) 794.

38. M.G. Ambia, M.N. Islam and M.O. Hakim Journal of materials science 27(1992) 5169.

39. H. Rupprecht. J. PHys. Chem. Solids. 6 (1958) 144.

40. A.R. Hutson. Physical Review vol. 108. No. 1 (1957) 222.

41. E. Mollwo. Reichsber, Physik 1 (1943) 1.

42. S. Major, A. Banerjee. and K.L. Chopra. Thin Solid films 125(1985) 179.

43. James O. Barnes, David J. Leary and A.G Jordon J. Electrochem.Soc.Solid-State Science and Technology vol. 127. No. 7 (1980) 1636.

44. Mollwo E. Photo conducting conferance (1956) Wiley. N.Y.

45. J.C. Manifacir. M. de Murcia and J.P. Fillard. Mat. Res. Bull 10, (1975) 1215.

46. J.C. Manifacer L. Szepessy. J.F. Bresse, M. Perotin and R. Stuck. Mat. Bull. 14(1979)109 and 14 (1979) 163.

47. D.B. Fraser and H.D. Cook J. electrochem Soc. 119 (1972) 1368

48. G. Haacke. J. Appl. Phys. 47 (1776) 4086.

CHAPTER 3

THEORETICAL CONSIDERATIONS

Fabrication of films by vacuum and non-vacuum techniques yield films of different nature but the basic principles of condensation and nucleation of the films from its vapour phase (in the initial film growth stage) are the same. Since chemical spray deposition method is a non-vacuum technique and can operate in open atmosphere, so to have a good quality film a stern quality requirement is imposed on the films prepared by this method. Beside this, one should have a thorough knowledge of the principles that are associated with this method. In the first part of this chapter, a brief description of nucleation and film growth aspects is presented. The second part includes the methods of analysis of various properties of semiconducting thin films.

PART-I : SALIENT FEATURES OF THE FILM GROWTH PROCESS IN A CHEMICAL METHOD.

THEORETICAL CONSIDERATIONS OF CHEMICAL SPRAY METHOD.

To discuss something about this method, one has to consider first the chemistry, the thermodynamics and possible chemical kinetics which are the essential features of the chemical spray method. Some of the relevant usefulness of these studies are briefly described below.

3.1 CHEMISTRY OF THE METHOD

Chemical pyrolysis method can be defined as a material synthesis, in which the constituents of the vapour phase react to form a solid film at some surface, thus the occurrence of chemical reaction is an essential characteristic of the pyrolysis method.

To understand the process, one must know which chemical reactions occur in the reactor and to what extent. Furthermore, the effects of process variables such as temperature, pressure, input concentrations and flow rates on these reactions must be understood. The nature and extent of chemical reactions can be deduced if one knows the composition of the solid and vapour phases in pyrolysis system. The composition of the solid product can be analysed after the deposition but that of the vapour phase must be determined in situ at the particular reaction condition, otherwise high temperature species may disappear or change on cooling to room temperature. Several experimental method are employed for this purpose such as mass spectrometry, Raman spectroscopy, absorption spectroscopy, gas chromatography etc.

3.2 CHEMICAL REACTION

The types of reactions which generally take part in chemical method to form solid film are as follows.

(i) Pyrolysis (ii) Hydrolysis (iii) Oxidation (iv) Reduction (v) Synthesis reaction (vi) Disproportionation (vii) Carbide and Nitride formation (viii) Combined reaction etc.

Among these various types of reactions the first four types are very important and have roles in spray pyrolysis method.

The thermal decomposition (by the action of heat) of a compound to yield a deposit of the stable residue is called pyrolysis where as the chemical decomposition that are caused by the action of water is called Hydrolysis. In the formation of ZnO thin films by pyrolytic method the hydrolysis and pyrolysis reactions are involved. Hydrolysis reaction occurs first in preparing aqueous ionic solution of starting material and pyrolysis reaction takes place during the film deposition. For ZnO, the reaction involving the anion A (for aqueous solution) is in principle of the type:

$$(Zn\ A_2)aq + H_2O \rightleftharpoons ZnO + 2HA \quad \ldots\ldots\ldots\ldots\ldots\ldots (3.1)$$

It occurs under nonequilibrium conditions and probably through reaction paths of considerable complexity. Aqueous solutions have been investigated here. For kinetic reasons complete dissociation of the salt is required, corresponding to the cation forming hydrated complexes with only water molecules in the first phase of coordination. The heat of reaction of equation. (3.1) are 30 k cal/mol for the Chloride,-0.1 k cal/mol. for the acetate, and -10 k cal/mol for nitrate at room temperature[1].

3.3 REACTOR SYSTEM

The reactor is an important part of a pyrolytic deposition system. Its design and equipments should be adequate enough to accomplish the following functions:

(i) Transport, meter and time the diluent and reactant gases entering the reactor

(ii) Supply heat to the reaction site, namely substrate material being coated, and control of this temperature

(iii) Remove the by product exhaust gases from the deposition zone and safely dispose of them.

The quality of the film depends on the degree of fulfillment of the above mentioned functions and to meet these requirements one should give attention to avoid the complexity in the construction of the reactor.

The geometry and construction material of the reactor is selected by the physical and chemical characteristics of the entire system and by the process parameters. For the chemical spray deposition method usually three types of reactors are found.

(iva) Low temperature reactor system whose temperature is kept $<500^{\circ}C$ at normal pressure.

(ivb) High temperature reactors whoes operating temperature $> 500^{\circ}C$ at normal pressure.

(ivc) Low pressure reactors.

Low pressure reactors are generally hot-wall type but the low

temperature or high temperature reactor may be either of hot wall or cold-wall type.

It is expected that a fully developed thermal field exists in hot-wall reactors because of the fact that low gas velocities are employed there. These type of reactors are generally tubular in form. In cold wall reactors the situation is more complex.

The existane of rather sharp temperature gradients perpendicular to, as well as along the surface of this substrate (in the horizontal configuration)[2] affect the gas flow and transport phenomena considerably as shown diagramically in figure 3.1.

Hot-wall reactors are used in the case of system where the deposition reaction is exothermic in nature since the high wall temperature minimizes or even presents undesirable deposition on the reactor walls. In the case of endothermic reaction cold wall reactors are more useful.

3.4 TRANSPORT PHENOMENA IN THE REACTOR

Transport phenomena in fluids are related to the nature of the fluid flow. The following parameters affect the nature of gas flow in reactors :-

(i) Velocity of flow

(ii) Temperature and temperature distribution in the system

(iii) Pressure in the system

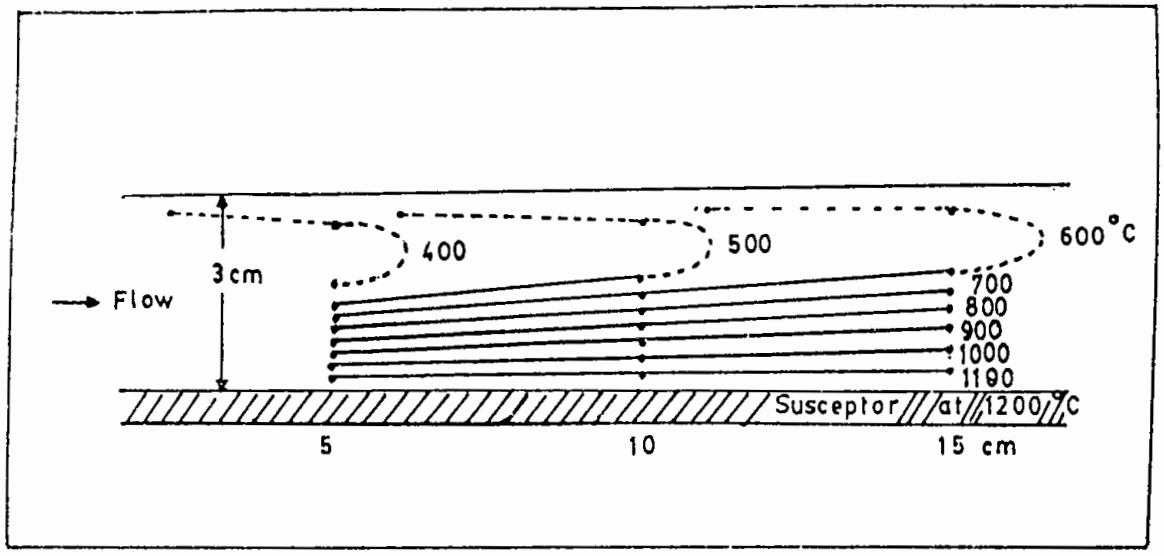

Figure 3.1: Isotherms in horizontal reactor when heated from the bottom .[V.S. Ban, J. Electrochem. Soc. 125, 317 (1978)]

(iv) geometry of the system and

(v) Gas or Vapour characteristics.

For two basic reasons the study of transport phenomena is important.

(1) The requirement of thickness and semiconducting doping uniformity which can be fulfilled only when equal amounts of the reactant gases and dopants are delivered to all the substrates in the system.

(2) The requirement of high chemical efficiency to achieve satisfactory growth rates and utilization of input chemicals; this means that sufficient amounts of reactants must be delivered to the film growth surfaces.

All the above points should be brought under consideration at the time of designing the reactor.

3.5 THERMODYNAMICS OF PYROLYTIC DEPOSITION

The main functions of thermodynamics in relation to chemical spray method are to predict the feasibility of the process under some specified conditions and to provide quantitative information about the process. Properly performed thermodynamic calculations give the theoretically obtainable amount of a deposit and partial pressures of all species under specific experimental conditions, such as the temperature and pressure in the reactor and the input concentrations of the reactants.

Thus, thermodynamics can be used as a guide line for establishing general process parameters. Intial step of a chemical spray deposition process is to perform the necessary thermodynamic calculations to obtain the general conditions the process requires. In order to perform the calculations, one needs reliable thermodynamic data. The most useful data are free energy of formation of all vapour and condensed constituents of the system.

G°_{f} is the standard free energy of formation of a compound and $\Delta G^{\circ}_{f} = 0$ for all elements in their standard state. The free energy of some chemical reaction (ΔG°_{r}) can be calculated if (ΔG°_{f}) values are known[3].

$$\Delta G^{\circ}_{r} = \Sigma \Delta G^{\circ}_{f} \text{ products} - \Sigma \Delta G^{\circ}_{f} \text{ reactant} \quad \ldots\ldots\ldots\ldots (3.2)$$

In chemical spray deposition, one usually deals with a multicomponent and multiphase system. Most often, there are only two phases, the Vapour and solid; although more than one condensed phase may be present. There are several ways for computing thermodynamic equilibrium in multicomponent system. Most important method is the optimization method.

3.6 OPTIMIZATION METHOD

Let us suppose a system in which a chemical reaction proceeds to some degree of completion. This is denoted by ϵ:

$$(1-\epsilon)\ (\text{reactants}) \rightarrow \epsilon\ (\text{Products}) \ldots\ldots\ldots\ldots\ldots\ldots (3.3)$$

If one plots the free energy of the system versus ϵ, one sees that the energy curve has a minimum at some value of ϵ. This value of ϵ, is the equilibrium concentrations of reactants and products.

3.7 KINETICS OF THE METHOD

The situation in spray pyrolysis reaction might differ from the prediction of thermodynamical equilibrium calculations. The deposition reaction is almost always a heterogeneous reaction. The sequence of events in the usual heterogeneous processes can be described as follows:

(i) Diffusion of reactants to the surface;

(ii) Adsorption of reactants at the surface,

(iii) Surface events, such a chemical reaction, surface motion, lattice incorporation, etc.

(iv) Desorption of products from the surface,

(v) Diffusion of products away from the surface.

The application of kinetics in film deposition process has been exemplified by Eversteijn[4].

Some of the factors that causes deviation from equilibrium are

(vi) Temperature dependence of deposition rate:

For a given substrate the nature of the rate controlling step, changes with temperature. The rate controlling steps are (via) adsorption of reactants on the substrate surface; (vib) diffusion of reactants and products to and from the substrate surface respectively. The rate of deposition r is exponentially dependent

on temperature T as given by Arrhenius rate equation:

$$r = a \exp(-\Delta E/K_B T) \quad \ldots\ldots\ldots\ldots\ldots\ldots\ldots 3.4$$

Where ΔE is the activation energy for the process and a is the frequency factor.

(vii) Dependence of the deposition rate on substrate orientation: This is another important aspect of the film deposition process where kinetics has its role to play. The other kinetic effect in pyrolytic deposition is the effects of dopants in the case of semiconductor films growth rate[5] and the existence of metastable phases. It is important to keep in mind that while thermodynamics specifies what ought to happen in the reactor,the kinetics determine what actually will happen.

3.8 FILM GROWTH ASPECTS

The properties of thin film depend very much on their structure. So it is important to know the factors that govern the structure of the film. A brief discussion about the nucleation and formation of polycrystalline and amorphous thin films has been given in the following section.

3.9 Condensation

Generally thin films are prepared by depositing the film material, atom by atom, on a substrate. The best understood process of film formation is that by condensation from the vapour phase.

Condensation simply means the transformation of a gas into a liquid or solid. Thermodynamically, the only requirement for condensation to occur is that the partial pressure of the film material in the gas phase be equal to or larger than its vapour pressure in the condensed phase at that temperature[6]

However, this is true only if condensation takes place on film material already condensed or on a substrate made of the same material. In general the substrate will have a chemical nature different from that of the film material. Under these conditions still a third phase must be considered namely the adsorbed phase in which vapour atoms are adsorbed on the substrate but have not yet combined with other adsorbed atoms.

Condensation is initiated by the formation of small clusters through combination of several adsorbed atoms. These clusters are called nuclei and the process of cluster formation is called nucleation. Since small particles display a higher vapour pressure than the bulk material under the same conditions, a supersaturation ratio large than unity is required for nucleation to occur. The process of enlargement of the nuclei to form finally a coherent film is termed growth.

The modern theory of nucleation is based upon the atomostic nucleation concept[3] which states that not all surfaces have equal bonding characteristics. Those with strong bonds are particularly favourable nucleation sites. Again, after nuclei reach a certain

size it becames energetically more favourable for them to grow than to reevaporate. The growing nuclei come into contact and finally coalesce to form continuous film.

The sequence of the nucleation and growth steps to form a continuous film as revealed by an electron microscopic observation[7,8] are -

3.9 (i) The island stage

When a substrate under impingement of condensate monomers is observed, the first evidence of condensation is a sudden burst of nuclei of uniform size. Growth of nuclei is three dimentional. These nuclei then grow to form islands, whose shapes are determined by interfacial energies and deposition conditions.

The growth is diffusion controlled, that adatoms and subcritical clusters diffuse over the substrate surface and are captured by the stable islands.

3.9 (ii) The coalescence stage

In a given distribution of immobile nuclei, the separation between neighbours is continuously decreased by their growth, when contact occurs the nuclei are said to have coalesced. The coalescence occurs in less than 0.1 sec. The character of coalescence is liquidlike and enlargement of the islands occurs covering larger areas of the substrate.

3.9 (iii) The channel stage

When larger islands grow together they leave channels of interconnected holes of exposed substrate in the form of a network structure on the substrate. As deposition continues, secondary nucleation occurs in these channels and forms the last stage of the nucleation viz

3.9 (iv) **The continuous film:** Which then becomes thicker as the time passes.

3.10 POLYCRYSTALLINE AND AMORPHOUS THIN FILMS

The films deposited by spray pyrolysis are generally polycrystalline or amorphous in structure. Lower temperature and higher gas phase concentration are actually favourable in forming polycrystalline film. In these situation the rate of arrival of the aerosol (spray particles) at the surface is high, but the surface mobility of adsorbed atoms is low. A large number of differently oriented nuclei are formed, after coalesce between them the films that are obtained possess grains of different orientation. Further decrease in temperature and increase in supersaturation result in even more nuclei and consequently in finer grained films. When crystallization is completely stopped formation of amorphous film is favoured.

3.11 THE INCORPORATION OF DEFECTS DURING GROWTH

When the islands during the initial stages of thin film growth are still quite small, they are observed to be perfect single crystal[8]. However, as soon as the islands become large enough so that they touch, grain boundaries or lattice defects will be incorporated into the film, unless the islands coalesce to form a single grain. A large number of defects are incorporated in the film during their recrystallization process at the early stage of film formation. The defects that are usually encountered in spray deposited films are lattice vacancies, stoichiometric excess and grain boundary. Another type of defect namely surface roughness which stems from the quality of the sprayer is especially important in the use of spray deposited films. The properties of the film are strongly affected due to surface roughness if the thickness of film is small. The most frequently encountered defects in evaporated films are dislocations which are less important in chemical spray deposited films.

3.12 THE GRAIN BOUNDARIES

In polycrystalline thin film, the grain size and the boundary regions markedly depend on the deposition variables such as (i) film thickness, (ii) substrate temperature, (iii) annealing temperature and (iv) the deposition rate. Thus the number of such boundaries are controllable parameters.

The variation of crystallite size with the parameters mentioned above are shown schematically[9] in figure 3.2. From this figure the dependence of grain size on film thickness is that the larger grains are expected as the new grains are nucleated on the top of the old ones after a certain film thickness has been reached. Another possibility of getting larger gain sizes are expected for increasing substrate or annealing temperature because of an increase in surface mobility. Thus allowance is made to the film to decrease its total energy by growing large grains and thereby decreasing its grain-boundary area. Annealing at temperatures higher than the deposition temperature increases the grain size, hut the growth effect is significantly different from that obtained by using the same temperature during deposition[10]. The dependence of grain size on deposition rate is less obvious but can be understood on the basis that film atoms just impinged on the surface, although they may possess a large surface mobility, become buried under subsequent layers, at high deposition rates, before much diffusion can take place[9]. In order for this effect to operate, however, a certain minimum rate must be expected. Rather than this threshold rate, grain size is limited by temperature alone and above it the grain size is decreased more and more for higher and higher rate.

Dependence of grain size of spray pyrolized ZnO thin film on the substrate temperature has been studied by Cossement et. al.[11] and Chris Eberspacher et. al.[12] on the SnO_2 and InP substrate

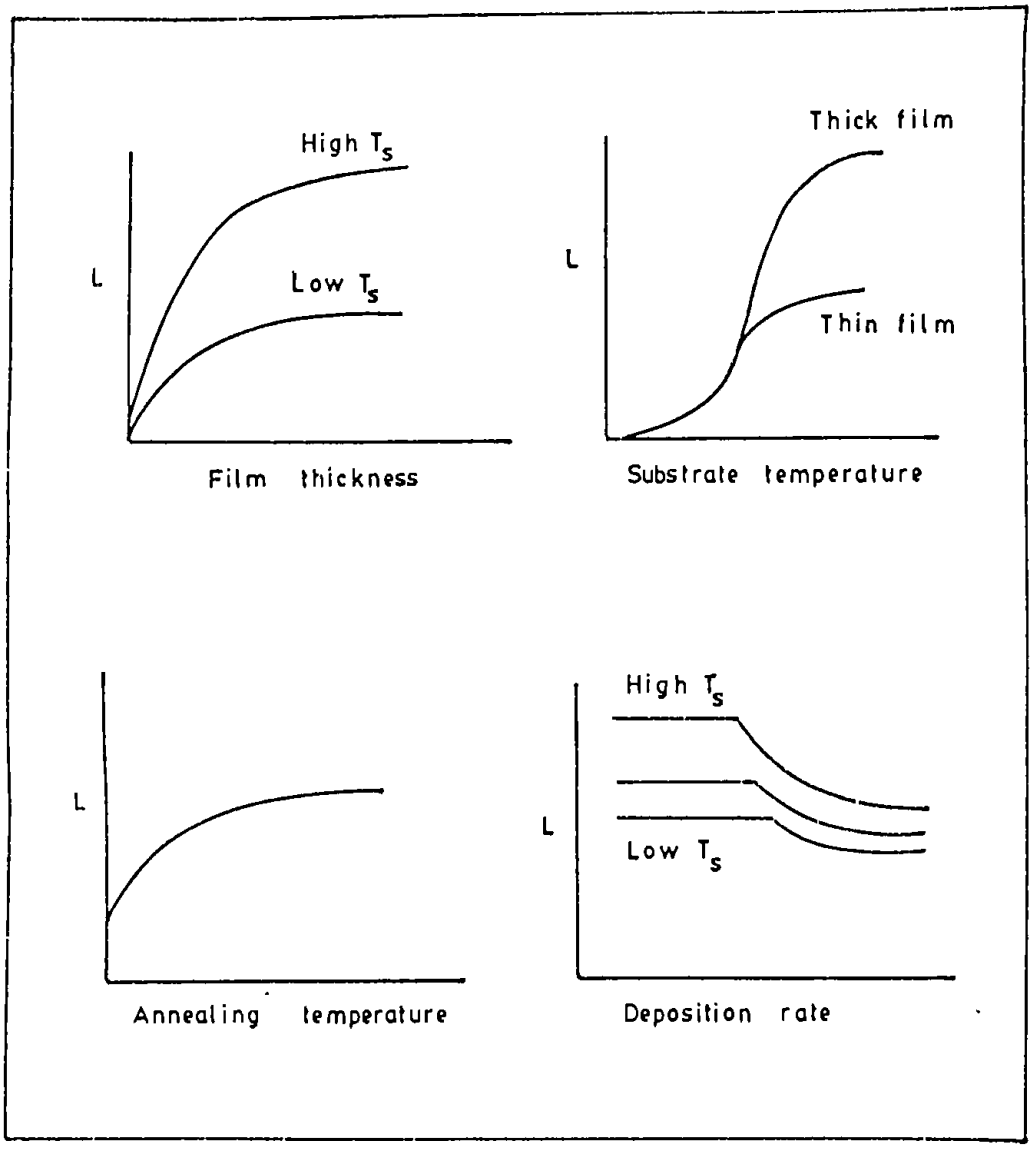

Figure 3.2: Dependence of grain size L on film thickness, substrate temperature T_s, annealing temperature and deposition rate.

respectively, where it was observed that grain size increases with the substrate temperature. Variation of carrier concentration with substrate temperature can thus take place. Nobbs et. al.[13] reported another evidence that the grain size of ZnO thin film increases with the film thickness.

3.13 DEFECT STRUCTURE IN ZNO THIN FILM

It is known that the physical properties of oxide films strongly depend on the deviation from the stoichiometric composition and on the nature and concentration of the foreign atoms incorporated into the host lattice. In undoped ZnO the imperfections are introduced either by the Oxygen vacancies or by interstitial zinc atoms which act as donors and the material as a whole exhibits n-type behavior.

In In-doped ZnO indium initially replaces Zn in the ZnO. lattice, while its role as a donor but above a certain dopant concentration, indium is no longer substituted in the lattice rather it is localized in the form of In $(OH)_3$ in the grain boundaries[11]

In the case of Al-doped ZnO prepared by sputtering, the Al atoms are expected to enter substitutionally on Zn sites in the ZnO lattice so that they act as singly Ionized donors. Doping of pure ZnO is likely to be associated with Oxygen deficiency[14].

Part-II ANALYTICAL METHODS FOR THE STUDY OF FILM PROPERTIES

Statistical methods are generally employed for analysing the electrical and optical properties of semiconducting materials.

Undoped ZnO thin films deposited with spray pyrolysis are found in both the non-degenerate and degenerate condition but doped films are always obtained almost in the degenerate condition. Therefore, in this part of the chapter different theoretical principles undermentioned the various analytical methods for the properties of semiconducting materials have been briefly discussed with both non-degenerate and degenerate models.

3.14 DEGENERATE AND NON-DEGENERATE SEMICONDUCTOR

Fermi level in most of the semiconductor lies in about $2K_BT$ below the bottom of the conduction band edge. In that case the electrons in conduction band follow closely Boltzmann statistics, and the electron gas is said to be non-degenerate. In some cases of an n-type semiconductor, when the Fermi level enters into the conduction band or goes close to the band edge from the mid gap the electron gas may become degenerate. The conditions that are in favour of such a situation are-

(i) Relatively high donor density ($\sim 10^{19}$ cm^{-3}) for n-type material

(ii) Small donor ionization energy and

(iii) Low density of states near the bottom of the conduction band i.e. small effective mass of the electrons.

Under these conditions all the statistical calculations should be performed by using the Fermi-Dirac statistics.

When the temperature increases from absolute Zero, the donors begin to ionize and the lower energy states in the bottom of the conduction band become completely occupied due to its low density of states. The position of the Fermi level relative to the bottom of the conduction band is then given by [15]

$$E_f = (h^2/8m^*_e)\ (3n/\pi)^{2/3} \quad \ldots\ldots\ldots\ldots\ldots\ldots \quad (3.5)$$

Where n is the density of electrons in the conduction band. If $E_f >> K_B T$, the electron gas is degenerate. It is observed that degeneracy may occur at electron concentrations ($\sim 10^{18}$ cm^{-3}) with the reduced electron effective mass m^*_e, As the temperature is increased further the degeneracy may be removed and Fermi level leaves the conduction band again. The approximate condition for degeneracy is that the Fermi level be no lower than $K_B T$ (at T = 300K) below the conduction band-edge and the temperature T_{deg} at which this condition is satisfied can be obtained from equation (3.5)

$$T_{deg} = \left(\frac{h^2}{8k_B m^*_e}\right)(3n_{deg}/\pi)^{3/2} \quad \ldots\ldots\ldots \quad (3.6)$$

Where T_{deg} is the temperature at which degeneracy starts and is termed as degeneracy temperature and n_{deg}, the carrier concentration at T_{deg} is called degeneracy concentration (Concentration for the onset of degeneracy). This concentration is the demarkation line between degenerate and non-degenerate semiconductors.

3.15 THE HALL CONSTANT, ELECTRICAL CONDUCTIVITY AND MOBILITY

When a magnetic field is applied at right angle to the direction of current in a conductor, Hall effect is produced as shown in figure 3.3. In presence of a magnetic field, a magnetic force eB acts on the electrons having on average velocity v due to the current I. The force acts in the direction perpendicular to both B and v causes the electrons to deflect (for n-type materials) toword the surface of one side of the conductor. As a result of this an additional electric field E_H is produced. Under equilibrium condition, the sideways force on the moving carriers due to this field just balances that arising from the magnetic field.

The magnitude of the transverse Hall field E_H, is found by equating the sideways forces

$$e\,E_H = ev\,B \quad \ldots\ldots\ldots\ldots\ldots\ldots\ldots\ldots 3.7$$

expressing v in terms of current density J and the conduction electron density n from the relation J = nev, we have E_H,

$$E_H = (1/ne)\,JB = B_H JB \quad \ldots\ldots\ldots\ldots\ldots\ldots (3.8)$$

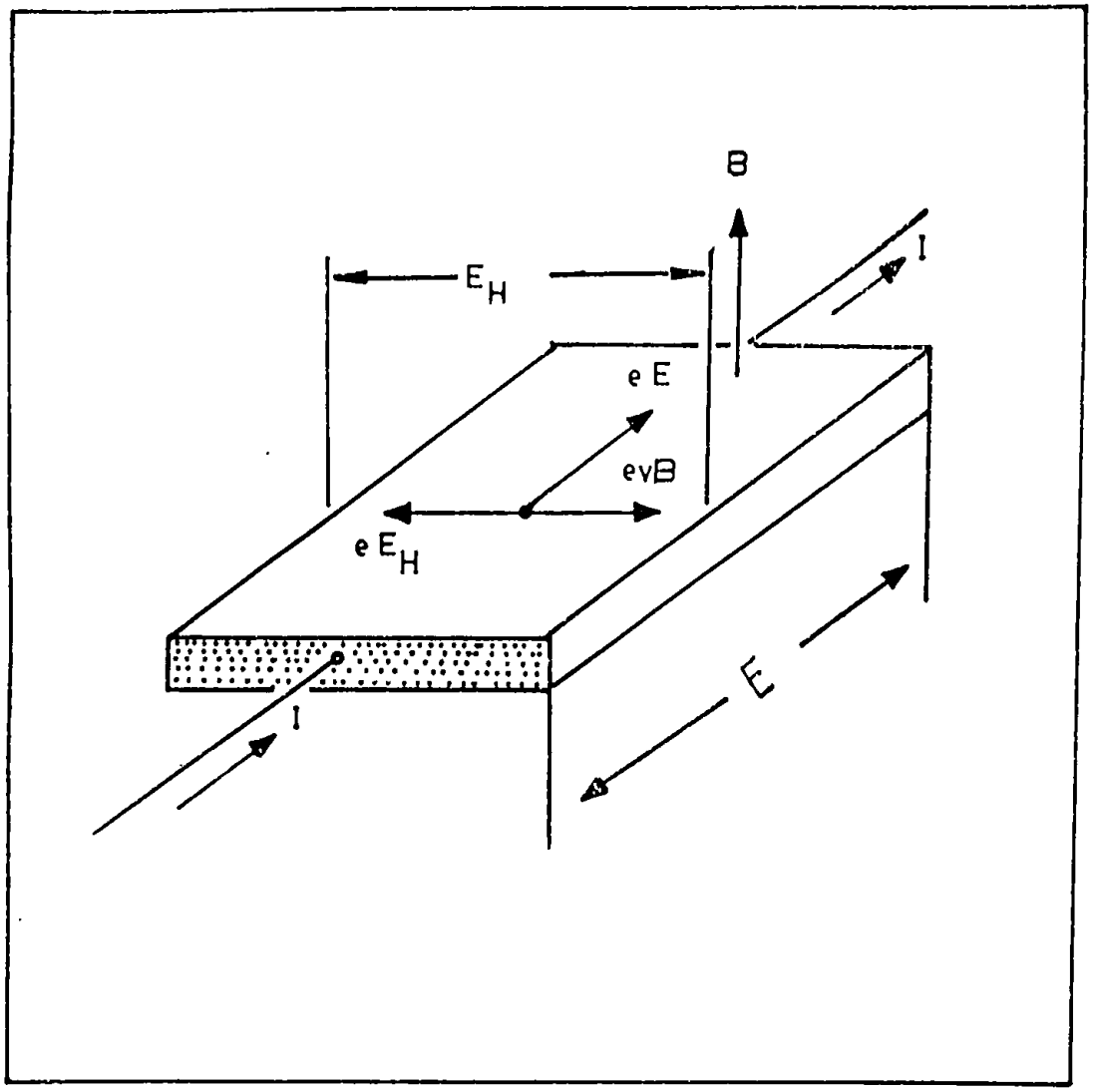

Figure 3.3: The forces acting on a current carrier in a conductor placed in a magnetic field leading to the observable Hall field E_H.

where the Hall constant

$$R_H = 1/ne \quad \ldots\ldots\ldots\ldots\ldots\ldots\ldots\ldots \quad (2.9)$$

gives the carrier concentration directly. The experimental observed quantity is the Hall voltage V_H, which is obtained form the equation (3.8) since

$$E_H = V_H/W, \text{ and } J = I/wt.$$

where w is the sample width and t is thickness. Therefore equation (3.8) becomes

$$R_H = 1/ne = V_H t/IB \quad \ldots\ldots\ldots\ldots\ldots\ldots \quad (3.10)$$

In equation (3.10), e is the magnitude of electronic charge and the algebraic sign of the Hall voltage indicates whether the carries are holes or electrons. This treatment of Hall effect is very simple and is applied for specimens with a constant energy surface. But a more rigorous treatment for multivally semiconductors with ellipsoidal constant energy surfaces leads to the expression for the Hall constant[16]

$$R_H = \left(\frac{r}{ne}\right) 3k(k+2)/(2k+1)^2 \quad \ldots\ldots\ldots \quad (3.11)$$

Where r is a constant equal to 1 for degenerate semiconductors and K is the ratio of the longitudinal to transverse effective masses of the carriers.

3.16 HALL MOBILITY μ AND ELECTRICAL CONDUCTIVITY σ

When the charge carrier is moving in an electric field E with the average velocity v then the Hall mobility μ is defined as the velocity of electrons per unit electric field, i.e.

$$\mu = v/E \quad \ldots\ldots\ldots\ldots\ldots\ldots\ldots \quad (3.12)$$

Combining this with the Ohm's law $\sigma = J/E$, using $J = nev$, the expression for conductivity is-

$$\sigma = ne\mu$$

$$\text{or } \mu = R_H\sigma \quad \ldots\ldots\ldots\ldots\ldots\ldots \quad (3.13)$$

Due to thermal energies the electrons and holes in a semiconductor are set to rapid random motion and collide among themselves. If τ is the average time between such collisions then the rate of change of velocity is $- v/\tau$. In steady state condition this rate of change must be equal to the acceleration due to the field $-eE/m^*$. Therefore

$$eE/m^* = v/\tau = \mu E/\tau$$

$$\text{or } \mu = e\tau/m^* \text{ and } \sigma = ne^2\tau/m^* \quad \ldots\ldots\ldots\ldots \quad (3.14)$$

In this expression τ has been assumed to be free from the electron's velocity v for simplicity.

For semiconductor with spherical constant energy surfaces it has been found that over a considerable range of energies [17]

$$\tau = aE^{-r} \quad \ldots\ldots\ldots\ldots\ldots\ldots \quad (3.15)$$

Where r is a constant and may vary with temperature. The value of r is generally derived from the observed variation of mobility with temperature and is dependent on the scattering processes. So it is a fundamental problem in semiconductor physics to determine the exact nature of the dependence of τ on energy of the electrons.

3.17 VARIATION OF CARRIER CONCENTRATION WITH TEMPERATURE (FOR EXTRINSIC SEMICONDUCTOR)

The variation of electron concentration n (or hole concentration p) with temperature in extrinsic semiconductor have been considered in the following manner. We suppose that the donor centers are partially ionized so that $n<N_D$ (or $p<N_A$) where N_D is the donor density. In the case of n-type material, ($N_D>N_A$), the rate of loss of electrons from donor centres to the conduction band is proportional to the number of filled donors $[N_D - (N_A + n)]$ and to the number of empty conduction bands states N_c, thus it is given by

$$k_1 N_c (N_D - N_A - n)$$

where K_1 is a constant of proportionality. The rate of return of electrons to the donors is proportional to the number of electrons in the conduction band n and to the number of empty donor states, $(N_A + n)$ each of which must be counted twice, however, as there are two possible ways for the electron to enter it (spin up or spin down). This rate, is

$$K_2 n [2 (n + N_A)]$$

At equilibrium these ratios are equal, so that

$$\frac{n[2(n+N_A)}{N_c(N_O-N_A-n)} = \frac{K_1}{K_2} = K \quad \ldots\ldots\ldots \quad (3.16)$$

where k is the equilibrium constant, a function only of temperature. In the classical approximation it is given by

$$K = \exp\,[-(E_c - E_0)/k_BT]$$

where $(E_c - E_0)$ is the donor ionization energy, E_c is the conduction band edge and

$$N_c = 2(2\pi\, m_e^*\, k_BT/h^2)^{3/2}$$

is the effective density of states. For degenerate case, N_c given by

$$N_c = 4\pi/h^3\ (2m_e^* k_BT)^{3/2}$$

considering the approximation to equation (3.16). If $n \ll N_A$, (3.16) reduces to

$$n = [(N_D - N_A)/N_A.\ \ N_c/2]\ \exp\,[-(E_c - E_D)/k_BT) \quad \ldots \quad (3.17)$$

In a second approximation to (3.16) when $n \gg N_A$ (3.16) reduces to

$$2n^2/N_c\ N_D = \exp\,[-[Ec - E_D)K_BT)$$

$$\text{or, } n = (N_c/_2.N_D)^{1/2}\ \exp\,[-(E_c - E_D)/2K_BT] \quad \ldots\ldots\ldots \quad (3.18)$$

The pre-exponential term of equation (3.18) slightly depends on temperature and is usually neglected. Equation (3.17) and (2.18) operate so long as the sample is extrinsic and remain outside the saturation or exhaustion range. In the exhaustion region, the supply of electrons to the conduction band is stopped because all the donor atoms are completely ionized and the electron

concentration remains, approximately constant with the temperature. In that case the concentration where the (n vs. T) plot is horizontal equals the donor concentration N_D.

3.18 THE ACTIVATION ENERGY

The activation energy which is related to the electron transport process in the material can be expressed by a conventional Arrhenius type relation-

$$\sigma = \sigma_0 \exp(-E_a/K_BT) \quad \ldots\ldots\ldots \quad (3.18i)$$

Where E_a is the activation energy and σ is the electrical conductivity. For semiconductors the following two distinct cases may arise.

Case-I

3.18 (i) (For intrinsic semiconductor)

The carrier concentration for n-type conductivity in intrinsic semiconductor is expressed as

$$n=(N_vN_c)^{1/2} \exp(-E_g/2K_BT) \quad \ldots\ldots \quad (3.18ii)$$

Where N_v and N_c are the carrier concentration in the valence and conduction bands respectively, and E_g is the band gap. At constant mobility, σ is directly proportional to the carrier concentration, n

$$(\sigma=ne\mu)$$

So the activation energy can be obtained by comparing equation

(3.18i) and (3.18ii) and is given by

$$E_a = E_g/2 = \text{half the band gap} \quad \ldots\ldots\ldots \quad (3.18iii)$$

Case-II

3.18 (ii) **Extrinsic semiconductor:**

Extrinsic semiconductor contains impurity atoms which create an additional impurity or trap level in the regular band gap. In this case, the activation energy can be obtained by comparing equation (3.17) and equation (3.18) with the equation (3.18i). Two cases may arise-

3.18 (iia) **Uncompensated semiconductor:**

In this situation $N_D > n >> N_A$ and the activation energy is obtained from equation (3.18)

$$E_a = (E_c - E_D)/2 = \text{half the trap depth} \quad \ldots\ldots \quad (3.18iv)$$

3.18 (iib) **Partly compensated semiconductor**

In this case $n << N_A < N_D$ and the activation energy is

$$E_a = (E_c - E_D) = \text{the trap depth} \quad (3.18v)$$

3.18 (iii) **Compensated semiconductor**

In this regime the activation energy is compared with half the band gap because the semiconductors hehave like intrinsic material.

Depending on the temperature a sample of one category may change to other one. An intrinsic conduction may set in an extrinsic sample when its temperature is high enough. It is clear from the above discussion that great care should be taken in the study of the activation energy determination for semiconductor sample.

3.19 THOMSON COEFFICIENT AND THERMOELECTRIC POWER

It has been seen that even in the absence of current, there must be an electric field if a temperature gradient is present in a conductor. This indicates the elementary concept of thermoelectric effect in conductors. Phenomenologically one may define the Thomson coefficient as the coefficient of proportionality relating the electric field and the temperature gradient as follows:

$$E_x = - T_h \, (\delta T/\delta x) \quad . . . . . \quad (3.19)$$

Practically, this effect arises as a result of increased energy of electrons at the hot end of the material causing a diffusion of electrons towards the cold end; the charge imbalance due to diffusion sets up an electric field (Seebeck back e.m.f) in the material and this field strongly opposes further flow of charge in this direction. A quantity commonly used to describe the effect is thermoelectric power Q_{ab}. This refers to two materials denoted by 'a' and 'b'. If we have a circuit containing two junctions at A and B as shown in figure 3.4, at temperature T_2 and T_1 , the material

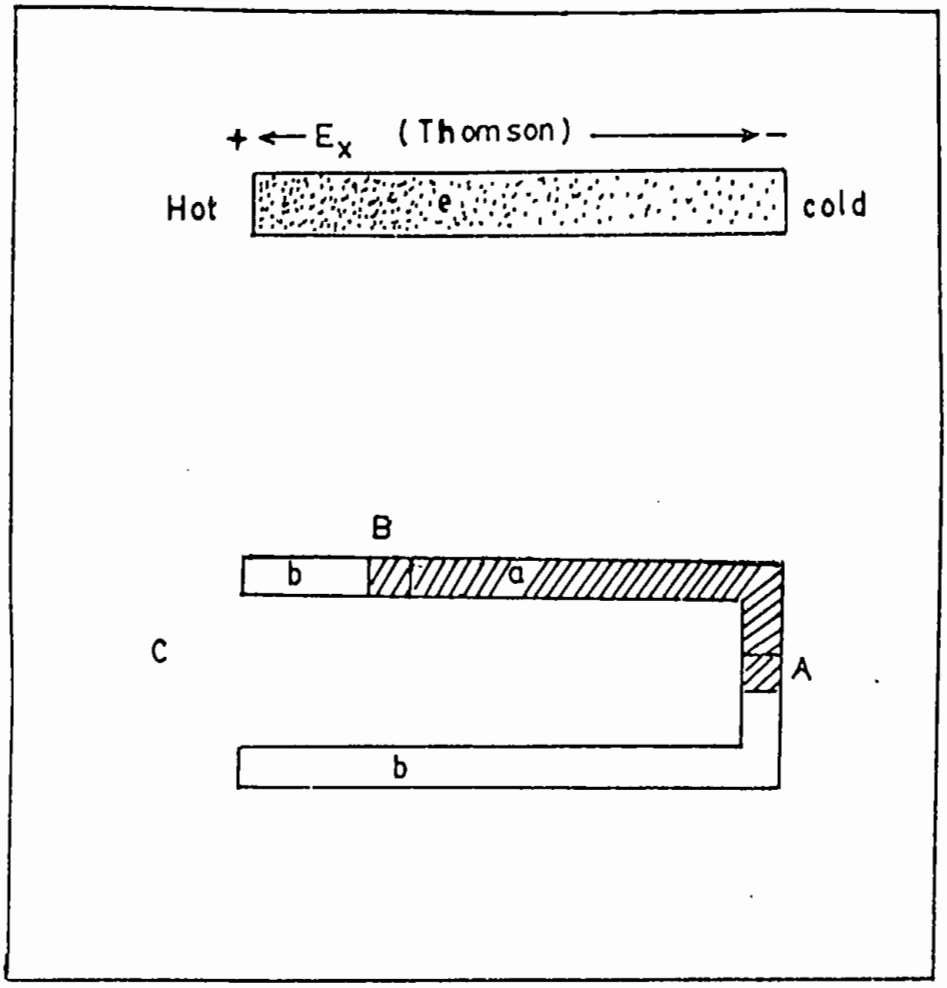

Figure 3.4: Origin of thermopower in semiconductor. A and B are two junctions in two types of materials a and b.

is being open at point C which is assumed to be at temperature T_0, then the open circuit voltage v_0 at C is given by

$$V_o = \int_{T_1}^{T_2} Q_{ab}(T)\, dT$$

If $T_2 = T_1 + \Delta T$, when ΔT is small, we have

$$V_0 = Q_{ab}\ \Delta T$$

$$or \quad Q_{ab} = \frac{V_o}{\Delta T} \quad . \quad . \quad . \quad . \quad . \quad . \quad . \quad . \quad . \quad (3.20)$$

Where Q_{ab} is the thermoelectric power of the material "a" with respect to material 'b' and indicates specific thermoelectric power.

3.19 (i) Absolute thermoelectric power

If T_h (a), T_h (b) are the thomson coefficients for the two materials then from thermodynamical argument[11] we have

$$T_h(a) - T_h(b) = T\frac{dQ_{ab}}{dT} \quad . \quad . \quad . \quad . \quad . \quad . \quad . \quad . \quad (3.21)$$

If we choose the material b as one for which T_h (b) = 0 (usually lead,Pb) the thermoelectric power relative to this material we write $Q_{ab} = Q_a$,then Q_a is sometimes called the absolute thermoelectric power. In this case we have

$$T_h\ (a) = T\frac{dQ_a}{dT} \quad . \quad . \quad . \quad . \quad . \quad . \quad . \quad . \quad . \quad (3.22)$$

3.20 THE POSITION OF FERMI LEVEL

For a non degenerate n-type crystalline semiconductor with spherical constant energy surface under thermal equilibrium the thermoelectric power is given by [18]

$$Q = -\frac{K_B}{e}\left(\frac{E_c - E_F}{k_B T} + A\right) \quad \ldots\ldots\ldots \quad (3.23)$$

Here A is a constant that depends on the nature of the scattering process. When the energy is measured with reference to the bottom of the conduction band the equation (3.23) reduces to

$$Q = -\frac{k_B}{e}\left(A + \frac{E_F}{K_B T}\right) \quad \ldots\ldots\ldots \quad (3.24)$$

Where E_f is the position of the Fermi level in the band gap. Harry et. al.[19] have pointed out that A = 5/2 -r where r is the scattering index.

According to Mott and Davis[18], for limited temperature range, the Fermi energy is

$$E_c - E_f = E_0 - \gamma T - \quad \ldots\ldots\ldots\ldots \quad (3.25)$$

Where E_0 is the low temperature limit of $(E_c - E_f)$ and corresponds to the activation energy equivalent to the band gap, and γ is the temperature coefficient of activation energy. Substituting Equation 3.25 into 3.23

$$Q = -\frac{E_o}{eT} + \left(\frac{\gamma}{e} - \frac{AK_B}{e}\right) \quad \ldots\ldots\ldots \quad 3.26$$

Now, the Peltier Coefficient, $\pi = QT$. can be expressed as

$$\pi = -\frac{E_o}{e} + \left(\frac{\gamma}{e} - \frac{AK_B}{e}\right)T \quad \ldots\ldots\ldots \quad (3.27)$$

From equation (3.27) the plot of π versus T yields a straight line From its slope γ is obtained. Using the value of γ in equation (3.27), the value of E_0 can be found out. From the knowledge of γ and E_0, the value of Fermi energy, $(E_c - E_F)$ can be obtained from equation (3.25).

3.21 EFFECTIVE MASS OF ELECTRONS

In extrinsic polycrystalline semiconductors the electrical conductivity is mainly controlled by impurity level. In that case, the carrier concentration n is a function of temperature which is given by[20].

$$n = (n_0 N_d)^{1/2} \exp(-E_d/2K_BT) \quad \ldots\ldots\ldots \quad 3.28$$

Where E_d is the donor ionization energy, N_d is the donor density, and $n_0 = 2(2\pi m_e^* K_B T/h^2)^{3/2}$

The plot of $\ln(nT^{-3/4})$ versus $1/T$ gives E_d. Using the value of E_d and considering hydrogenic model for the impurity, the effective electron mass m_e^* can be obtained from the relation

$$E_d = e^4 m_s^* / (2\epsilon^2 \hbar^2) \quad \ldots\ldots\ldots\ldots\ldots\ldots \quad (3.29)$$

Where ϵ is the dielectric constant.

3.22 SCATTERING PROCESSES

When the electrons move in a real crystal, they suffer numerous collisions among themselves as well as with the lattice phonons, impurities and imperfections resulting in a phenomenon known as scattering. The effect of any particular interaction i may be evaluated by calculating relaxation time τ_i associated with the process. The overall free time τ may then be expressed as

$$\frac{1}{\tau} = \sum_i \frac{1}{\tau_i} \quad \ldots\ldots\ldots\ldots \quad (3.30)$$

It is clear from this that the Scattering process which leads to the shortest free time τ_i is the dominant one. Once the free time τ is Known, the mobility may be easily determined. Process responsible for carrier scattering which in turn affect the mobility are described below briefly :

3.22 (i) Lattice Scattering

The possibility of lattice scattering may either be by electronic potential resulting from optical polarization of the lattice or by acoustic lattice vibration that can create lattice deformation potential via Lattice dialation or via piezoelectric polarization field. A number of theoretical physicists dealt with

optical scattering. Howarth and Sondheimer[21] have given a very useful expression of the mobility for non-degenerate semiconductors.

$$\mu_o = [\hbar^2/e(2K_B)^{\frac{1}{2}}]\,\Theta_D^{-\frac{1}{2}} m_e^{*-\frac{1}{2}} \left[\frac{\epsilon\epsilon_\infty}{(\epsilon-\epsilon_\infty)}\right]\left[\exp\left(\frac{\Theta_D}{T}\right)-1\right] \text{ at } T<<\Theta_D. \quad \ldots\ldots \quad (3.31)$$

Where Θ_D is the Debye temperature, ϵ is the dielectric constant and ϵ_∞ is the high frequency (optical) dielectric constant. For degenerate semiconductor, similar formula may also be found.[22] Bardeen and Shockley calculated the mobility and showed that scattering due to lattice dialation caused by the acoustic lattice vibration, is

$$\mu_a = (8\pi)^{1/2}\,\hbar^4\, C_{ii}/[3E_{in}\, m_e^{*\,5/2}(k_BT)^{3/2}] \quad \ldots\ldots \quad (3.32)$$

Where, C_{ii} is the average longitudinal elastic constants and E_{in} is the shift of the conduction band edge per unit dialation in eV.

Piezoelectric scattering is important in ZnO films because it has been proved that ZnO is a piezoelectric crystal. This type of scattering mechanism arises from the electrostatic potential induced by the polarization accompanying the acoustic phonons due to piezoelectric effect. The exact calculation of the transport properties taking into account the anisotropy of the piezoelectric, elastic constants and dielectric constants is very complicated. Hutson[23] and Zook[24] have taken into account the anisotropy of the piezoelectric effect and assumed dielectric and elastic isotropy which is a sufficiently accurate approximation for the application

to II-VI compounds. Because the scattering can be considered elastic, a relaxation time can be defined and it is proportional to the square root of the carrier energy. The transport coefficients in the relaxation time approximation is given by Blatt[25] as

$$\mu = \left(\frac{16}{3}\sqrt{2\pi}\right)\left[\frac{\hbar^2}{q\left(m_e^{*\frac{3}{2}}\right)}(k_B T)^{\frac{1}{2}}\right]\left[\frac{\sum_{modes}\langle K^2\rangle}{k_s \epsilon_0}\right]^{-1} \quad . \quad . \quad . \quad (3.33)$$

Where $\langle K^2\rangle$ is a suitable average of the piezoelectric electromechanical coupling constant and ϵ_0 is the permitivity of free space.

3.22 (ii) Impurity scattering

Impurity scattering is important in impure and non-stoichiometric semiconductors in which ionized and neutral atoms are present. Both of them may scatter under specific conditions.

3.22 (iia) Ionized impurity scattering

Ionized impurity scattering predominates, when the concentration of ionized donors is high. The charge carriers suffer Rutherford scattering due to the presence of ions. When it is assumed that the ions are distributed throughout the lattice in a regular fashion, the average distance between the ions a_i is given by $a_i^3 = 1/N_i$, where N_i is the number of ions per unit volume. Thus if V is the velocity of an electron, the mean free time between collisions is $\tau_c = a_i/v$. The relaxation time is in general given by

$$\tau = \tau_c / (1 - \langle \cos\beta \rangle) \quad \ldots\ldots\ldots\ldots\ldots \quad (3.34)$$

Where cosß is the average of the cosine of the scattering angle. Making use of the Rutherford scattering formula, Conwell and Weisskopf[26] have calculated an approximate expression for τ with the result that

$$\mu = \frac{e\tau}{m^*} = \frac{\epsilon^2 m^* v^3}{2\pi N_I e^3}\left[\log\left(1 + \frac{\epsilon^2 m^* v^4}{(4e^4)N_I^{\frac{3}{2}}}\right)\right]^{-1} \quad \ldots \quad (3.35)$$

It is observed that this type of scattering leads to a mobility which varies approximately as $T^{3/2}$, in contrast with the $T^{-3/2}$ law for lattice scattering.

The Hall coefficient and Hall mobility associated with ionic scattering are found to be

$$R_H = \pm\ 1.93/nec, \quad \mu_H = 1.93\mu \quad \ldots\ldots\ldots\ldots \quad (3.36)$$

3.22 (iib) Neutral impurity scattering

In this type of scattering, the scattering of charge carriers by neutral impurities is quite similar to the scattering of electron by hydrogen atoms. By using a modified theory, Erginsoy[27] calculated the mobility associated with this type of scattering alone. He found

$$\frac{e\tau}{m^*} = \mu = \frac{m^* e^3}{20 N \epsilon \hbar^3} \quad \ldots\ldots\ldots \quad (3.37)$$

Where N is the density of neutral impurity and ϵ is the dielectric

constant. The relaxation time is independent of the velocity in this case, so that the Hall coefficient is the same as that for metals, viz;,

$$R_H = \pm \frac{1}{nec} \quad \ldots\ldots\ldots \quad (3.38)$$

3.22 (iii) Scattering at Dislocation

Distortions of the crystalline lattice cause scattering of electrons and holes. This form of scattering has been discussed theoretically by Dexter and Seitz[28] and shown to make a negligible contribution unless the dislocation density is in excess of 10^{18} cm^{-2}. When the density is of the order of 10^{11} cm^{-2} scattering should be comparable to lattice scattering at room temperature. Dislocation may be regarded as charged cylinder in the path of an electron and causes scattering. The relaxation time τ_d for the process is given by

$$\tau_d = 3/(8RNv) \quad \ldots\ldots\ldots\ldots\ldots\ldots \quad (3.39)$$

Where N is dislocation density and R is the radius of the dislocation line and V is the velocity of the electron. At room temperature this type of scattering is not important but at low temperature it may be important. For spray-deposited samples dislocations are less important.

3.22(iv) Scattering by Grain Boundaries

Grain boundary scattering is very important for polycrystalline samples either in bulk or thin films form. From the theories of grain[29-31] boundary potential it is known that the boundary regions are characterized by a potential barrier of height E_μ and density of traps Q_t. These two quantities are related by

$$E_\mu = e^2\theta_t^2/(8\epsilon_0\epsilon n) \quad \ldots\ldots\ldots\ldots\ldots\ldots \quad (3.40)$$

where n is the carrier concentration. The barrier height is also dependent on the grain size. However, according to the nature of this barrier height the carrier transport that depends upon the scattering process in the sample may be influenced by all or any of the following mechanisms.

3.22(iva) thermionic emission of carriers over the barrier
(ivb) quantum mechanical tunnelling
(ivc) barrier reflection mechanism

In degenerate semiconductors a more complex situation may arise due to all these possibilities. Jones et. al.[32] have pointed out that when $E_\mu << E_F$ quantum mechanical barrier reflection model would be applicable for a strongly degenerate sample with the Fermi level E_F at least $2k_BT$ above the conduction band edge. In this case, the relaxation time τ for the material with grain size L can be given by

$$\tau_B = 2L\hbar^2E/(m_e^* a^2 E_\mu^2 v) \quad \ldots\ldots\ldots \quad (3.41)$$

Since $E = \frac{1}{2}(m_e^* v^2)$ is the energy of the electron having velocity v and $a = Q_t/n$ is the width of the square barrier of height E_μ, thus equation (3.41) takes the form $\tau \alpha E^{-r}$ and yields the value of $r = -\frac{1}{2}$ for barrier scattering. It is to be noted that for pure lattice scattering $r = \frac{1}{2}$. For strongly degenerate case the temperature broadening of the Fermi surface will create a little change in the velocity distribution of the electrons and as a result of which barrier reflection scattering mechanism becomes almost temperature independent. On the other hand, Petritz[33] pointed out that when the carriers predominate due to thermionic emission, the associated mobility becomes strongly temperature dependent, whereas in the case of tunnelling, carrier transport is temperature independent.[34] Recently, the nature of grain boundary scattering in polycrystalline semiconductors has become an interesting subject of research to many workers.

3.22(v) Carrier-Carrier scattering

In highly degenerate electron gas model, the scattering between carriers is important but it offers little contribution so they are generally neglected. In some cases, however, this type of scattering can play an important role in determining the band shape of the specimen. The effect of inter-electron collision on mobility has been discussed by Fröhlich et. al.[35]. When the effective mass of holes are larger than those of electrons, the electron-hole

collision may reduce the electron mobility.

3.22(vi) Inter-Valley Scattering

Inter-valley scattering[36] is accounted for semiconductors which contain multivalley conduction band. In such scattering process energetic phonons are generally involved and they become highly inelastic and strongly temperature dependent. This is however, noticed at high temperature only because at low temperature energetic phonons are not available.

3.23 EFFECT OF INHOMOGENEITY ON MOBILITY

Naturally thin film samples sometimes become inhomogeneous in their structure. The inhomogeneity creates a large effect on the carrier mobility. Such inhomogeneity may arise from (i) anisotropic impurity separation, (ii) impurity complex formation (iii) formation of cluster in solid solution samples or (iv) compositions during growth. The carriers suffer hard-sphere like collision by the space charge region which surround the inhomogeneity. The mobility is therefore given by[37]

$$\mu = (e/NS)(2m_e^* K_B T)^{-\frac{1}{2}} \quad . \quad . \quad . \quad . \quad . \quad . \quad . \quad . \quad . \quad . \quad . \quad . \quad . \quad (3.42)$$

where N is the density of space charge region with effective scattering cross-section of S. This type of scattering is prominent in high resistive materials.

3.24 OPTICAL PROCESSES

The optical behaviors of a semiconductor are investigated in term of the three phenomena namely transmission, reflection and absorption. So it is necessary to study the ultraviolet (uv), visible and infrared (IR) characteristics of the material. ZnO thin films are transparent to visible radiation and therefore its UV and IR characteristics are important.

3.24 (i) Inter Band Optical Transition and the Band Gap

When photon energy is incident on a material, the valence electron absorbs energy from incident photon and is excited. When incident energy exceeds threshold value, the electron may make a transition to the conduction band under suitable conditions. If this transition occurs between the bands at the same value of the wave vector K, the transition is considered as vertical and is allowed. Non vertical transitions are normally forbidden. For the simple case shown in figure 3.5(a) the minimum absorption of radiation occurs at $h\nu = E_g$ and it would intensify for all $h\nu > E_g$ where E_g is called the absorption edge or optical band gap. During the process of this type of transitions no phonon is involved for the conservation of energy except the creation of an electron and a hole and is termed as direct absorption process. Bardeen, Blatt and Hall[38] have given an expression for the absorption process as

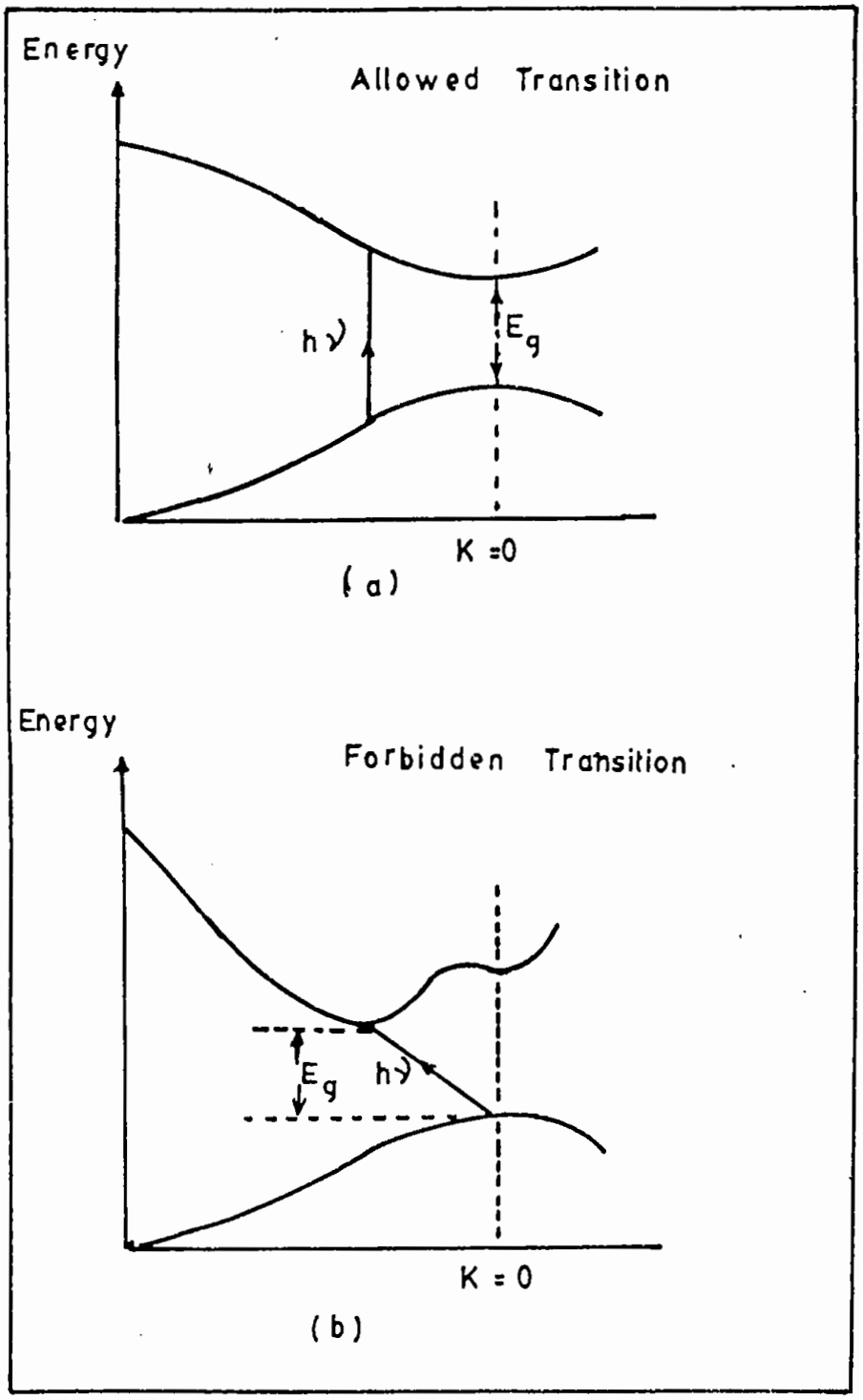

Figure 3.5: Optical transition in semiconductor, (a) Allowed transition (b) Forbidden transition.

$$\alpha_d = B(h\nu - E_g)^s / h\nu \quad \ldots\ldots\ldots \quad (3.43)$$

where S = ½ for allowed transition and 3/2 for the forbidden transition, B is a constant and α_d is the absorption coefficient.

The process of indirect transition has also been treated by the same authors[38]. In this transition phonons generation are always involved. The absorption coefficient is given by

$$\alpha_i = A(h\nu - E_g \pm E_p)^s / h\nu \quad \ldots\ldots\ldots \quad (3.44)$$

where S = 2 for allowed transition and 3 for forbidden one. The probability of allowed transition is less in indirect process. Here E_p is the energy of the phonon absorbed (+)/or emitted (-).

It is clear from all these expression that a graph of $(\alpha h\nu)^s$ vs. $h\nu$ would provide the value of E_g when carefully drawn for a particular transition process.

3.24(ii) Dependence of optical Absorption edge on the carrier concentration

A material with a fixed carrier concentration has an unique optical absorption edge which is often found to depend on the carrier concentration for degenerate semiconductor. The effect has been explained independently by Moss[39] and Burstein[40] when they observed in InSb sample a shift of the absorption edge towards higher energy as a function of its carrier concentration.

The magnitude of this shift is determined by two competing mechanisms. One of them is a band gap narrowing which is a consequence[41] of many body interactions on the conduction and valence bands. This shrinkage is counteracted by the Moss-Bursteen effect[40] which gives a band gap widening as a result of the blocking of the bottom (lowest states) of the conduction band. Either of the two mechanisms may predominate when the carrier density exceeds the Mott-critical density.

3.24(iii) Theory of the shift (Moss-Burstein)

The energy E by which an electron can make a transition from some place of the valence band to the conduction band at the same wave vector K is given by

$$E = h^2k^2/(2m_e^*) + E_{go} + h^2k^2/(2m_h^*) \quad \ldots\ldots\ldots \quad (3.45)$$

where E_{go} is the intrinsic band gap.
As the density of state in k-space is simply

$$dN/dk = 2(4\pi k^2) \quad \ldots\ldots\ldots\ldots\ldots\ldots \quad (3.46)$$

We obtain directly

$$dN(E)/dE = 8\pi h^{-3}\left[2m_r^{*3}(E-E_{go})\right] \quad (3.47)$$

Here N(E) is the density of states function and m_r^* is the reduced effective mass given by
integrating (3.47) within the limit 0 to ΔE_g (figure 3.6)

$$\frac{1}{m_r^*} = \frac{1}{m_e^*} + \frac{1}{m_h^*} \qquad (3.48)$$

we have

$$N = \int_0^{\Delta E_g} dN(E) = [8\pi/(3h^3)]\,(2m_r^*\Delta E_g)^{3/2}$$

Thus the Moss-Burstein shift is given by

$$\Delta E_g^{MB} = (\hbar^2/2m_r^*)\,(3\pi^2 N)^{2/3} \qquad (3.49)$$

This expression is exactly similar to equation (3.5) which gives the position of Fermi level in degenerate semiconductor.

This method of obtaining ΔE_g is very simple because the self energies due to electron-electron (e-e) and electron-impurity (e-i) scattering have not been encountered here. Considering the effect of these factors, the expression for the shifted band gap can be represented as[42]

$$\Delta E_g = \Delta E_g^{MB} + \hbar\Sigma_c(K_F, \omega) - \hbar\Sigma_v(K_F, \omega) \qquad (3.50)$$

where $\hbar\Sigma_c$ and $\hbar\Sigma_v$ represent the self energies due to (e-e) and (e-i) scattering and can be derived by quantum mechanical methods. In deriving the equation (3.50) it has been assumed that the conduction band is parabolic. But for a non-parabolic band with linear dependence of E on k one may obtain[43] $\Delta E_g \propto N^{1/3}$ in place of $N^{2/3}$ in equation (3.49)

3.25 REFRACTIVE INDEX OF TRANSPARENT FILMS

Figure 3.7(a) represents a thin film with a complex refractive index $n = n_f - ik$, bounded by transparent media with refractive indices n_0 and n_1. Assuming a unit amplitude for the incident light and in the case of normal incidence the amplitude of the transmitted wave is given by[44]

$$A = t_1 t_2 \exp(-2\pi i \eta t/\lambda)/[1 + r_1 r_2 \exp(-4\pi i \eta t/\lambda)] \qquad (3.51)$$

in which t_1, t_2, r_1 and r_2 are the transmission and reflection co-efficients at the front and rear faces. The transmission of the layer is given by

$$T = \frac{n_1}{n_0} [A]^2 \qquad (3.52)$$

For transparent film (weak absorption) with

$K^2 << (n_f - n_0)^2$ and $K^2 << (n_f - n_1)^2$

where K is the extinction coefficient, the expression for T is given by

$$T = (16 n_0 n_1 n_f^2 k)/[C_1^2 + C_2^2 k^2 + 2 c_1 c_2 K \cos(4\pi n_f t/\lambda)] \quad . . . . \quad (3.53)$$

Where $C_1 = (n_f + n_0)(n_1 + n_f)$

$C_2 = (n_f - n_0)(n_1 - n_f)$ and

$$K = \exp(-4\pi K t/\lambda) = \exp(-\alpha t) \quad . . . . . \quad (3.54)$$

α is the absorption co-efficient of the thin film.

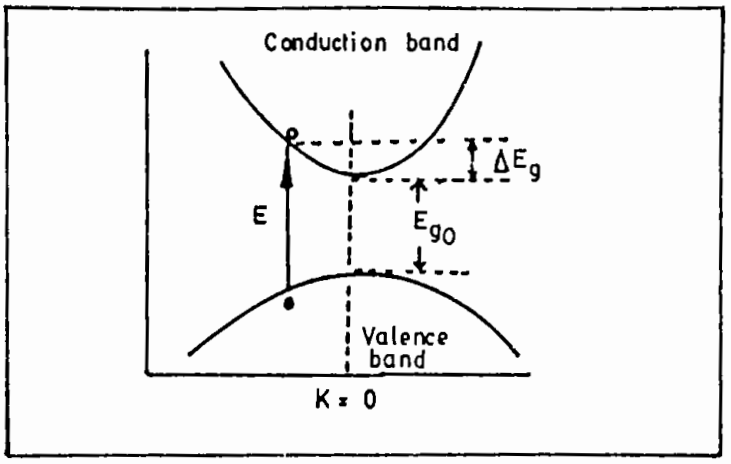

Figure 3.6: Origin of Burstein-Moss shift

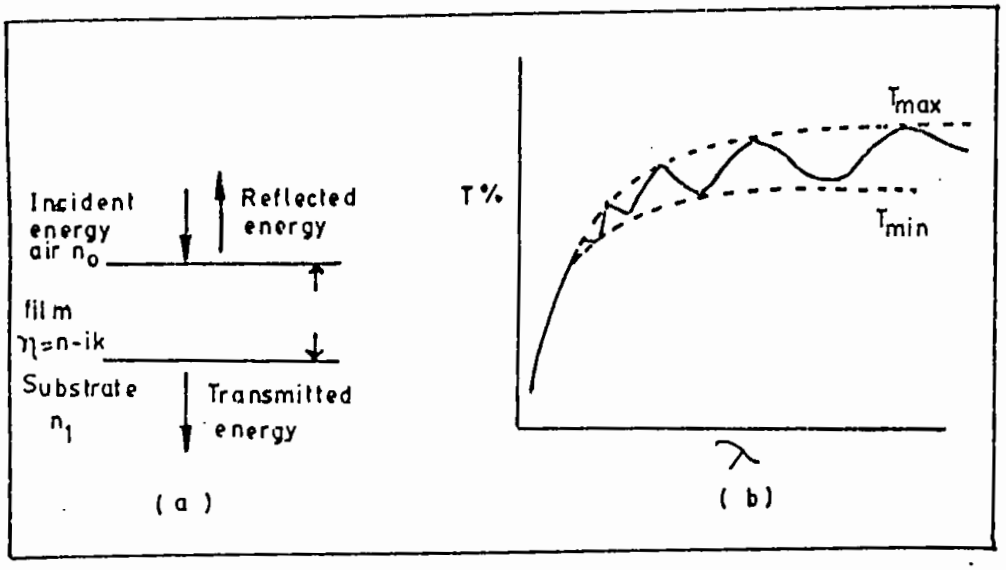

Figure 3.7: Typical transmission spectrum for a thin film of uniform thickness t.

Generally outside the region of fundamental absorption ($h\nu > E_g$) or of the free carrier absorption (at higher wavelengths), the dispersion of n_f and K is not very large. The maxima and minima of T in equation (3.53) occur for,

$$4\pi n_f t/\lambda = m\pi \quad \ldots\ldots\ldots\ldots\ldots\ldots \quad (3.55)$$

where m is the order number. Using equation (3.55) in (3.53) for transparent film on a non absorbing substrate we obtain[45]

$$n_f = [N + (N^2 - n_0^2 n_1^2)^{\frac{1}{2}}]^{\frac{1}{2}} \quad \ldots\ldots\ldots\ldots \quad (3.56)$$

where $N = (n_0^2 + n_1^2)/2 + 2n_0 n_1 (T_{max} - T_{min})/T_{max}\, T_{min}$

T_{max} and T_{min} are shown in figure 3.7(b).

3.26 I-R CHARACTERISTICS

In transmission region the major portion of IR losses are due to the free carrier absorption within the film. For the derivation of α (absorption coefficient) in this region, the classical dispersion relation can be adopted for the complex dielectric function

$\epsilon = \epsilon' - i\epsilon''$ for a free carrier gas, where

$$\epsilon' = n_f - k^2 = \epsilon_L [1 - \omega_p^2/(\omega^2 + \gamma^2)] \quad \ldots\ldots\ldots\ldots \quad (3.57)$$

$$\text{and } \epsilon'' = 2n_f k = (\gamma/\omega)\, \omega_p^2 \epsilon_L/(\omega_p^2 + \gamma^2) \quad \ldots\ldots\ldots\ldots \quad (3.58)$$

ϵ_L is the dielectric constant of the material in the absence of free electrons,

$\gamma = e/(m_e^* \mu) = 1/\tau$, τ is the relaxation time. The screened Plasma frequency ω_p is given by

$$\omega_p = [4\pi ne^2/\epsilon_0 \epsilon_L m_e^*]^{\frac{1}{2}} \quad \ldots\ldots\ldots\ldots\ldots\ldots \quad (3.59)$$

or, the plasma edge

$$\lambda_p = C_0 \, [(\epsilon \epsilon_L \, m_e^* \pi/ne^2]^{\frac{1}{2}} \text{ in C.G.S} \quad \ldots\ldots\ldots \quad (3.60)$$

Since the absorption coefficient

$$\alpha = 4\pi k/\lambda \quad \ldots\ldots\ldots\ldots\ldots\ldots\ldots\ldots \quad (3.61)$$

combining equations (3.57) to (3.58) we obtain

$$\alpha = (\lambda^2 e^3 n)/(4\pi \epsilon_0 C_0^3 n_f m_e^* \mu) \quad \ldots\ldots\ldots\ldots\ldots\ldots \quad (3.62)$$

where, C_0 is the velocity of light in free space, and other symbols have their usual meanings.

3.26(i) IR Reflectivity

One of the important optical characteristics of thin films is their IR reflectivity. This phenomenon plays a dominant role for ZnO thin films. In classical dispersion relation[45] using $\rho = 1/ne\mu$, the expression for the reflectivity in the free carrier absorption region can be found as

$$1 - R = 4(\pi \epsilon_0 C_0 \rho/\lambda)^{\frac{1}{2}} \quad \ldots\ldots\ldots\ldots\ldots\ldots \quad (3.63)$$

The IR reflectivity for very thin film can be calculated briefly using the impedance change description. In this case the impedance at the film surface is counted as a sheet resistance of the film $R_{\square}$ shunted by the background impedance. For simplicity if it is assumed that the value of the latter is to be equal as in the foreground, i.e; the free space impedance

$1/\epsilon_0 C_0 = 376\Omega$, we obtain

$$R = (1 + 2\epsilon_0 C_0 R_{\square})^{-2} \quad \ldots\ldots\ldots\ldots\ldots\ldots \quad (3.64)$$

in which some substitution have been made to obtain the IR reflection loss at high reflection level and in this case the approximate relation

$$1-R = (4\epsilon_0 C_0/e)/(1/nt\mu) \quad \ldots\ldots\ldots\ldots \quad (3.65)$$

A comparison of equation (3.62) with (3.65) reveals that both the losses can not be minimized simultaneously.

REFERENCES

1. J. Aranovich, A. ortiz and R.H.Bube. J.Vac. Sci. Technol. 16(4) (1979) 994.
2. M.S. Tomar and F.J. Garcia, Prog. Cryst. growth charact. 4, (1981) 221.
3. W. Kern and V.S. Ban. "Thin film process", (Ed. J.L. Vossen and W. Kern, Academic Press, New York 1978).
4. F.C. Eversteijn, Philips Res. Rept. 29, (1974)45.
5. C.A. Chang. J. Electrochem. Soc. 123. (1976)1245.
6. Leon I. Maisseel and Reinhard Ghang. "Handbook of Thin Film Technology", McGraw Hill Book Co. (1970).
7. D.W. Pashley, Proc. Phys. Soc. London, A64, (1951)1113 A210, (1952)355 A65, (1952)33.
8. G.A. Bassett, J.W. Menter and D.W. Pashley, "Structure and Properties of Thin films" (Ed. C.A. Neugebauer, J.B. Newkirk and D.A. vermilyea, John Wiley and Sons Inc., 1959).
9. R. Thun, "Physics of thin film", (Ed. G. Hass, Academic Press Inc., New York, vol-1. 1964) 187.
10. R.B. Belser, J. Appl. Phys. 28: (1957)109.
11. D. Cossement and J.M. Streydio. Journal of crystal growth 72(1985) 57.
12. Chris Eberspacher, Alan L. Fahrenbruch and Richard H. Bube. Thin Solid Films 136(1986) 1.
13. J. Mek. Nobbs and F.C. Gillespie Phys-Chem. Solids. Pergamon Press vol. 31. (1970) 2353.

14. B.E. Sernelius, K-F. Berggren, z-C. Jin, I. Hamberg and C.G. Grangvist. Phys. Rev. B. vol. 37, No.-17 (1988) 10244.

15. N.B. Hannay, "Semiconductors" (Reinhald Publishing Corporation, New York 1959).

16. A.R. Smith, "Semiconductors" (Cambridge University Press, 1968).

17. A.R. Smith, The physical principles of Thermodynanics (Chapman and Hall, 1952) 84.

18. N.F. Mott and E.A. Davis, "Electronic processes in non crystalline materials", 2nd Edn (Clarendon Press, Oxford, 1979).

19. H.Harry, B. Kwok and R.H. Bube. J. Appl. Phys. 44 (1973)138.

20. C. Kittel, Introduction to solid state Physics, 4th Ed. (Wilely, New York, 1971).

21. D.J. Howarth and E.H. Sondheimer, proc. Roy. Soc. A219, (1953) 53.

22. E.H. Putley, "The Hall effect and semiconductor physics" (Dover, New York, 1968).

23. Hutson A.R. J. Appl. Phys. 32. (1961) 2287.

24. Zook. D. Phys. Rev. 136(1964)869.

25. Blalt. F. Solid State Phys. 4(1954)200.

26. E.M. Conwell and V.F. Weisskopf, Phys. Rev. 77, (1950) 388.

27. C.Erginsoy, Phys. Rev 79, (1950) 1013.

28. D.L. Dexter and F. Seitz, Phys. Rev. 86. (1952)964.

29. J.Y.W: Seto, J. Appl. Phys. 46, (1975) 5247.

30. G. Baccarani, B. Ricco and G. spadini, J. Appl. Phys. 49, (1978) 5565.

31. A.K. Ghosh, C. Fishman and T. Feng, J. Appl. Phys. 51 (1980) 446.

32. R.E. Jones Jr. and S.P. Wesolowski, J. Appl Phys. 56. (1984) 1701.

33. R.L. Petritz, Phys. Rev. 104, (1956) 1508.

34. M.V. Garcia-Cuenca, J.L. Morenza and J. Esteve, J. Appll. Phys. 56, (1984) 1738.

35. H. Frohlich, B.V. Paranjape, C.G. Kuper and S. Nakajima, Proc. Phys. Soc. B 69, (1956) 842.

36. C. Herring, Bell Syst. Tech. J. 34, (1955) 237.

37. L.R. Weisberg, J. Appl. Phys. 33. (1962) 1817.

38. J. Bardeen, F.J. Blatt and L.H. Hall, "Photoconductivity conference", (Ed. R. Breckenridge, B. Russel and E. Hahn, New York, John wiley, 1956).

39. T.S. Moss, Proc. Phys. Soc., London B67, (1954) 775.

40. E. Burstein Phys. Rev. 93, (1954) 632.

41. K.F. Berggren and B.E. Sernelius, Phys. Rev. B24, (1981) 1971.

42. I. Hamberg, C.G. Ganquist, K.F Berggren, B.E. Sernelius and L. Engstron, Phys. Rev. B30, (1984) 3240.

43. T.S. Moss, "Optical propertis of semiconductors", (Butterworths Publications Ltd. 1959).

44. J.C. Manifacier, J. Gasiot and J.P. Fillard, J. Phys. E. 9, (1967) 1002.

45. G. Frank, E.Kauer and H. Kostlin, Thin Solid Films, 77, (1981) 107.

CHAPTER 4

EXPERIMENTAL DETAILS

This chapter mainly includes the design and construction of the film deposition equipments of pyrosol process and illustrates the preparation of experimental samples of ZnO on glass substrate. A detail discussion about every experimental setup with appropriate method adopted throughout the course of the work for the analysis of the structural, electrical and optical properties of the deposited films have also been presented here.

4.1 INTRODUCTION

There are a number of methods available up to date for the thin film deposition. Among them spray pyrolysis is well known as one of the simplest and least expensive one. By this method a large area of thin film can be prepared in relatively short time. The variety of properties of the deposited material can be varied easily with precise control over all the associated parameters. Nevertheless, there it has been faced a number of difficulties in controlling the process variables because of its extreme simplicity. The qualities of the deposited films are relatively inferior to those of films obtained in other complex methods in which very sophisticated instruments are used. Experimental arrangements have been put forward by many workers[1-8] to promote ease of preparation and to overcome difficulties which were often

encountered at the time of film deposition. But still more work is necessary to improve the process of deposition and to reduce the cost of production which is a necessary precondition in producing semiconductor thin films for the fabrication of solar cells and other device applications.

Pyrosol process[7,8] is a chemical spray deposition process which contains two sections. In one section of the apparatus an aerosol is produced from the working liquid and simultaneously carried to the other section where pyrolysis of the aerosol takes place. In the following sections we have given a description about a modified apparatus for this process. With the helf of this apparatus ZnO as well as several other semiconducting thin films of binary and ternary compounds such as SnO_2, In_2O_3 CdS ZnTe $CuInSe_2$ etc. can also be easily prepared only by adjusting some of the parameters of the process. The common defects that are usually noticed in the films prepared by this process, are the surface roughness and thickness inhomogeneties. Therefore the role of the deposition apparatus is very important in preparing good quality films free from these defects.

4.2 TROUBLE WITH THE CONVENTIONAL PNEUMATIC SPRAY SYSTEM

The spray particles that are outflow from the exit nozzle during the time of spraying become of different sizes. They do not depend on the fineness of the spray nozzle. But it is an inherent properties of a pneumatic spray gun. The size of the droplets also

depends on the cone angle covered by the spray particles [9,10]. Aerosol droplets behave differently depending on their size[11]. This creates problem in the film deposition process. The chemical reaction that takes place in the vapour phase is a fundamental mechanism of the process. Droplet of different sizes take different time to reach at the same site of the substrate. Beside this, at a constant substance temperature they take different fraction of time to complete their vaporization and reaction. As a result of which unwanted interaction between the reacted and unreacted species may take place at the substrate surface. This undesired factors create problem to obtain a film of uniform in structure and homogeneous in composition.

To obtain good results, one should has to be assured first about the fineness and uniformity of the spray particles. In order to achieve this, it should be given equal importance in making a fine spray nozzle and at the same time arrangement should be kept to filter the spray particles so that a very fine and uniform droplets may be supplied from the out put. Keeping this points in view we shall describe here about a new apparatus for the spray system.

4.3 DESIGN OF A NEW SPRAY DEPOSITION APPARATUS

The spray deposited apparatus furnishes a number of functions. These are the production of aerosol and their filtration for uniformity, transport of them to the reactor section and formation

of films. The different stages of the apparatus required for these purposes are described below.

4.4 THE SPRAY NOZZLE AND ITS MODIFICATION

In the chemical spray method the performance characteristics of the spray nozzle plays a very important role for the thin film deposition. The different performance characteristics of the spray nozzle are

(i) The spray rate that determines the amount of liquid sprayed during a given interval of time under any injection condition.

(ii) The size of the droplets.

(iii) Cone angle of spray that determines the total coverage of the spray i.e. degree of mixing of the spraying liquid with the surrounding atmosphere. Among these spray rate and size of the droplets have significant effect on the property of the deposited film

In a conventional compressed air sprayer, the spray nozzle consists of two capillary glass tube fitted at right angle to each other as shown in figure 4.1(a). When a high speed compressed air is allowed to pass through the upper tube A in a direction tangential to the mouth of the lower tube B, some air in the upper part of it (tube B) is pushed forward by the air current .As a result of which a partial vacuum (or air gap) is created at the upper end of the tube B whose lower end is kept immersed in the

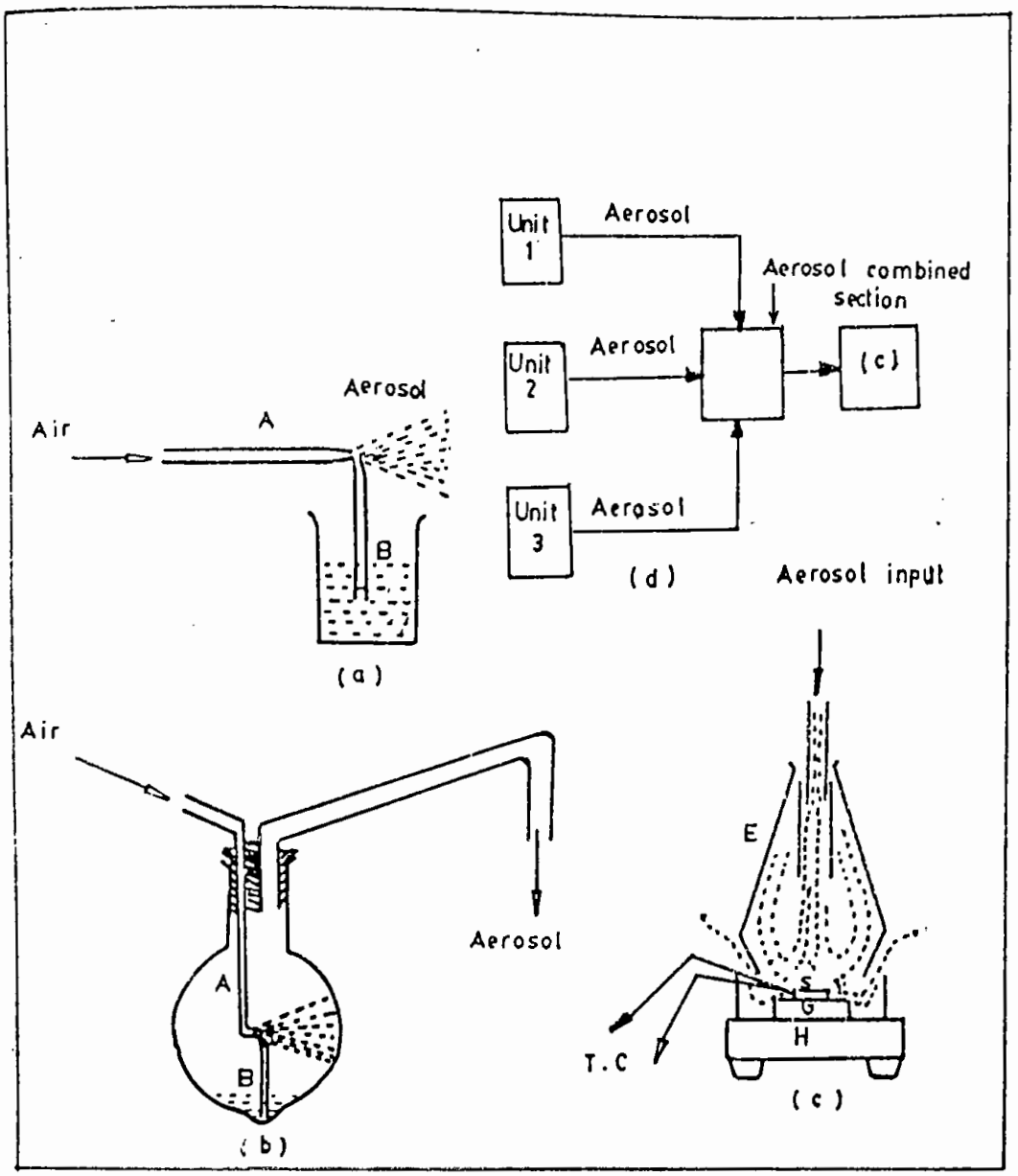

Figure4.1:(a) Conventional pneumatic spray gun
(b) and(c) are respectively the spray system and the pyrolysis reactor designed in our laboratory.
(d) The outputs of three sprayer of fig.(b) are combined.

spray liquid. To fill up this air gap, liquid is ejected up through the tube B and by the action of the compressed air this liquid emerges from the tube B as a fine spray particles (aerosol)

This type of spray guns have been directly used by many of the earlier workers for the deposition of thin films of various materials[1-6]. But the problem of nonuniformity of droplet size remains with this type of spray guns.

Considering this aspect, Islam and Kakim[8] in 1985 have made a simple modification on the conventional spray gun system in our laboratory in a way as shown in figure 4.1 (b). In this setup, larger droplets and heavier precipitates are discouraged to reach the substrate. Here the spray gun has been kept in a large capacity (1500 ml) round bottom glass container F in the bottom of which there is a little protuberance and at the top of it an outlet, a bent pipe C is connected. The protuberance is blown there because a very small amount of fresh liquid (not more than 10 ml) can then be used at each run for a single sprayer without wastage.

When the aerosol is produced in the flask, they mix with the surrounding atmosphere and form a cloud of the spray particles. Then this cloud of spray particles in the confined space of the flask are carried out by the carrier gas through the outlet pipe C and during their way out they are automatically separated into heavier and lighter droplets due to the action of vertical air current and gravitational effects. In this process the larger

droplets would be coalesced in the flask/or in the conduit pipe C and ultimately drop down in the flask to be fed back. On the other hand very light and relatively smaller droplets will be carried by the same incoming carrier gas to the reactor zone. This is how a virtual filtration process acts in the spray system and produces almost uniform and very small droplet size at the outlet of the sprayer. If it is necessary the solution spray rate may be increased by increasing the number of spray nozzles. This may be done in two ways (i) using a number of nozzle in a single container. (ii) using a number of spray nozzles, each of which is fitted in a separate container. the outlet pipe from each of the container are finally combined to a single outlet pipe whose open end is fitted to the reactor inlet. This is shown in fig (4.1d). The system is therefore economic in many respect. The facilities which are associated with this arrangement are

(i) The solution flow rate can be controlled to a better accuracy by suitable design of the spray nozzle and adjusting the air flow rate. In the present work, the solution flow rate was maintained constant to 0.80 ml/min in preparing ZnO thin films. This rate is about (50-100) times less than that used by the earlier workers[1-8].

(ii) Due to this small flow rate, the time of deposition is increased which provides a better thickness control and larger grain size[6] of the film.

(iii) Extra loss of working solution which was apparent in conventional setup[1-6] can be reduced sufficiently by setting the flow rate to its required lower limit.

(iv) Very fine droplets that are supplied to the reactor section may be vaporized easily without any extra pre-heating furnace[6] which saves excess power consumption.

4.5 THE DESIGN OF THE REACTOR

The reactor is an essential part of the spray deposition apparatus. The completion of the chemical reaction occurred here to form solid film. It is a batch type reactor which is shown in the figure 4.1.(c). It consists of the following components :- (i) a stainless steel enclosure E having a pyrex glass jacket inside (ii) a heater H on which a thick graphite block susceptor G is placed. (iii) a chromel-alumel thermocouple T.C used to monitor the substrate temperature. Substrate is placed on the susceptor block and the thermocouple is kept in contact with the substrate. The heater is equipped with an electronic power controller for requirements of different temperature. For the rapid expulsion of the byproduct gases there are openings at the side and at the top of the reactor. The double cone shape of the reactor wall E has dual action. It helps focussing the incoming aerosol towards the substrate and provides a chimney action to the exhaust gas upwards.

This type of reactor system plays an intermediate role between the hot-wall and cold-wall type reactor. Endothermic chemical

reaction occurs for the formation of ZnO and therefore a cold-wall reactor should be adequate. Since the incoming aerosol is cold and if the reactor is cold wall one, it will cause a sudden fall of substrate temperature and give a tremendous thermal shock to the heated substrate. As a result of this the glass substrate may be cracked at once. Furthermore, the reaction process would be distributed due to this rapid fall of substrate temperature and will give an unexpected result. To overcome these difficulties the temperature of the reactor wall should be maintained at a level much higher to the room temperature but lower to that of the optimum temperature for the reaction temperature. This temperature is maintained automatically here by the metallic enclosure E placed over the heater H, and thus it provides a pre-heating action easily to the input aerosol.

4.6 THE HEATER

The heater H is an ordinary round shaped hot plate having a heating coil of 2 KW nichrome wire. It is placed on an insulated horizontal platform. The top of the plate is covered by a piece of asbestos sheet with a small rectangular opening at the centre where a mica sheet is attached. A thick stainless steel or graphite plate G is placed on this mica sheet (figure 4.1.C). It serves as heat susceptor. Substrate that is placed on this susceptor plate G have a uniform temperature throughout the substrate surface. To avoid the chemical corrosion, another mica sheet is placed between the

susceptor block and the substrate. An electronic power supply unit is connected with the heater power line to supply proper heat to the substrate.

4.7 THE FUME CHAMBER

It is a large box provided with a slanting top. The top and the side walls of it is made of glass. There is a chimney at the top of the box. An exhaust fan with regulated power supply unit is fitted at the mouth of the chimney. At the front face of the chamber some air tight doors are provided. The chamber has purging facilities also. The spray system and the reactor are kept inside the fume chamber at the time of film deposition because it establishes safety film deposition atmosphere and checks air current disturbances at the deposition site. These two points are very important for pyrosol process where deposition is carried out in open atmosphere.

4.8 THE CARRIER GAS

The carrier gas is selected according to the criterion of the chemical reaction taking place. In some cases carrier gas takes active part in chemical reaction for the formation of the film, in the other cases it remains inactive with deposition material but serves only to transport the spray particles to the reactor section. For the deposition of an oxide layer air or oxygen may be used so as to supply oxygen needed for the reaction. Other gases

like nitrogen, argon, helium may be used to serve this purpose. In the present work dry compressed air has been used as carrier gas. The pressure of the gas can be varied by adjusting the outlet value of the air compressor and should maintain constant according to the requirement of the spray rate during the deposition run. The standard pressure for the spray system has been found to be 20 psi.

4.9 THE AIR COMPRESSOR

It is a reservoir type electrical air compressor. A rotary pump in its suction mode draws atmospheric air and keeps it reserve in a large capacity air tank. To keep the outlet pressure constant there is a bypass valve through which excess air can pass out. The air is forced to pass through a silica gel column in order to make it dry before passing it into the sprayer. A pressure gauge is fitted at the end of the delivery tube with a control valve. This records the carrier gas pressure for the sprayer.

4.10 SELECTION OF THE SPRAY SOLUTION

4.10 (i) Source compound

There are several numbers of source compounds which are found available. Among then the most suitable one is selected in order to fulfil a number of essential requirements. It should be a stable compound at room temperature, it should not oxidize in air or in the presence of water at room temperature, its decomposition temperature should not be very high (not>500°C), the decomposition

reaction leading to the formation of solid film should be thermodynamically favorable so that the residue of the reactant will not be left behind in the deposition material and the products of the decomposition reaction other than the desired one should be volatile so that they can easily escape from the deposition chamber. On the basis of these criteria, Zinc acted compound $\{Zn(C_2H_3O_2)_2\ 2H_2O\}$ is selected for the preparation of ZnO thin films.

4.10 (ii) Solvent

Different types of solvents may be used to prepare ionic solution for a single source compound. Among them the most suitable one is chosen so that it can permit a high aerosol flow rate in connection with the concentration and viscosity of this solvent. The spray system which is used in the present experiment has a spray nozzle of capillary bore type. The ejection of spray liquid through the spray nozzle depends on the solution concentration. Higher solution concentration causes to reduce the spray rate because it has to pass through a partial vacuum path. So the concentration of the solution prepared by the solvent should be such that it could at least be drawn by the nozzle. Preference is given in selecting a solvent that is not easily inflammable to avoid sudden combustion in the reactor. The most commonly used solvent is water which facilitates the hydrolysis action. Besides this, water and methanol or water and ethyl alcohol may be used. In this experiment water is used as a solvent because there is no

possibility of occurring any accident with it in the reactor and it acts as a powerful oxidizing agent.

4.10 (iii) Preparation of the ionic solution for ZnO film

The ionic solution is prepared by dissolving a soluble salt of the anion (metal) in water. Different quantity of source compound {$Zn(C_2H_3O_2)_2\ 2H_2O$, reagent grade} are used to obtain different molar concentration. The optimum solution concentration has been found to be 0.4m. A few drops of acetic acid was added in order to obtain an optically clear and complete dissolution of Zinc acetate solution. The film is not affected or contaminated by the addition of acetic acid because it is volatile and escape during the film formation.

In the case of doping, indium was used as a dopant for preparing ZnO: In films. Indium was added in the form of $InCl_3$ in the working liquid. For the present study 0.5 to 8 at % (In to Zn atomic ratio) In doping have been used.

4.11 SUBSTRATE CLEANING

The cleanliness of the substrate surface exerts decisive influence on film growth and adhesion. A thoroughly cleaned substrate is a pre-requisite for the preparation of films with reproducible properties. The choice of cleaning techniques depends on the nature of the substrate, the type of contamination and the degree of cleanliness required. Residues from manufacturing and packaging, lint , fingerprints, oil, and airborne particulate

matters are examples of frequently encountered contaminants. For the deposition of polycrystalline films, generally, glass quartz, plastic and ceramic substrates are used. In our work, we have used ordinary microscope slides and cover slides (supplied by the corning glass works U.S.A) as substrate. For its cleaning, the following procedure was adopted in our laboratory. At first the substrates are immersed in a luke warm aqueous solution of Sodium Carbonate in an ultrasonic clearer for the removal of gross contaminations. After this, they are washed in a stream of cold water and again dip in to dilute nitric acid for several minute. Then they are transferred into chromic acid (a mixture of Potassium dichromate in Sulfuric acid) for several days. Taking them out from the Chromic acid the traces of impurities that are loosely in contact with the substrate are eliminated by treating with cold water. Finally rinsing with deionized water for several times they are made dry by blowing hot air. Subsequent contamination was avoided by storing the substrate in desiccator. Cleanliness was tested by carrying out the water-break cleaning test[12]. During the whole process the substrate were always held by slide holding forceps.

4.12 PATTERN OF THE SAMPLE AND PREPARATION OF MASKS

In order to study the various properties of thin films, specific shape and size of films are necessary. The most commonly used methods of patterning thin films are

(i) physical masking (ii) photoresist (iii) inverse photoresist and (iv) inverse metal masking. In the present work, physical masking has been used. These are suitably shaped apertures through which deposition is made to have a desired pattern of the film. Specially for the chemical spray deposition system, the material for the masks should he selected in such a way that is remained inert to the chemicals used for the deposition. Mica and stainless steel is a suitable masking material for this process because of their chemical inertness and capacity for high temperature tolerance. The film uniformity strongly depends on the dimension of mask. As the film thicknesses are of the order of 1000—4000Å so the mask should be as thin as possible. The smaller is dimension of the pattern the thinner should be the mask. In figure 4.2 (a), (b) and (c), the effect of the mask thickness on the film size and uniformity has been clearly shown. In the pyrosol process it is assumed that the chemical reaction takes place in the vapour phase at the substrate surface or in its close vicinity. So the effect of mask dimension on the uniformity of film thickness is very important and should be taken into account. This problem can be properly solved by preparing mask using single layer mica sheet.

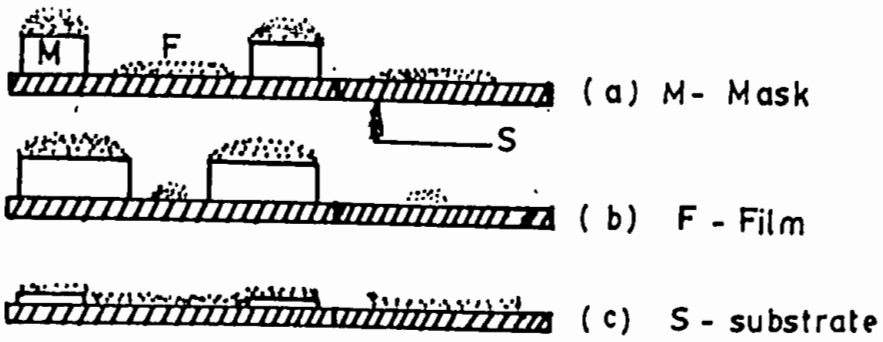

Figure 4.2

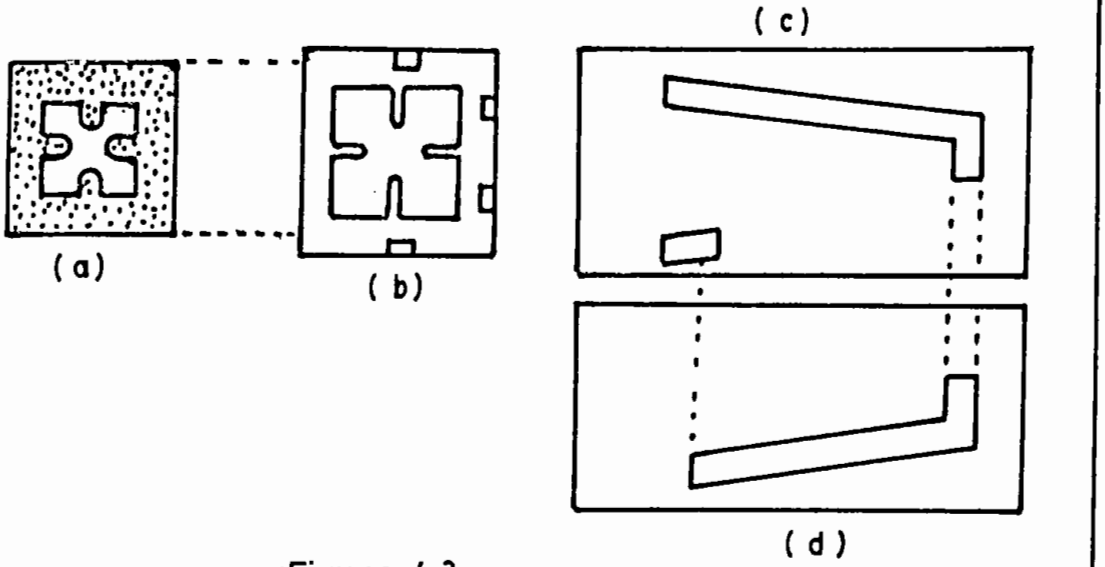

Figure 4.3

Figure 4.2: The effect of size of mask on the deposited film in pyrosol process.

Figure 4.3: (a) Mica mask with the design cut on it,

(b) A stainless steel frame to hold the mask and the substrate intimately in contact,

(c) Mask to deposite pb-film for thermopower reference contact,

(d) Mask to deposite experimental sample for the thermopower measurement.

For the measurement of resistivity and Hall co-efficient of our samples Vander Pauw's method[13] was followed . In order to do this, it is necessary to deposit the sample of such a pattern that can take the shape of Vander Pauw specimen and this can done by a suitable mask (mica) as shown in figure 4.3(a). To keep this mask in contact with the substrate surface, a stainless steel frame is cut in the shape shown in figure 4.3 (b). This frame can hold the mask with substrate surface by giving suitable pressure. Other type of mask is shown in figure in 4.3(c) and (d)(for the study of thermoelectric power of our samples. Figure 4.3 (c) shows the mask, made of mica for the deposition of ZnO films whereas figure (d) illustrate the mask made of stainless steel or aluminium sheet and is used to deposit metal film (Pb) as to form a junction with ZnO films. Metal film was deposited by vacuum evaporation method. The pattern shown in figure 4.3 are cut in the mask materials. A great care was taken in preparing mask with a thin mica sheet because of its brittle nature. Only fresh cleaved mica was used to avoid cleaning procedure and mask was cut by a sharp knife to have sharp edge which became favourable in measuring film thickness by optical method.

The pattern of the film may also be obtained by chemical etching technique instead of using mask. In this case, the film surface is covered by paraffin wax, the required shape is marked on the wax layer. The unwanted portion of the film is then etched out by using etching chemical (Hcl in the case of ZnO). After

completion of etching the wax is removed from the film surface by using organic solvent.

4.13 FILM DEPOSITION PARAMETERS

In the chemical spray deposition system, the structure, composition and other characteristics of the deposited films depend on a number of process variables (deposition parameters). The variable quantities that can produce effect on the properties of the films are, the substrate temperature, solution and gas flow rate,deposition time, quality of the substrate material, size of atomized particles, solution concentration, substrate to nozzle distance and the doping levels of doped films. It is obvious that the substrate temperature is the most important factor and it is controlled with great care.

For the deposition of ZnO thin film, all the above mentioned parameters except (i) substrate temperatures T_s (ii) deposition time t_d (iii) solution concentration (iv) spray rate and doping levels were kept unchanged. To study the effect of any one of these five parameters on the film properties the remaining other were kept constant.

Air current disturbances becomes another parameter which creates problem to get uniformity of thickness and homogeneity of the film.

4.14 FILM DEPOSITION

Before starting deposition, the whole setup is thoroughly cleaned. A little amount of the spray solution (≈ 10 ml) is taken in each of the flask F. (figure 4.1b) In order to obtain sufficient aerosol supply three sprayers were used in separate solution container. A clean substrate with suitable mask is placed on the heat susceptor of the heater H;. A Chromel-Alumel thermocouple is put in contact with the substrate surface on which film is to be deposited. Before supplying the compressed air the heater is kept on for some time. For this the substrate and the reactor wall E attain the requisite temperature. The substrate temperature T_s is raised to level which is several degree higher than that of the required substrate temperature because at the onset of deposition the substrate temperature is dropped down somewhat.

As soon as the compressed air is passed through the tube A at a constant pressure of 20 psi, a fine aerosol in the form of cloud is produced in the flask. These aerosol is carried by the incoming air current to the reactor zone. On reaching the substrate surface ZnO is formed by the pyrolytic action and deposits on the surface. Films of ZnO with appreciable thickness (≈ 2000Å) were obtained at a substrate temperature of T_s = 360°C in a deposition tiem of 25 minutes

4.15 FILM THICKNESS CONTROL

In the present spray deposition process, it is found that the required film thickness may be obtained by controlling the deposition time t_d provided that the other parameter are kept constant. A longer deposition time Yields a thicker film. So deposition time is the only thickness controlling factor in this process. Direct and in situ control of thickness t is a difficult task because the deposition is carried out in normal atmosphere. In order to control the film thickness, a previously prepared calibration charts, which would be a t_d vs. t plot, may be used. The charts should be prepared at different constant substrate temperatures and priority is given for a particular experimental sample using the same solution and deposition variables. The rate of deposition is small and the reaction rate (the film formation for ZnO) is slow in the present set up, Therefore the thickness may be controlled easily.

4.16 EVAPORATION OF METAL FILM FOR CONTACT

For the study of thermoelectric power of ZnO thin film, a reference material is required with respect to which thermopower is measured. In this experiment pure metallic lead (Pb) was used as a reference contact material which has been thermally evaporated on a requisite substrate in a high vacuum coating unit at a pressure of 10^{-5} Torr. Molybdenum boat was used as a resistive heating element for the evaporation of Pb.

4.17 OPTIMIZATION OF THE DEPOSITION PROCESS

To obtain the optimum condition of the film deposition process, it is essential to select at first the requirements with respect to which the process should be optimized. The optimization process is very lengthy because there are a number of process variables. Our basic requirement was to get a film of high transparency as well as high electrical conductivity (i.e film of high figure of merit). We have proceeded to optimize the process under certain limitations and it can not be taken as the ultimate optimization.

For the process of optimization following sets of films have been deposited. (i) The first set of films was deposited at various substrate temperatures T_s keeping all other deposition parameters constant at an arbitrary level. From this set of films the substrate temperature T_s was selected with respect to the best conducting and transparent films. (ii) After obtaining the optimum values of T_s, second set of films was deposited by varying the substrate—nozzle distance 'd' using the optimized T_s and other parameters were kepte constant to the arbitary level as they were in the first set. From this second set of films the suitable distance d was selected corresponding to the best film. (iii) Fixing the distance d and substrate temperature T_s, a third set of films was deposited by varying the pressure P of the carrier gas. From this set, adequate pressure P of the carrier gas was selected

(iv) Keeping T_s, d and P as fixed, fourth set of films was deposited by taking spray rate S_p as variable parameters. (v) Selecting the suitable spray rate from the set, the fifth set of films was deposited. In this case solution concentration C was varied for selecting accurate concentration of the working solution.

Thus in all cases the optimum values of parameters (T_s, d, P, S_p C,) were selected for febrifaction of films that exhibit good conductivity and high transparency. The resulting optimization is undoubtedly a tentative one because the process variables are in some degree mutually interdependent. We found the optimum values of the variables for the ZnO thin film as T_s=360°C, d = 6 cm, P = 20 psi, S_p = 0.8 ml/min, and C = 0.4 M (molar). The experimental samples have been prepared by taking these values of the parameters.

4.18 LEAD ATTACHMENT TO THE FILM

Electrical measurements are performed by attaching leads to the films. Two methods are generally employed for this purpose, (i) Solid phase bonding and (ii) Alloy bonding. The solid phase bonds are formed by thermocompression and ultrasonic means, on the other hand, the alloy bonds are formed by soldering. The soldering material be selected in such a way that it could provide a ohmic contact with the films.

In the present work, metallic indium (without flux) was used as soldering material to make electrical contacts. Very small indium dots were first soldered to the clear surface of the film using a low wattage (15 watts) fine-tip soldering iron. Insulated fine copper wire was used as connecting lead. One end of the fine copper wire was wetted by indium and then placed in contact with the indium dot on the film and soldered by the fine-tip soldering iron.The upper part of the indium dot was melted by taking heat from the soldering iron and make a good ohmic contact with the film. To obtain tight contact, a slight pressure was applied at the contact points.

For taking measurements at high temperature (>100°C), a pressure contact was used, sometimes indium contact point were covered by thick insulating hard adhesive resin. Inspite of low melting point of indium (≈ 155°C), it works nicely up to ~ 200°C.

4.19 MEASUREMENT OF FILM THICKNESS

Film thickness plays an important role on the electrical and optical properties of thin film and thus it is one of the most significant film parameters. Almost electrical parameters except the Hall mobility need for their evaluation the value of film thickness. Therefore, the thickness should be measured with great care as far as possible to have an accurate value. The thickness may be measured either by monitoring the rate of deposition or after the film is taken out of the deposition chamber. The latter

type is appropriate for the spray deposition technique because it is operated in open atmosphere. There are many techniques for measuring film thickness, some of which are briefly illustrated below.

4.19 (i) Method adopted for the present work

Optical interference method is one of the film thickness measuring methods by which the thickness of the thin film can be determined accurately. In this method two reflecting surfaces are brought into close proximity, interference fringes are produced, the measurement of which makes it possible a direct determination of the film thickness and surface topography with high accuracy. Our experimental samples are transparent to the visible light,the measurement of thickness by interferometric method would be adequate.

Weiner[14] was the first to use interference fringes for the measurement of film thickness. Latter on using Fizeau fringes, Tolansky[15] developed this method (Interferometric method) to a remarkable degree and is now accepted as a standard method.

For the experimental set up a low power microscope, a monochromatic source,a glass plate and an interferometer are required. To see the Fizeau fringes of equal thickness in a multiple beam interferometer a thin absorbing film on a glass substrate with an auxiliary reflecting coating on the film surface

is required. For a transparent film with a very smooth surface no such auxiliary coating is necessary[16].

The film whose thickness is to be measured is required to form a step on a glass substrate and over it another plane glass plate (Fizeau plate) in placed. This type of interferometer is shown in figure 4.4 (a). When the interferometer is illuminated with a parallel monochromatic beam of light (Sodium light) at normal incidence, a fringe system [as shown in figure 4.4 (b)] is produced and is viewed with a low power microscope. Dark fringes are also observed against a white background. The displacement h of the fringe system across the film-substrate step is then measured to calculate the film thickness t, using the relation

$$t = (h/\text{fringe spacing}) \times \lambda/2$$

The accuracy of the method depends on how accurately the fraction h of the fringe separation s has been measured. In this method, thickness from 30Å to 20,000Å can be measured with an accuracy of ± 30Å.

4.19 (ii) Other methods

At present there are several other methods of determining thicknesses of transparent films. A few of there are mentioned here.

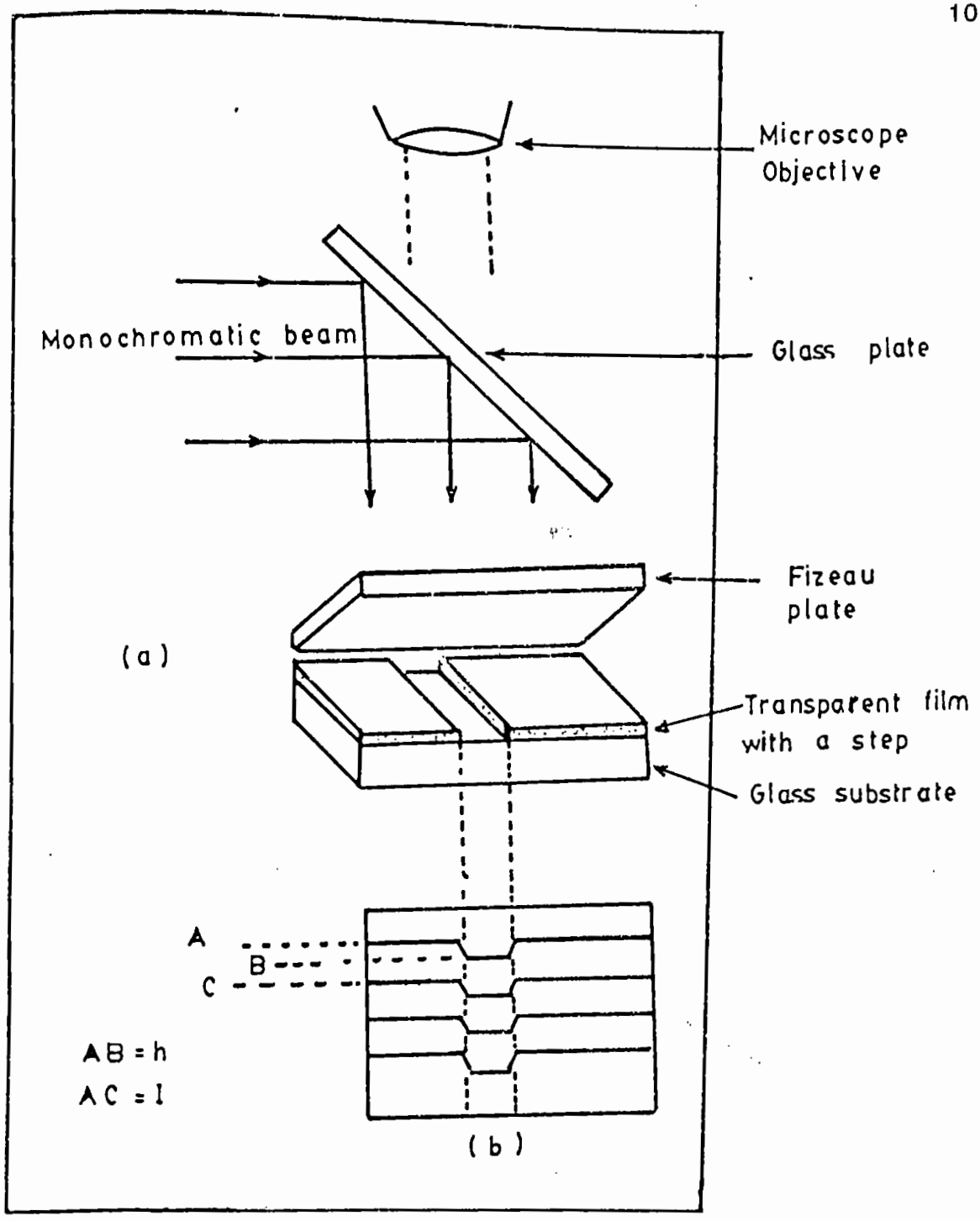

Figure 4.4:(a) Enlarged view of the interferometric arrangement for the measurement of film thickness, (b) The fringe pattern with step height h and fringe spacing l.

4.19(iia) Gravimetric method

It is one of the simplest and oldest methods of determining the film thickness. In this method, the mass m of a film of certain area A is determined by weighing the substrate before and after deposition by a very sensitive microbalance. The film thickness t can be calculated by taking the bulk densely ρ of film material. The thickness of the film is then given by

$$t = m/A\rho$$

Though the method is simple but there are a number of difficulties and sources of errors. The accurate bulk value of ρ hard to know and the method is therefore avoided.

4.19 (iib) Stylus instrument

It is a mechanical method and is widely used for the measurement of surface roughness and surface finishes. Here also a step is required.The instrument is acted on such a principle that compares the vertical movements of the stylus travelling across the sample surface with the movement of a "shoe" or "skid" on a smooth and flat reference surface, the substrate. There is an auto system that concerts the mechanical signals produced by the stylus movement into the electrical impulses which are then amplified and recorded on a strip chart. The thickness of the film can be evaluated by analysing the pattern of the chart. This method is very suitable for hard film like Zno. The main advantage of this method is that it is independent on the optical nature of the film.

This method can be applied successfully on the film which can merely support the load of the stylus. The accuracy depends on the sensitivity of the stylus.

4.19 (iic) Colour comparison

It is a crude method but very simple. The thickness of a transparent film on a reflecting substrate can be estimated rapidly. Transparent films display colors when they are exposed in ordinary day light. The colour depends on the thickness of the film. For a particular colour exhibition the film should have to attain a definite thickness. Various colors can be viewed from the layer of different thickness in the same film. First precise colour gauge was made by Blodgett[11] who had deposited Berium stearate on a lead-glass plate producing a very colourful and useful thickness gauge.

During colour comparison, one must be careful not to confuse different film thicknesses which give rise to similar colours but in different orders. This can be done by comparing the colours of the films while varying the angle of observation. These colour varieties with thickness were observed at the time of deposition of ZnO thin film when the deposition chamber was kept illuminated with light. The value of the refractive index however limits this method in some cases.

4.20 RESISTIVITY, HALL MOBILITY AND CARRIER CONCENTRATION MEASUREMENT

Vander pauw's technique[13] is one of the standard and widely used technique for the measurement of resistivity and Hall coefficient of thin film, we have followed this technique throughout the work.

Figure 4.5 shows the Vander pauw's specimen with four small contacts A, B, C and D in order, 1, 2, 3 and 4 indicate the terminals of the electrometer for the measurement of voltages and currents. The sample should not need to be of the shape as shown in figure. This method is applicable for any arbitrary shape of uniform sheet of material with four contacts applied to the periphery. Through commutative switches the connections are made between the film and the meter terminals. If a dc current I_{AB} entering the specimen through the contact A and leaving it through the contact B, produces a potential difference V_{CD} between the contacts D and C then $R_{AB,CD}$ is defined as V_{CD}/I_{AB}. Similarly, $R_{BC,DA}$ is defined as V_{DA}/I_{BC} and $R_{BD,AC}$ as V_{AC}/I_{BD}. $\Delta R_{BD,AC}$ measures the change in $R_{BD,AC}$ due to the application of magnetic field B. For a plate of arbitrary shape and constant thickness t, the resistivity and Hall constant are given by

$$\rho = [(\pi t/\ln 2)(R_{AB,CD} + R_{BC,DA})/2]\ f(R_{AB,CD}/R_{BC,DA}) \quad \ldots\ldots\ldots (4.1)$$

and the Hall constant $R_H = \Delta R_{BD,AC}\ (10^8 t/B) = \Delta R_{AC,BD}\ (10^8 t/B)\ cm^3/C$ .. (4.2)

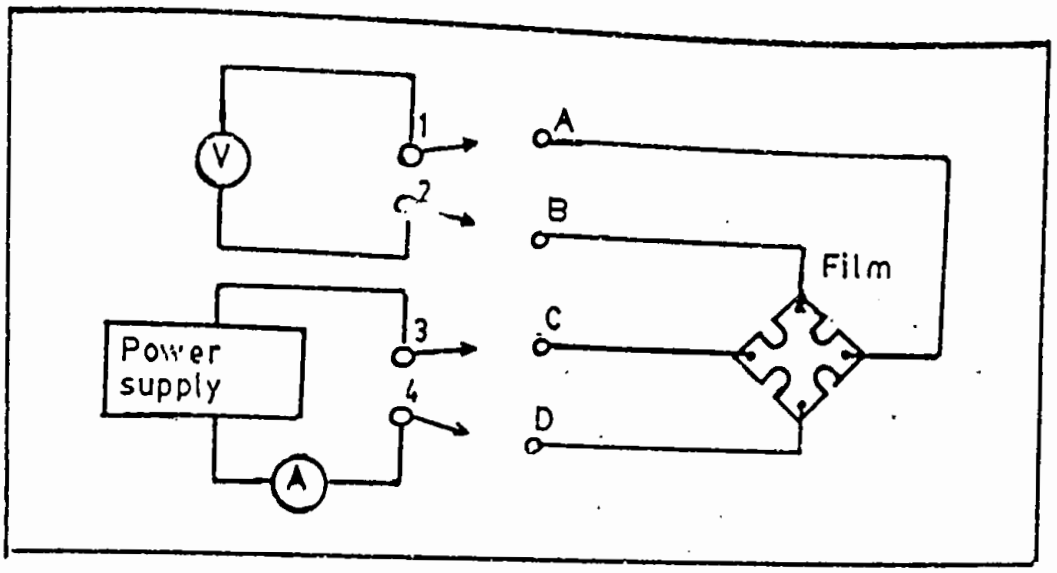

Figure4.5: Schematic diagram for the measurement of film resistivity. 1,2,3 & 4 are meter terminals and A, B, C & D are the film terminals. Arrows indicate commutating switches.

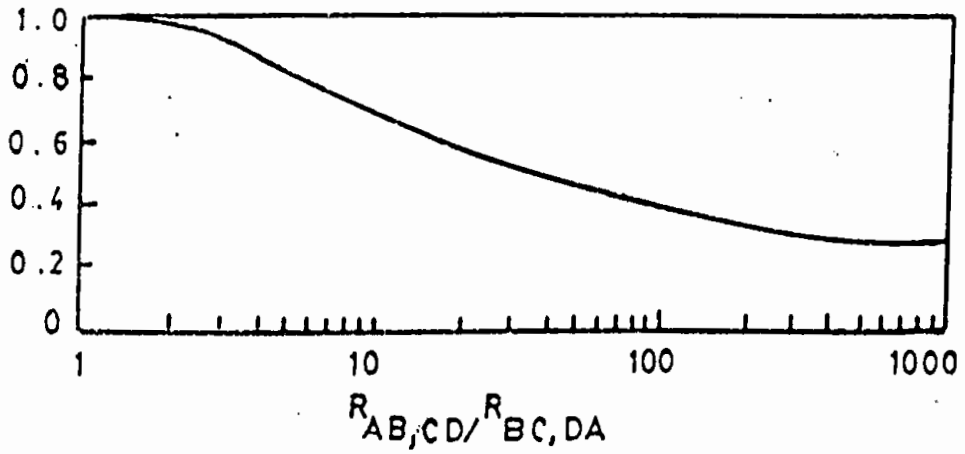

Figure4.6: The dependence of function f on the resistance ratio $R_{AB,CD}/R_{BC,DA}$.

where B is the magnetic filed in Gauss and film thickness is in cm. The function f can be evaluated from

$$(R_{AB,CD}-R_{BC,DA})/(R_{AB,CD}+R_{BC,DA}) = (f/\ln 2)\ \text{arc cosh}\ [[\exp(\ln 2/f)]/2] \quad \ldots\ldots (4.3)$$

The function f of this equation depends only on the ratio $R_{AB,CD}/R_{BC,DA}$. Figure 3.6 shows in graphical form, the dependence of f on the ratio $R_{AB,CD}/R_{BC,DA}$.

To keep the ratio $R_{AB,CD}/R_{BC,AD}$ approximately equal to unity and to eliminate the contacts effect, the shape of the sample has been taken in the form of a "quatrifoil leaf". In this situation the resistivity ρ is given by

$$\rho = 2.266t\ (R_{AB,CD} + R_{BC,DA})\ \text{ohm-cm} \quad \ldots\ldots\ldots\ldots\ldots (4.4)$$

The magnetic field B and the sample plane are kept perpendicular to each other.

The carrier concentration n and Hall mobility μ can be obtained from the relation $n = (1/R_H e)\ cm^{-3}$ and $\mu = R_H/\rho\ cm^2/V.S.$ In calculating ρ, appropriate correction factor evaluated from figure 4.6 was used where it was at all necessary.

4.21 THE MAGNETIC FIELD B

For the measurement of Hall constant, a magnetic field of intensity B has been used. An electromagnet (Type A designed and supplied by Newport instruments Ltd. England) was used for this purpose. It has plane pole faces of diameter 10 cm. The magnetic field may be varied by changing either the pole gap or the magnetizing current following through the coils of the electromagnet.

For the present experimental studies on ZnO, the magnetic field was varied by changing the current flowing through the coils and pole gap of the electromagnet was kept fixed at 3 cm. The electromagnet was energized by a "Newport power supply" type D104. We have used the fields of the order of 3.5 to 7.35 K Gauss for our study. Previously ,a plot of the magnetic field vs. current flowing through the coils of the electromagnet was drawn for calibration

4.22 MEASUREMENT AT ELEVATED TEMPERATURE

Some of our experiments were carried out at elevated temperature. The measurements were carried out at temperatures ranging from room temperature up to about 200°C. This temperature was obtained by using a nichrome wire flat heater whose dimension was 2.5 X 6 cm^2 and it was properly insulated by mica sheet in conjunction with thick aluminum heat sink (4 mm). The surface temperature of the heat sink could be kept constant for a

considerable time and its temperature could be varied from room temperature to about 300°C by applying ac voltage of the order 5 to 50 volts across the heater coil. A digital thermometer (RS components STK. No. 610-067, with thermocouple Type A) and some time chromel-alumel thermocouple were used to record the temperature of the specimen.

4.23 MEASUREMENT OF THERMOELECTRIC POWER (TEP)

For the measurement of thermoelectric power of ZnO thin films, the experimental set up is shown in the figure 4.7. For the measurement of thermoelectric power two functions are required at A and B. The shape of the sample DABC is obtained by the deposition of ZnO film AB first on glass substrate using mask of figure 4.3 (C). After the deposition, the substrate with the film having the mask of figure 4.3 (d) was placed inside the vacuum evaporation chamber to deposit a thick lead film of DA and BC by the thermal evaporation of pure metallic lead to form the junction A and B. Here pure lead (Pb) has been taken as the reference metal. The measurement of thermoelectric power was carried out by the integral method[118] in which junction A was heated by a flat nichrome strip heater with regulated power supply to keep it at different temperatures. A spring pressure clipping arrangement provided a close contact between the heater and the substrate. The cold junction B, was immersed into an ice-water bath of constant (0°C) temperature. The temperature of the hot junction was measured using

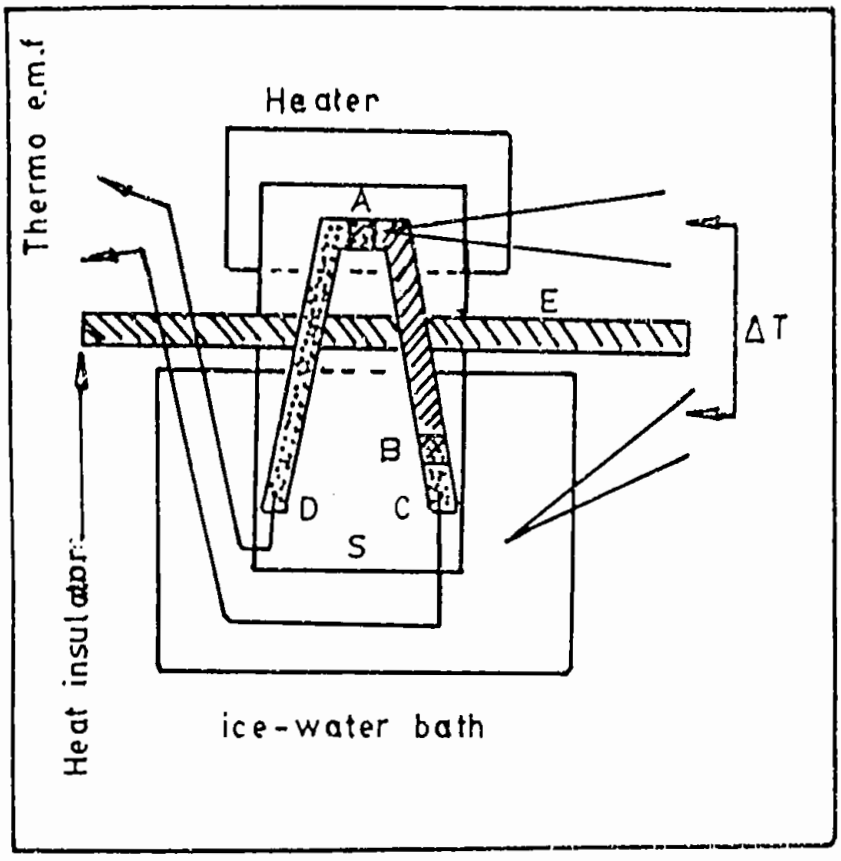

Figure 4.7: Schematic diagram of thermopower measuring apparatus AB; ZnO film; DA and BC; lead films; S, substrate; E; heat insulating barrier; ΔT is the temperature difference between hot and cold ends.

a chromel-alumel thermocouple attached to the sample. The generated thermo e.m.f was recorded using a digital voltmeter. The hot and cold junction were kept thermally isolated by inserting an insulated barrier, E between the junctions to minimize heat radiation from the hot to the cold end. The immersed portion of the sample was kept electrically insulated to remove any leakage of e.m.f. between D and C due to contact with the ice-water. The whole apparatus was kept in a suitable enclosure to minimize air current disturbances.

The temperature of the hot junction was raised slowly from room temperature, and at regular intervals of 5°C the thermo e.m.f was noted up to the highest temperature of 200°C. For the measurement of carrier concentration and Hall mobilities of these sample, during the preparation of thermopower samples another specimen having the shape of Vander Pauw specimen was also deposited in the same run. The substrate temperature was kept constant (≈ 360°C) for all the sample but they were of different thicknesses ranging from 900—2100Å. All the samples were annealed in vacuum before using for any measurement. This was necessary because the as-deposited samples were of very high resistivity.

4.24 POST-DEPOSITION HEAT TREATMENT EXPERIMENTS

As-deposited samples of ZnO are of very high resistance Electrical measurements of these samples were difficult. Most of the experimental samples except a few were annealed in vacuum at a

constant temperature of 250°C in a vacuum of the order of $2x10^{-5}$ Torr and they were preserved in a desiccator for electrical measurement.

For device applications, the temperature stability and reproducibility are the two important film properties which is necessary for the device operation and reliability. For the Fabrication and optimization of electronic devices it has been observed that a common process of heat treatment often comes in question. Polycrystalline Oxide films are more or less sensitive to the post deposition heat treatment but when the films are deposited in open atmosphere specially in the case films deposited by pyrosol process the sensitivity is very much pronounced. Therefore it is necessary to study the temperature effect on ZnO thin film so that an improved knowledge of the behaviuor of the deposited films under thermal cycling may be obtained.

For the heat treatment experiments a set of as-deposited undoped ZnO thin films were prepared at various substrate temperatures, Viz-300,330,360 and 390°C. All the films had a thicknesses of about 1730Å and were deposited onto glass substrate. After the deposition, the films were cooled at a rate of approximately 100°C/min. and were then preserved for heat treatment experiment.

Heat treatments were performed in four steps as described below. The heating and cooling rate was about 5°C/min for each

sample. The first step of heat treatment operation was carried out on as-deposited sample in air. After completing the 1st step of the heating and cooling cycle in air., the second step was performed on the sample in a similar manner. Then the sample was placed in a vacuum chamber making a vacuum of the order of 10^{-5} Torr,the sample was heat treated there for the first time. Then the sample was taken out of the vacuum chamber, and a third step of heat treatment was performed in air. The sample was then put into the vacuum chamber for a second time and again heat treated. After this second vacuum heat treatment, the sample was heat treated again in air for the fourth time. Successive heat treatment operation enables the sample to lower its resistivity to a minimum value.

Electrical resistivity and Hall coefficients wee measured simultaneously during heat treatment in air only. A flat Nichrome were strip heater was used to heat the sample. The maximum heating temperature was 200°C for all the samples. Temperatures were measured by a digital thermometer.

4.25 MEASUREMENT OF OPTICAL TRANSMISSION

Optical transmission have been measured in the wavelength range 3000—9000Å on both the as-deposited and vacuum heat treated films of ZnO. the deposition conditions were kept constant for both set of samples. For the measurement of transmission the samples were deposited on a special type of glass substrate which were transparent in this spectral range.

Shimadzu UV-180 double beam spectrophotometer was used for this purpose. A sample with substrate was placed in the incident beam with an uncoated substrate in the reference beam of the spectrometer. Optical transmission (in percentage) of the film for normal incidence was obtained from a graph that was automatically plotted against wavelengths during the period of spectral transmission.

Optical absorptions of these samples were calculated from the transmission data at different wave lengths. Since the samples were highly transparent in the visible region of the spectra, the reflection coefficients for the normal incidence were taken negligible in consideration. The value of the refractive index of the film were calculated from the transmission data.

4.26 ELECTROMECHANICAL PROPERTIES OF ZnO FILMS ON GLASS SUBSTRATES

For the study of electromechanical properties of ZnO a set of films both undoped and In-doped were deposited on microscope slide cover glass at a substrate temperature of 360°C having different thicknesses. The sample dimension was of 1.5 x 0.8 cm^2. Before taking measurement, all the samples were heat treated in vacuum at a pressure of 10^{-5} Torr for 1 hour at a constant temperature of 250°C.

Experimental arrangement consists of 1m long flat bar of mild steel which acts as a cantilever. The samples with the substrate

were pasted on this bar with a thin layer of strong adhesive. One end of this bar was firmly clamped and load was applied at the free end. As a result of this bar was bent thereby producing strain in the sample. For electrical resistance measurement conventional four probe method was used.

REFERENCES

1. J.C. Manifacier, M. De Murcia and J.P. Fillard, Mat. Res. Bull. 10, (1975) 1215.
2. B.K Gupta and O.P. Agnihotric, Solid state Commun. 23(1977) 295.
3. J. Aranovich, A. ortiz and R.H. Bube, J. Vac. Sci, Technol. 16, (1979) 994.
4. E. Shanthi, V. Gutta, A. Banerjee and K.L. Chopra, J. Appl. Phys. 51, (1980) 6243.
5. S. Kulaszewicz, Thin solid Films. 74. (1980) 211.
6. M.S. Tomar and F.J. Garcia, Prog.crust. Growth chract. 4. (1981) 221.
7. G. Blandenet, M. court and Y. Lagrade, Thin solid Films, 77, (1981) 81.
8. M.N. Islam and M.O. Hakim, J. Phys. Chem. solids, 46 (3), (1985) 339.
9. S.K. Som and S.G. Mukharjee, Acta Mech. 36, No.1-2 (1980)
10. C.M. Lampkin, Prog. cryst. Growth chract. 1, (1979) 405.
11. J.C. Viguie and J. Spitz, J. Electrochem. Soc.122 (4) (1975) 585.
12. R. Brown in "Handbook of thin Film Technology" (Eds. L.I. Maissel and R. Glang, Mc. Graw. Hill Inc. 1970)
13. L.J. Vander pauw, philips Res. Rept. 13, (1958) 1.
14. O. Wiener; Wied. Ann. 31 (1887) 629.

15. S. Tolansky, "Multiple Bean Interferometry of surfaces and Films" (Oxford university press, 1948)

16. J.G. Gottling and W.S. Nicol, J. opt. SOC. Am. 56, (1966) 1227.

17. K. Blodgett and I Langmuir, phys. Rev. 51, (1937) 964.

18. V. Damodara Das and J.C. Mohanty, J. Appl. Phys. 54, (1983) 977.

CHAPTER 5

RESULTS AND DISCUSSIONS

In this chapter the results and discussions of the various experimental investigations on ZnO thin film have been presented. In the previous chapter details of the experimental procedures for each of these studies have been described.

5.1 STRUCTURAL STUDIES

The microstructure of the films was studied with transmission electron microscope (TEM). Figure 5.1 shows such a micrograph of ZnO thin film of thickness 760 Å deposited at a substrate temperature of 360°C. From this micrograph it is seen that the crystals are well oriented possess small grain size, and uniformly distributed over the area of the substrate. The films are polycrystalline in structure. The composition of the film was tested by chemical method and ZnO phase was confirmed.

5.2 THE EFFECT OF SUBSTRATE TEMPERATURE

The film properties strongly depend on substrate temperature T_s, in spray pyrolysis method. The films were deposited at various substrate temperatures ranging from 270°C to 420°C. The films deposited at lower substrate temperature (<270°C) showed very high resistivity even after annealing in vacuum and the electrical measurements on these samples were not reliable. Below 250°C no

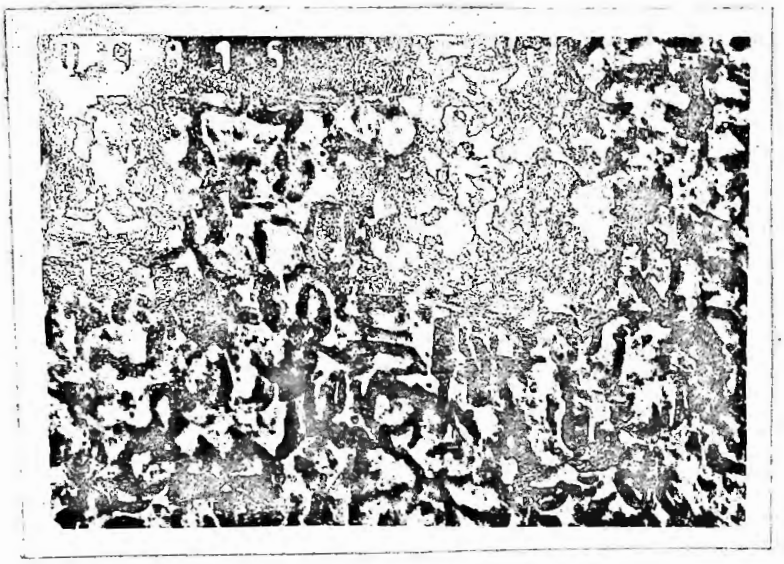

Figure 5.1 : Tansmission electron micrograph of 760Å ZnO film .

stable film but a white powdery deposit was found. This can occur possibly because of unreacted acetate that comes with the aerosol and vaporizes only leaving a dry white precipitate on the substrate.

Figure 5.2 (a) shows the plot of resistivity ρ versus substrate temperature T_s, of some as-deposited samples and figure 5.2 (b) illustrates the plot of resistivity ρ, carrier concentration n and Hall mobility μ of the same set of samples of figure 5.2 (a) after they were annealed in vacuum.

From figure 5.2 (a) it is observed that the resistivity of as-deposited sample is high in comparison to vacuum heat treated films. Minimum resistivity was found at a substrate temperature of 360°C, below or above of which it shows an increase. The nature of variation of resistivity of as-deposited and vacuum annealed samples follow the same general trend but with a drastically reduced magnitude. The measurement of Hall co-efficient of the as-deposited samples was not possible. The carrier concentration n and Hall mobility μ vary similarly with the substrate temperature T_s.

At low substrate temperature some unreacted species of starting material (Zinc acetate) may be present in the samples during the process of deposition. This unreacted species causes barrier to the carrier conduction, hence the resistivity is relatively high in the films deposited at lower substrate temperature. With the rise of T_s, n increases and ρ decreases. When

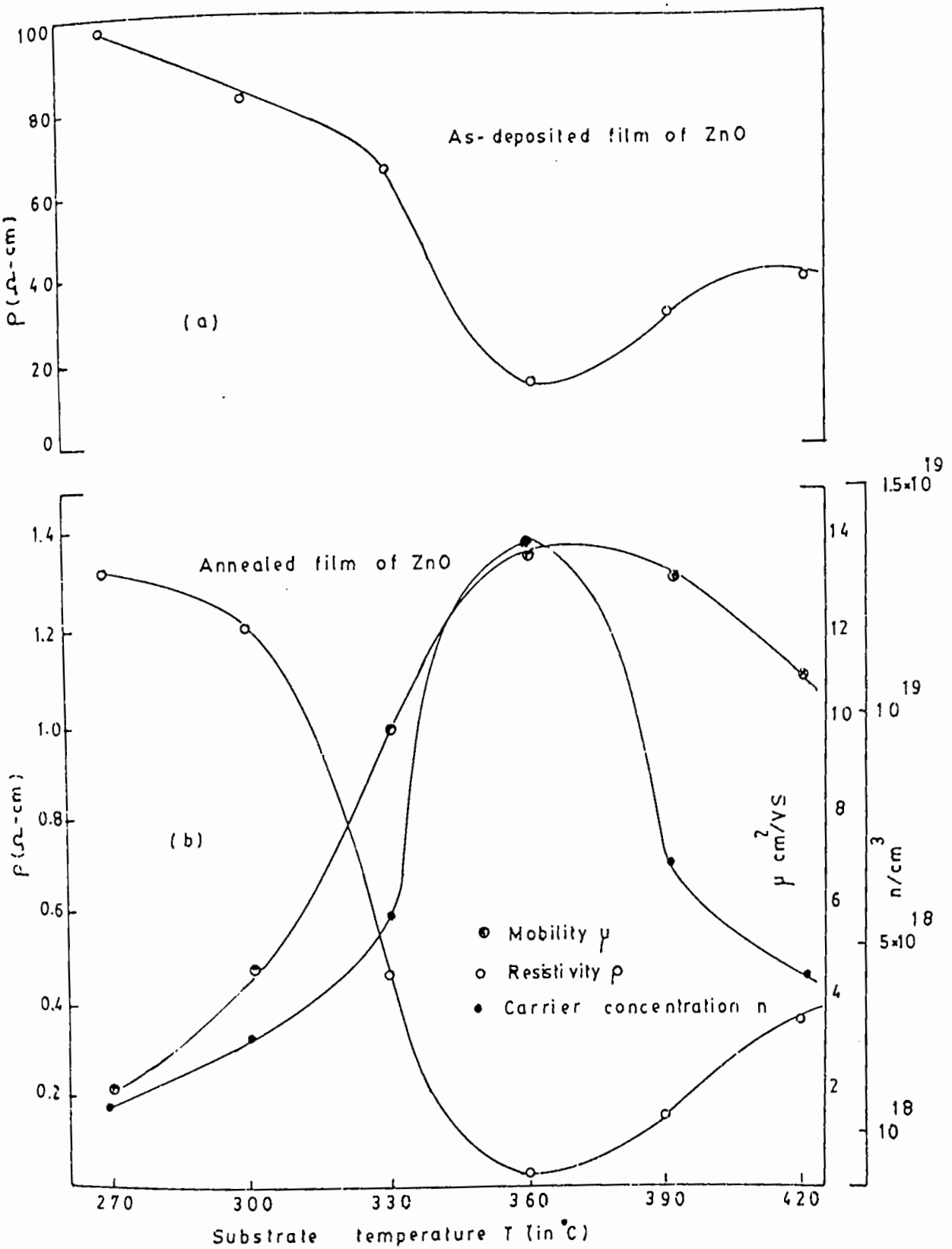

Figure 5.2(a): The plot of resistivity ρ vs. substrate temperature T of as-deposited ZnO films.
(b): The plot of resistivity ρ, carrier concentration n and mobility μ of vacuum heat treated ZnO films.

substrate temperature crosses 360°C both n and μ decrease but ρ increases. At higher substrate temperature, the variations of n and μ cause the increase in ρ. Furthermore the decrease in μ is probably due to an increase in the grain boundary barrier heights whereas the decrease in carrier concentration n is perhaps due to relatively better stoichiometry of the films at this temperature which in turn may increase the resistivity[1]

It is generally accepted[2] that the n-type conductivity in undeoped non-stoichiometric ZnO is due to lattice oxygen deficiency and interstitial Zinc atoms, which act as donors[2]. Wagner[3] has ruled out the alternative possibility that oxygen vacancies are produced in the lattice and that the conduction electrons are those which normally may occupy these vacancies by showing that the negative-ion transport number is very small compared with the positive-ion transport number. The small observed positive ionic current is carried either by ionized interstitial zinc atoms or by the normal Zinc ions. The films are polycrystalline in structure and the resistivity of the as-deposited films is very high. High resistivity may be due to the grain boundary effects. During the film deposition, a large number of oxygen molecular ions (O^-_2) are chemisorbed and incorporated at the grain boundaries and on the surface of the film producing potential barrier for the conduction electrons. This hinders the electrical transport and raises the resistivity[4]. Fujita[5] and Kwan proposed that when these films are heat treated, the chemisorbed (O^-_2) desorbed from the samples

donating an electron in the ZnO [$O^-_2 \rightarrow O_2+e$] hence causing the resistivity to decrease drastically. This is obviously due to a cumulative effect of lowering of grain boundary potential barriers and increase of carrier concentration in the sample. On the other hand, in the crystalline lattice the ions have a closed outer shell and the energy bands arise from the filled 2P levels of the O^{--} ion and empty 4S levels of the Zn^{++} ion. If the crystal is now caused to lose oxygen by heat treatment, the ions escape as neutral molecules (O_2)leaving two electron per atom behind. They in turn combine with the Zn^{++} atom. One electron is then easily ionized into the conduction band from the Zinc atom in this position[6]. Thus the conductivity of the heat treated film may easily increase.

5.3 EFFECT OF DEPOSITION TIME

The dependence of film thickness t, on the film deposition time t_d is Shown in figure 5.3. It is observed that the variation of t with t_d is not linear. But lnt varies almost linearly with t_d. This may naturally happen because at the starting of the spray a portion of the aerosol cannot reach at the substrate for its non-uniform distribution in the reaction chamber. This results in a lower deposition rate. After deposition to a certain thickness of the film a steady state of the process is attained, and it becomes energetically favorable for the rest of the film to grow easily on the initially deposited layer and thus the thickness of the film increases nonlinearly with time.

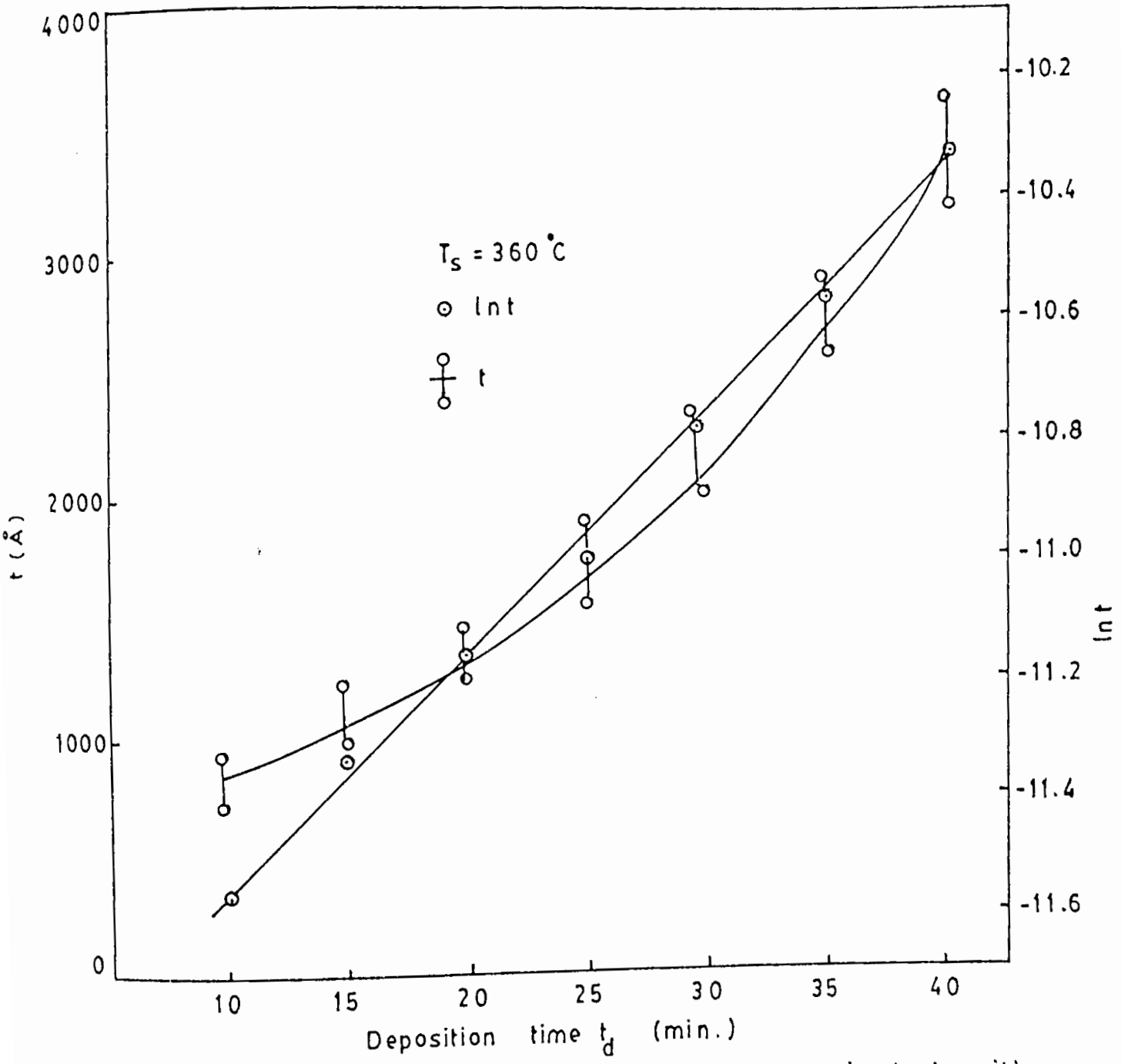

Figure 5.3: Variation of film thickness t and lnt against deposition time t_d of ZnO films.

5.4 EFFECT OF SUBSTRATE TEMPERATURE ON FILM THICKNESS

Figure 5.4 shows the variation of film thickness t with substrate temperature T_s. To study the effect of substrate temperature, a constant deposition time of 25 minutes was maintained. It is found that the film thickness decreases with the increase in substrate temperature. It is expected that when Zinc acetate solution is sprayed onto glass the growth rate decreases as the substrate temperature increases. Film growth is believed to be controlled by gas and droplet dynamics[7]. As the substrate temperature increases wetting decreases, and splitting, bouncing and the lateral mobility of the droplets increases. Laterally moving droplets in which the reaction proceeds more slowly have the opportunity to be swept away by the lateral wind. At higher substrate temperatures and air flow rate thinner films are thus expected.

5.5 FILM GROWTH ACTIVATION ENERGY

Figure 5.5 shows the plot of log t of film thickness t, against $1/T_s$. Considering the film growth process as a rate process the activation energy for the film growth can be determined from the slope of the plot and was found to be 0.22 eV in the temperature range 270°C to 420°C.

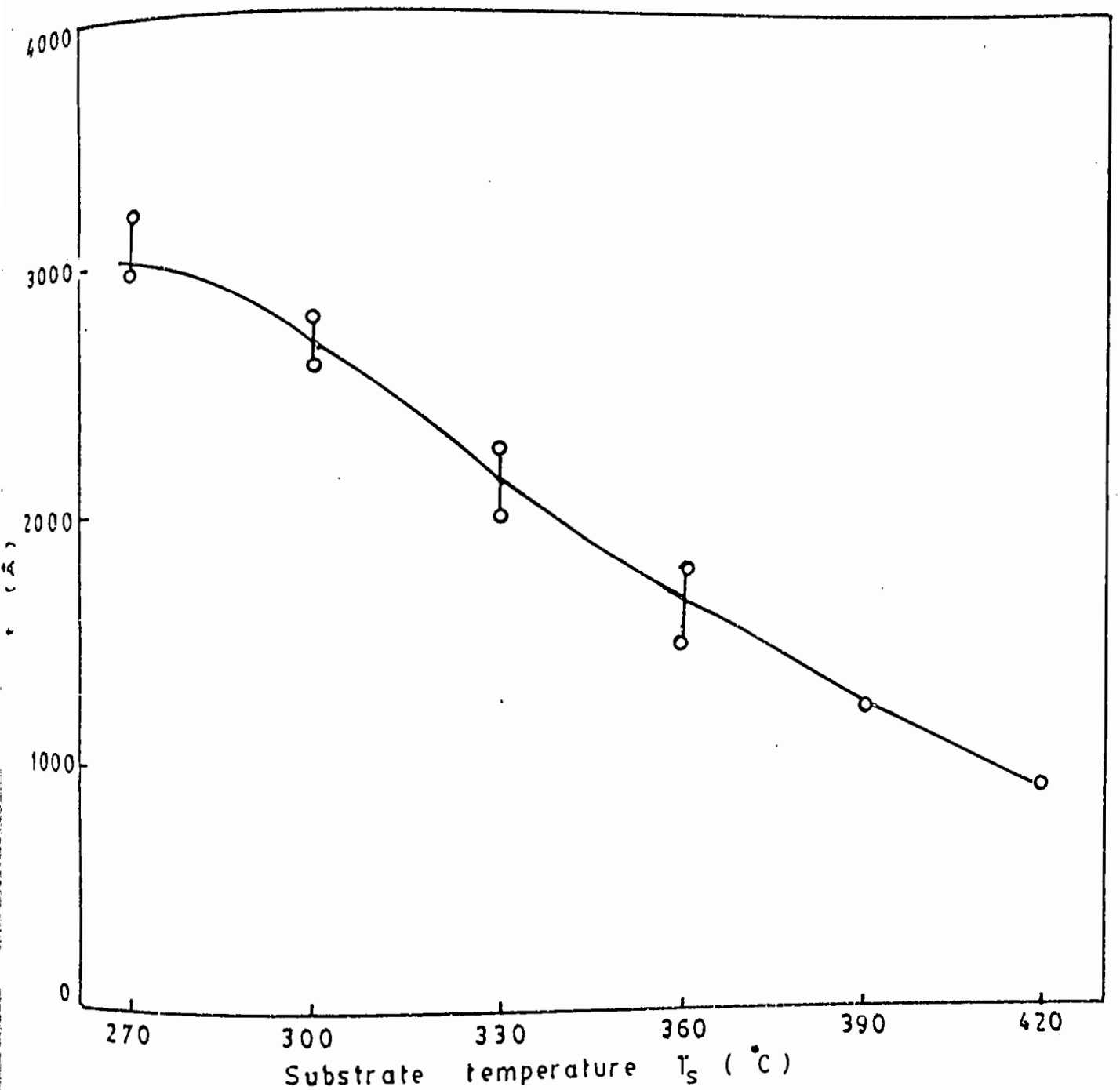

Figure 5.4 : Variation of film thickness t against substrate temperature T_s.

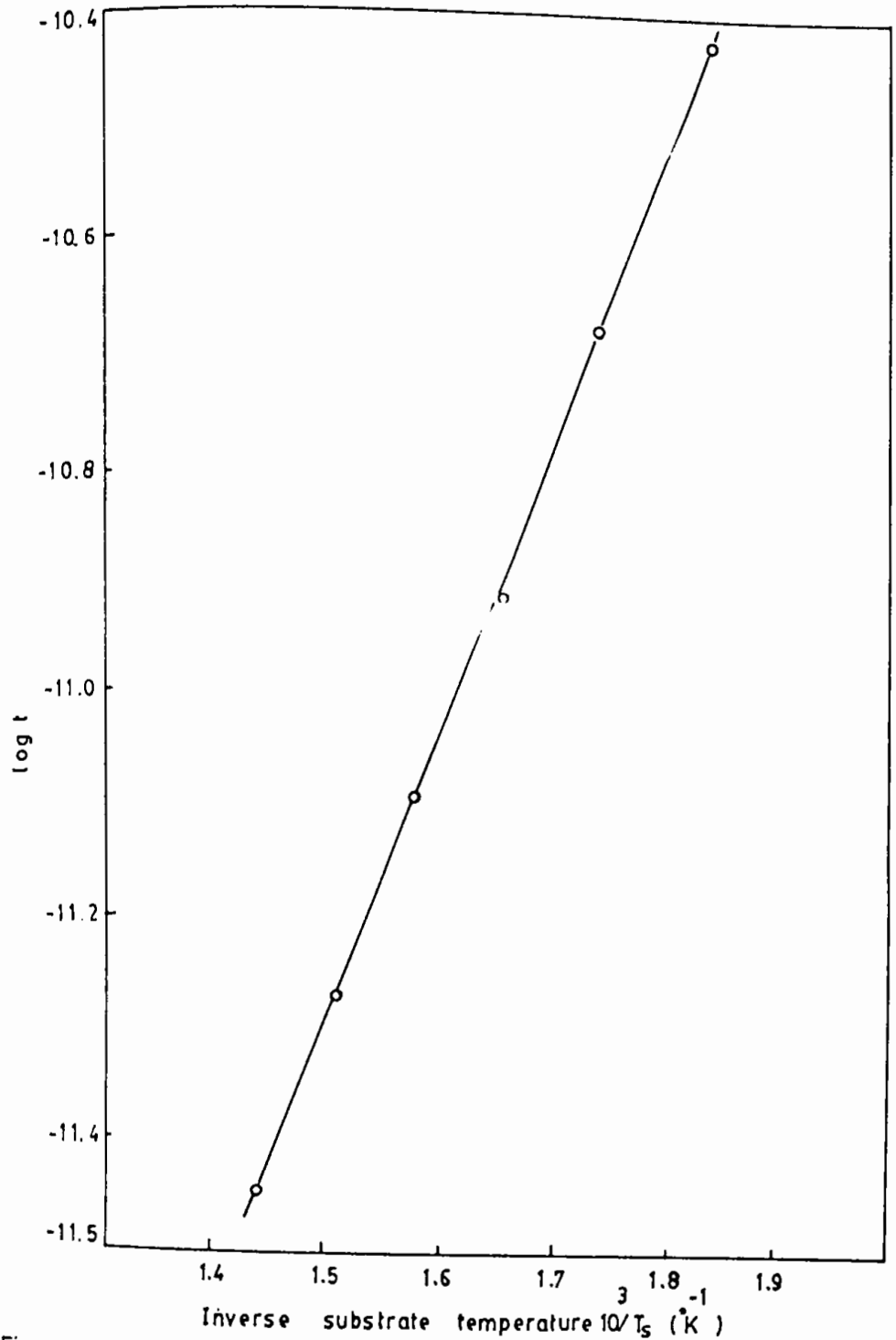

Figure 5-5: The plot of log of film thickness t against 1/T (Inverse substrate temperature) of ZnO films.

5.6 EFFECT OF SOLUTION CONCENTRATION ON FILM THICKNESS

The variation of the film thickness t with the working solution concentration C is shown in figure 5.6. It is observed that the thickness increases linearly with the increase in solution concentration. This is probable, because the mass of the vapour molecules on the substrate increases with the increase in solution concentration. This results in increasing the rate of deposition i.e thickness. Otherwise it can also be said that as the supply of the reactant increases the increase in product is expected accordingly.

5.7 EFFECT OF SPRAY RATE ON THE FILM THICKNESS

The variation of film thickness as a function of spray rate is shown in figure 5.7. The fixed substrate temperature was 360°C. The variation is not linear. It is seen that initially the thickness increases slowly with the spray rate, but at higher spray rate thickness tends to saturate. At lower spray rate, smaller quantity of aerosol reaches at the substrate but at higher spray rate,the quantity of reacting aerosol reaching the substrate increases and the thickness of the film increases. But a time will come at a fixed temperature when the reaction rate becomes optimum and more reactant supply could not increase the rate of formation of film rather the excess reactant will flow outside remaining unreacted. So a saturation of film thickness is obtained.

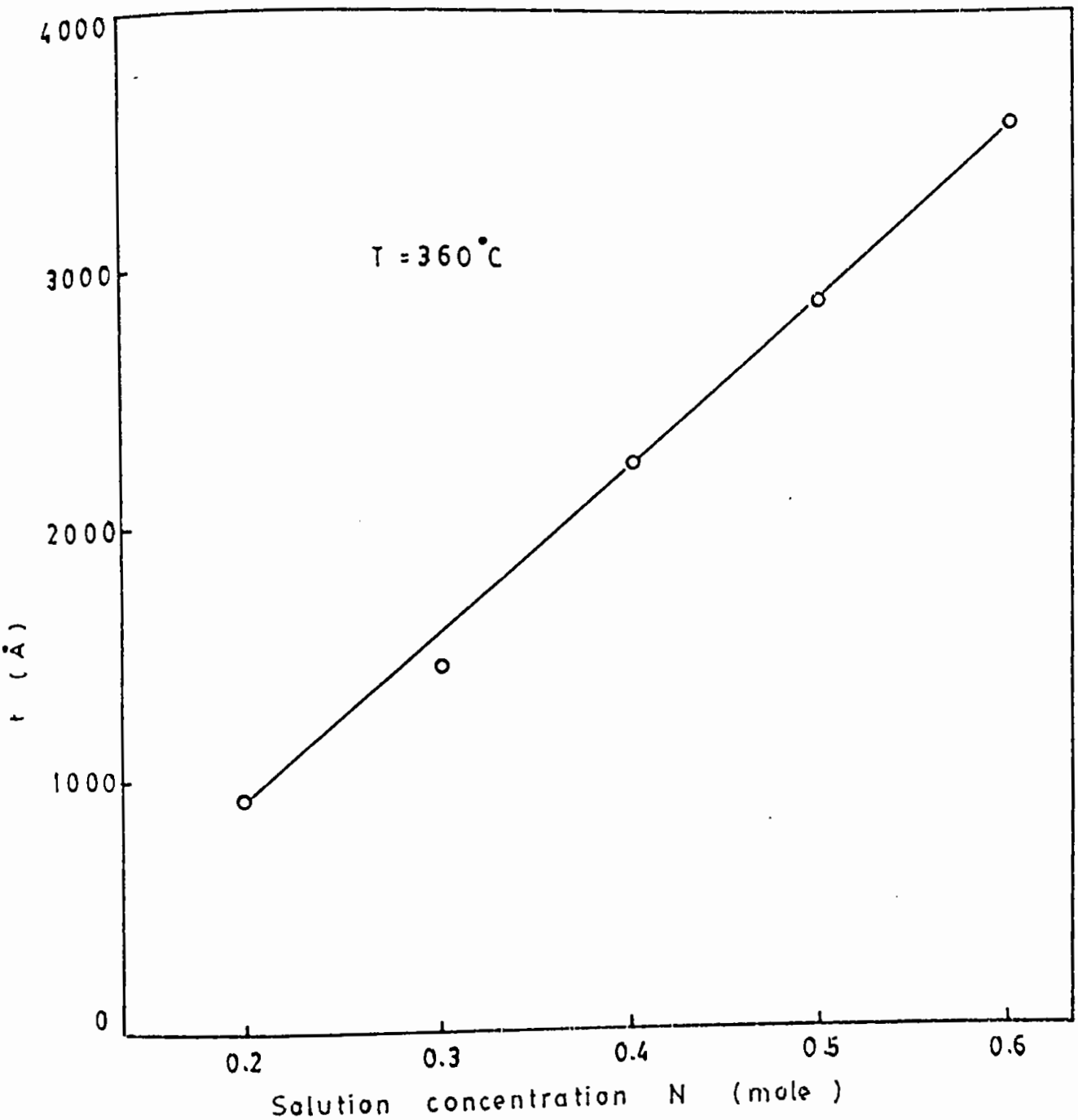

Figure 5.6: The plot thickness t vs. solution concentration N of ZnO films.

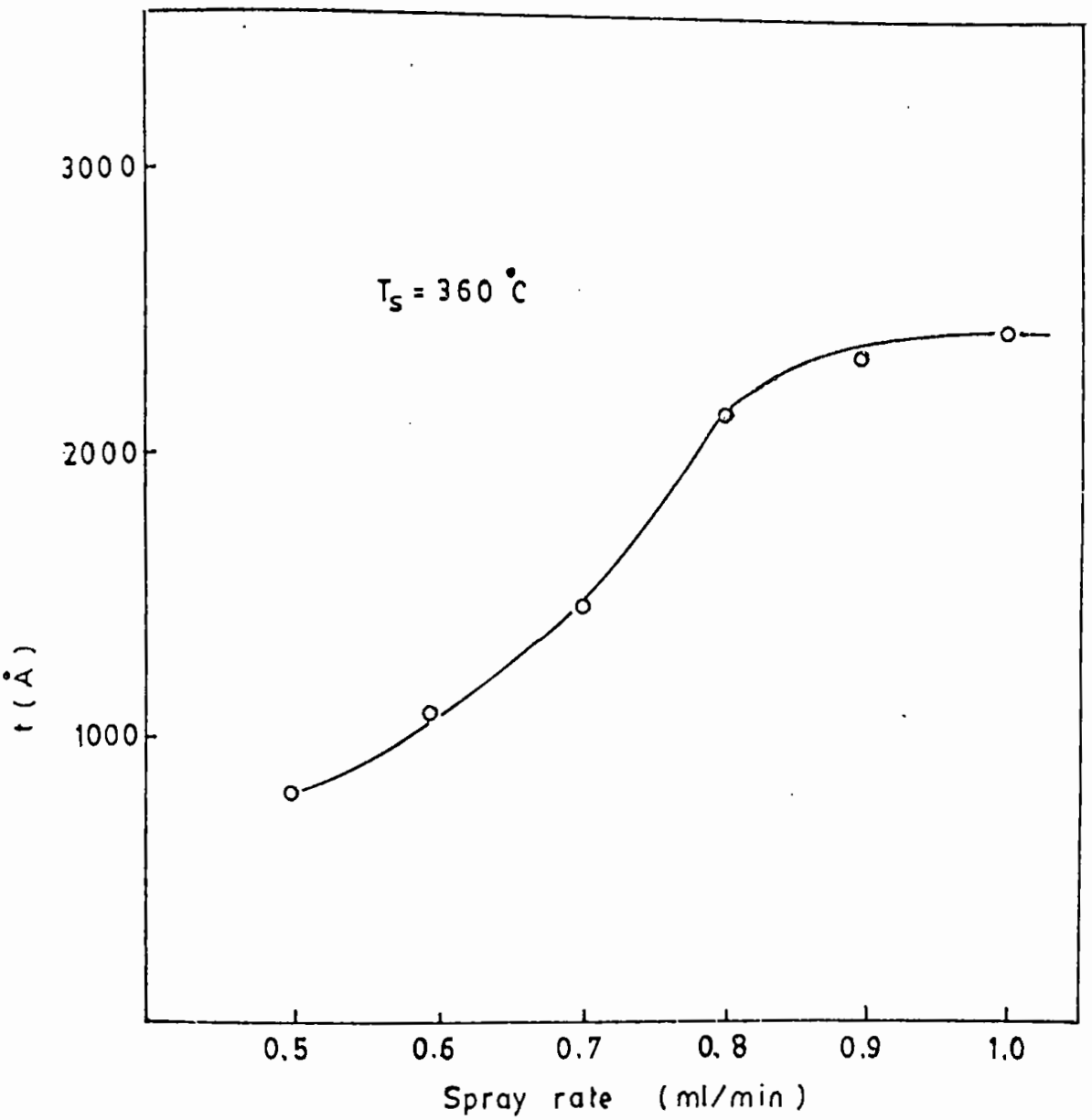

Figure 5.7: Variation of film thickness t as a function of spray rate of ZnO films.

From this observation, the optimum spray rate was found to be about 0.78 ml/min. towards better mobility and higher carrier concentration with minimum resistivity (Figure 5.9)

5.8 EFFECT OF NOZZLE DISTANCE FROM THE SUBSTRATE

The effect of distance 'd' between the substrate and the spray nozzle is shown in figure 5.8. It shows the plot of the film thickness t as a function of 'd' at constant substrate temperature T_s (≈360°C). From this plot it is observed that t decreases with the increase in d. At higher distance the decrease in t is more pronounced. At small d, the maximum amount of vapour molecules which come out from the nozzle can strike the substrate directly before getting the scope of distributing in the reaction chamber. As the nozzle to substrate distance d increases the vapour molecules get sufficient space to distribute laterally in the reaction chamber. As a result a smaller quantity of the aerosol can reach the substrate and cause a decrease in deposition rate (thickness). At sufficiently large d (d ≈ 30 cm), the substrate remains deprived of any coating even after a long time spraying. This is obviously due to the vaporization of the aerosol before reaching the substrate.

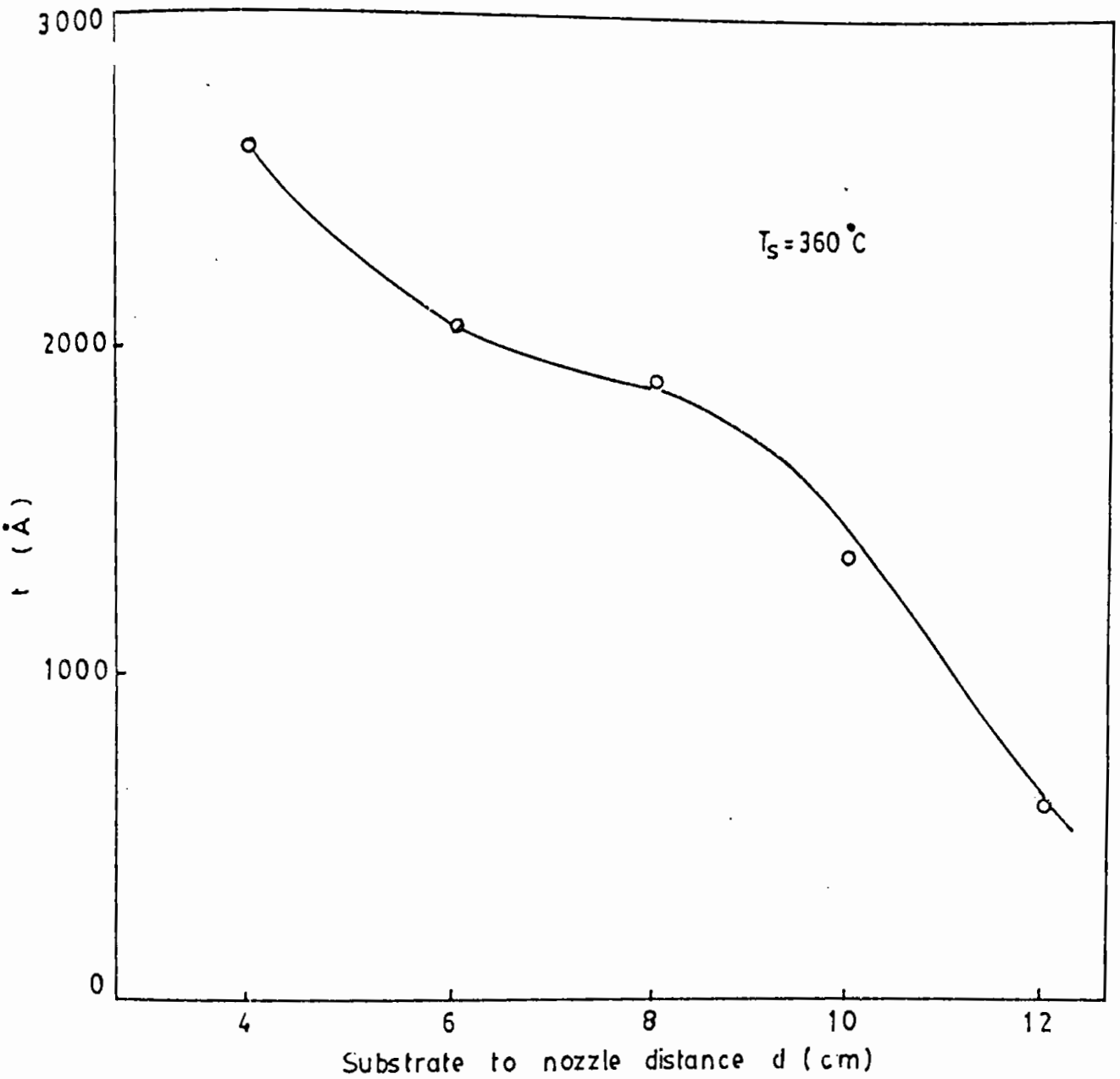

Figure 5.8: Variation of film thickness t, as a function of nozzle distance d (the distance between the substrate and spray nozzle) of ZnO films.

5.9 EFFECT OF SPRAY RATE ON THE RESISTIVITY, CARRIER CONCENTRATION AND HALL MOBILITY

In figure 5.9, the variation of carrier concentration n, mobility μ and resistivity ρ as a function of spray rate has been shown. All the films show n-type conductivity in Hall measurement. Both n and μ increase with increasing spray rate and reach to maximum around 0.8 ml/min of spray rate. Resistivity ρ attains its minimum value at this rate. Above this spray rate n and μ tend to decrease whilst ρ tends to increase. At higher solution flow rate the quality of the film becomes poorer. This happens perhaps due to the presence of unreacted species of Zinc acetate[8].

5.10 THE DEPENDENCE OF SHEET RESISTANCE ON THE FILM THICKNESS

Figure 5.10 shows the dependence of sheet resistance $R_{\square}$ on the film thickness. It is observed that sheet resistance $R_{\square}$, decreases as the film thickness increases. In the lower range of thickness a sharp increase in the sheet resistance is observed but in the higher range of thickness $R_{\square}$ tends to become almost independent of t.

This behavior is related to the sheet resistance size effects of spray deposited films. The effect comes into play in ZnO films significantly only below a thickness of about 1500 Å and above this thickness bulk properties may set in[9].

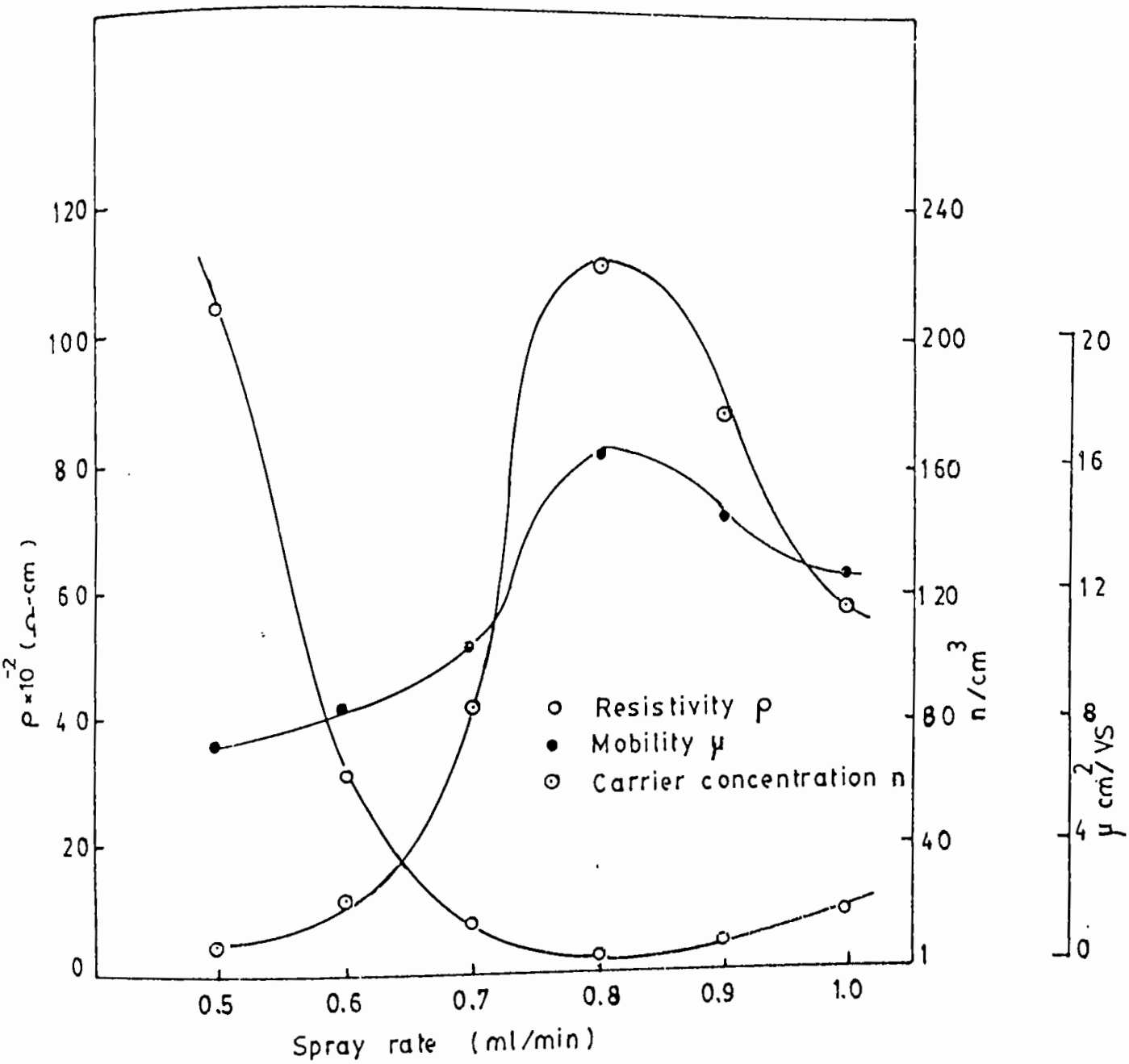

Figure 5.9 : Variation of carrier concentration n, mobility μ and resistivity ρ as a function of spray rate of ZnO films.

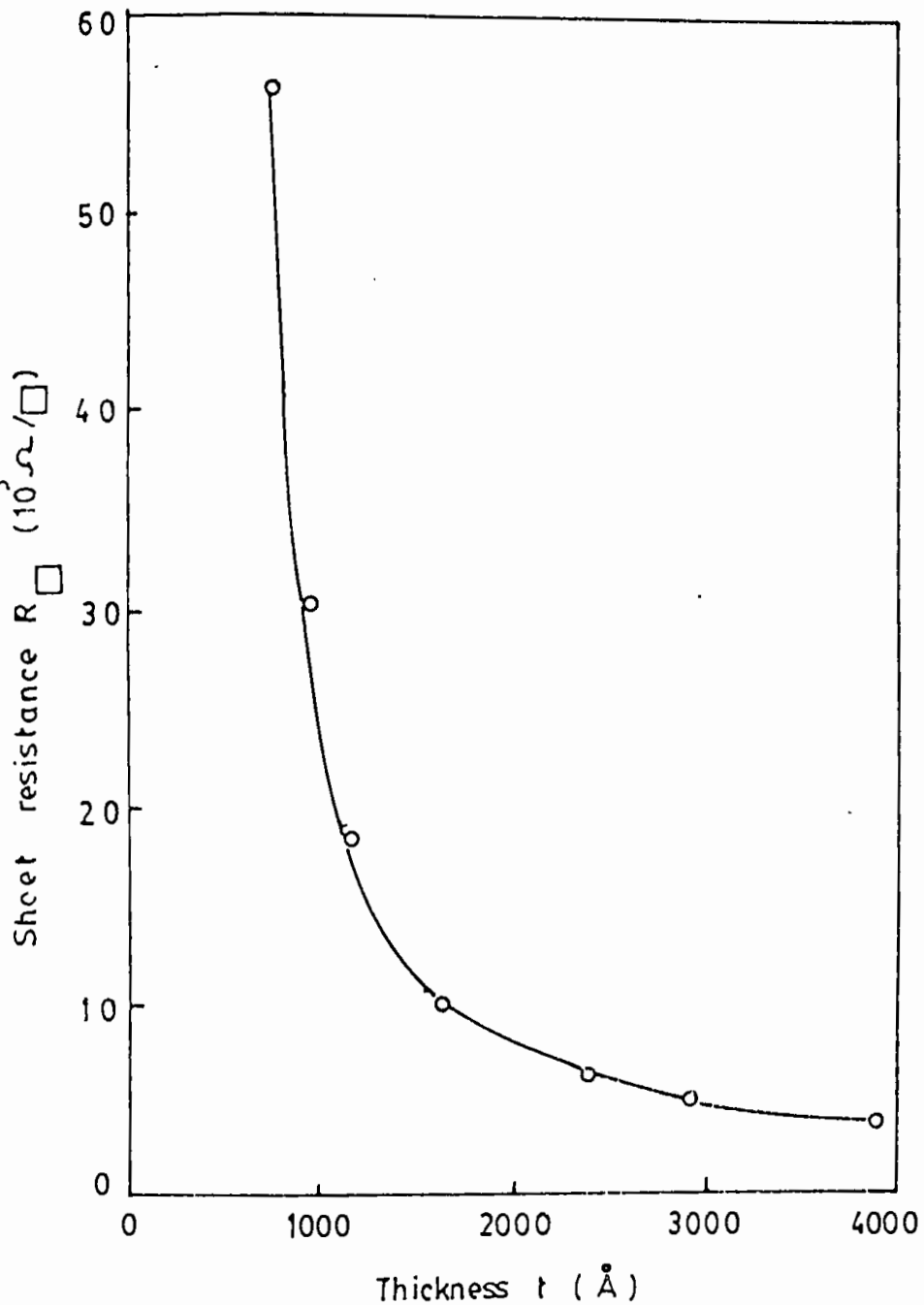

Figure 5.10: Thickness dependent of sheet resistance $R_{\square}$ of ZnO films.

5.11 EFFECT OF FILM THICKNESS ON THE CARRIER CONCENTRATION, MOBILITY AND RESISTIVITY

Figure 5.11 shows the thickness dependence of carrier concentration n, mobility μ and resistivity ρ for vacuum annealed undoped ZnO films. From the figure it is seen that the resistivity ρ increases very slowly with the decrease of thickness t, down to 1500 Å as of $R_{\square}$, and bellow this thickness a sharp increase of ρ is observed.

In the lower range of thickness n and μ are very sensitive to the film thickness t, but in the higher range of t, the dependence is rather feeble. This behavior may be attributed to the increase in grain size of the film with the increase in film thickness[10]. The increase in resistivity as observed with decreasing film thickness of the vacuum annealed films is mainly due to a decrease in Hall mobility. Chopra et al[10] suggested that the decrease in mobility is attributed to a decrease in grain size with thickness.

5.12 AGING EFFECT

Figure 5.12 shows the plot of conductivity σ against aging time T_{da}. Six samples were selected for this experiment. Four of these were undoped and other two were indium doped. For the undoped samples, the substrate temperatures were different e.g for sample no. 1 and 2 it was 360°C and for no. 3 and 4 it was 330°C and 300°C respectively. For In-doped samples (no.5 and 6), the substrate

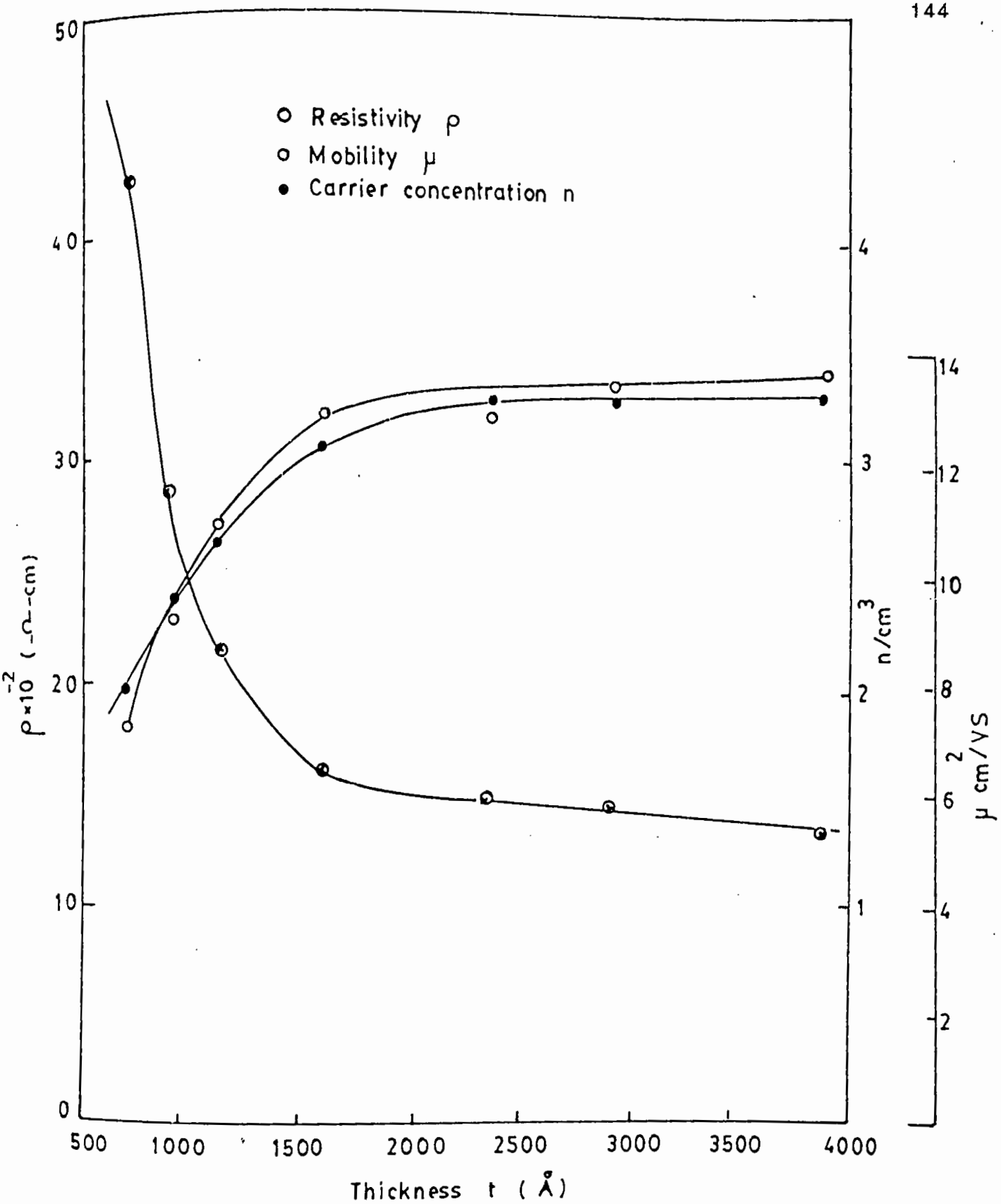

Figure 5.11: The thickness dependence of carrier concentration n, mobility μ and resistivity ρ of ZnO films.

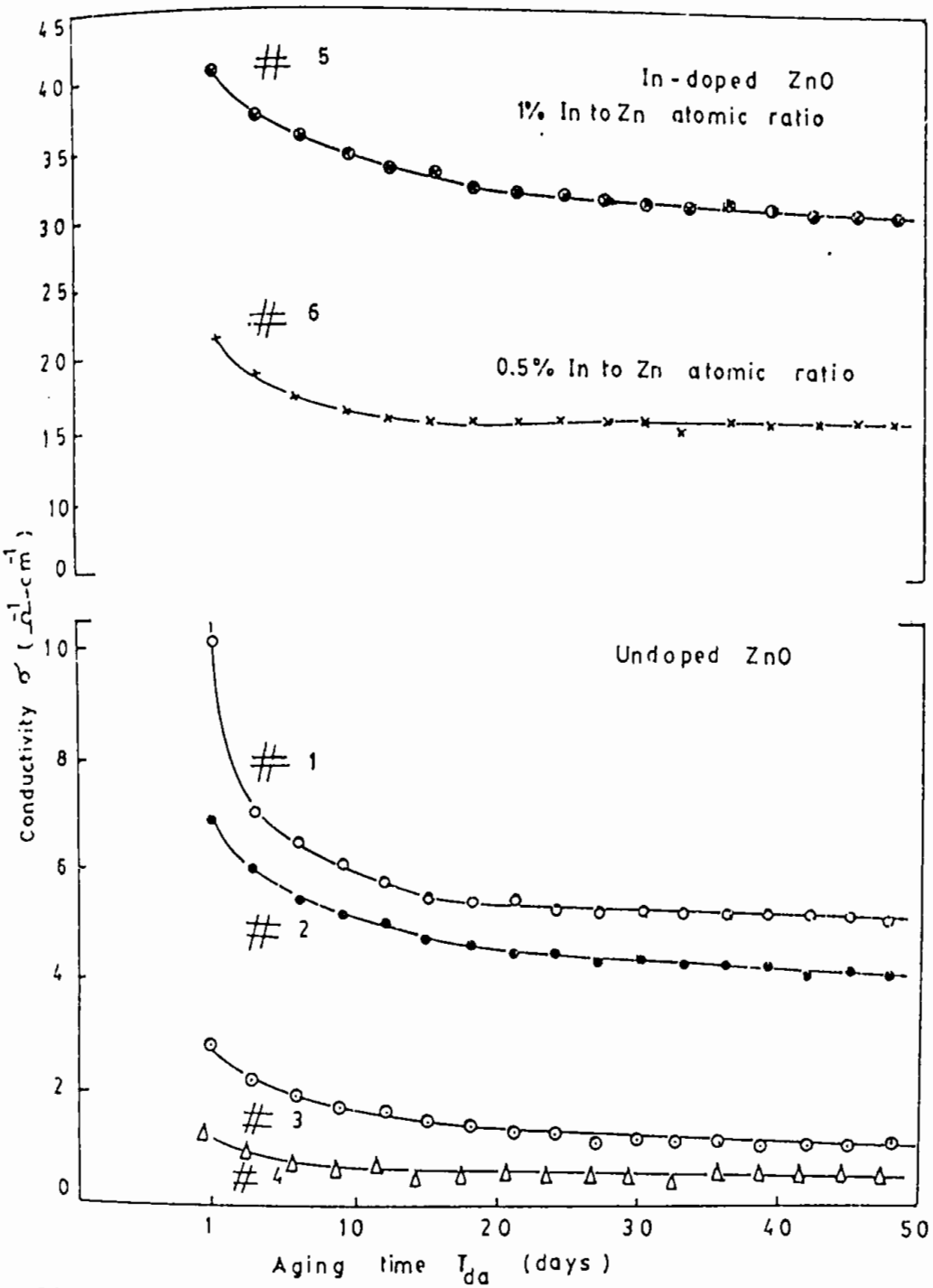

Figure 5.12: The plot of conductivity σ against aging time T_{da} of ZnO films.

temperature was 360°C. Their doping concentration have been shown in the figure. Measurements were performed in open air at room temperature. The samples were previously vacuum heat treated and they were kept in open atmosphere during the observation period. It is found from the figure that 30—50% of the films' conductivity decreases within the first two weeks of the deposition for undoped samples whereas 20—30% fall was noticed for In-doped samples during the same period. After this change, σ remains almost constant for all the samples during the rest of the period. Similar observations have been reported by other workers[7,11,12]. This decrease in conductivity can be interpreted in terms of oxygen absorption because further heat treatment in vacuum returns the films' original condition.

5.13 EFFECT OF DOPING

Doped ZnO films were prepared at a constant substrate temperature T_s=360°C using different doping concentrations. The films were doped with In. $InCl_3$ was used as a doping agent. In working solution 0.5-8 at% of In (In to Zn atomic ratio) was used for the present study.

Figure 5.13 and 5.14 show the variation of ρ, μ and n of ZnO film with the In-doping concentrations in the working solution. Figure 5.13 gives the results for the as-deposited In-doped samples whereas figure 5.14 shows the same when the samples where vacuum heat treated. From these figures it is observed that the nature of

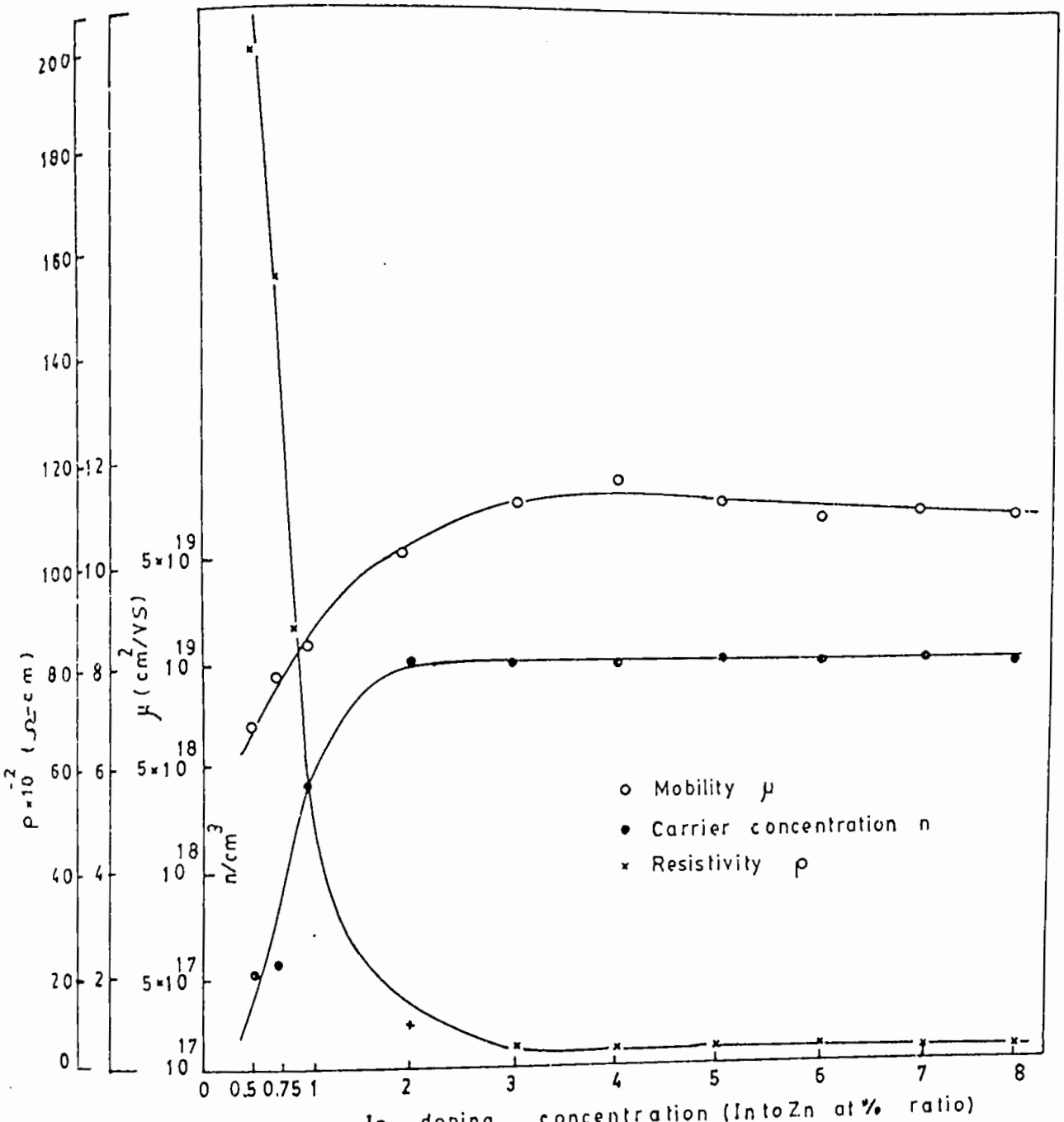

Figure 5.13: Variation of ρ, μ and n of ZnO films with the In - doping concentration for as-deposited samples.

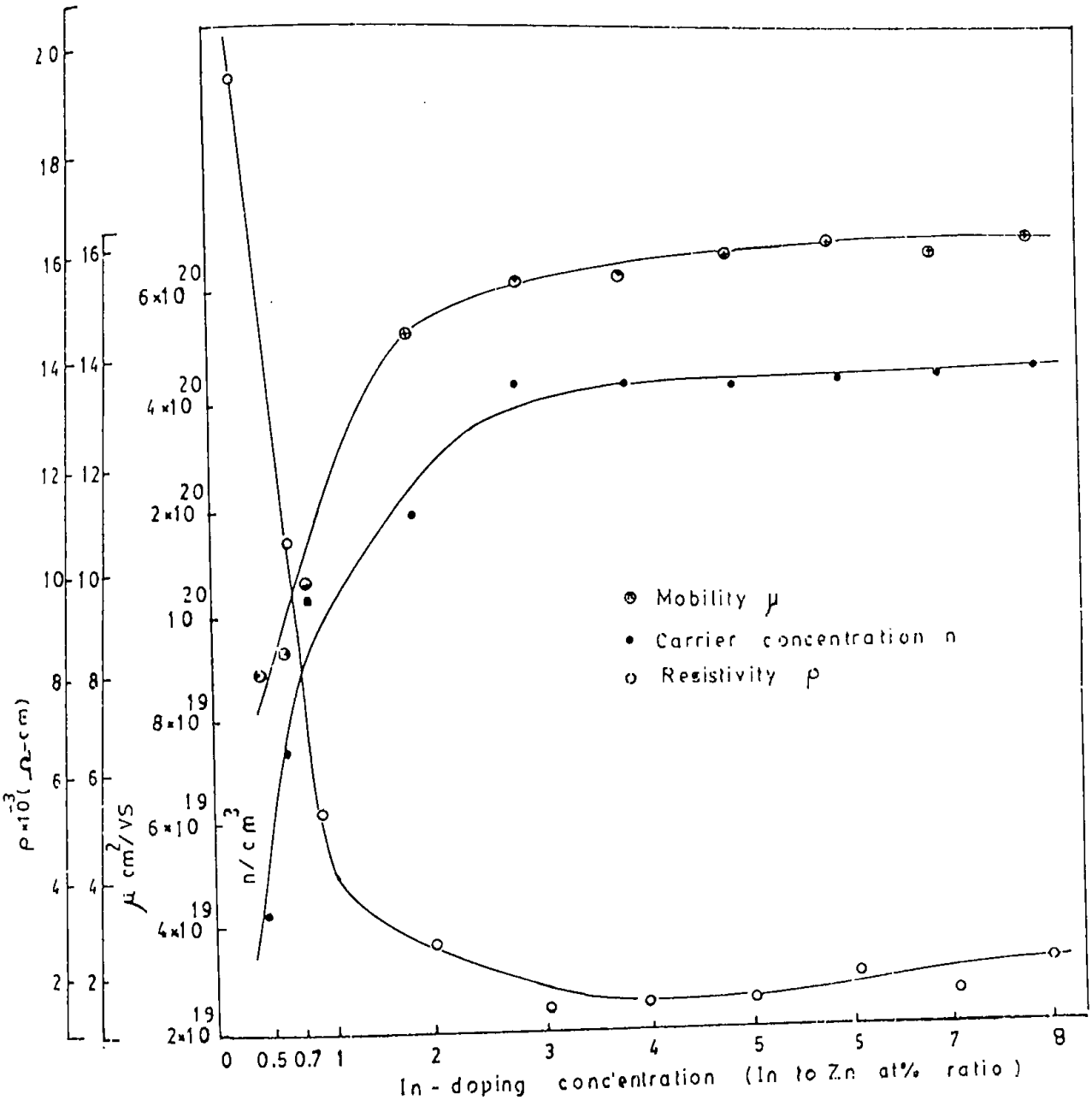

Figure 5.14: Variation of ρ, μ and n of ZnO films with the In-doping concentration of vacuum heat treated samples.

variations of ρ, μ and n of the films with the In-doping levels are almost similar in both as-deposited and vacuum heat treated films having differences only in magnitude of their values. In-doping causes to decrease the film resistivity substantially. The doping mechanism has efficiently improved the values of the electrical parameters of the films but they could not be free from the chemisorption effect during film deposition process. The indium dopant concentration is by far the most critical parameter to affect the electrical properties of these films, which is evident from figure 5.13 and figure 5.14. n increases with dopant concentration until it saturates at a value of about $6X10^{20}$ cm^{-3} at about 3 at% In for the case of vacuum heat treated films and about 10^{19} cm^{-3} at the same concentration of In for the case of as-deposited films. However, μ increases sharply to saturate at about 11 cm^2/VS for the as-deposited films. This sort of behaviour is expected in a micropolycrystalline materials with a high impurity and interface trap density and can be understood on the basis of a grain boundary trapping model[13,14]. Similar observations have been made by Seto[15] on polycrystalline silicon. The gross increase of electrical conductivity of doped as-deposited films is due to the additional donor levels in the doped material. Indium initially replaces Zn in ZnO lattice, while its role as a donor leads to increase the carrier concentration of 3 orders of magnitude for the as-deposited In-doped films. Zn is divalent element whereas Indium is trivalent one. Two valence electrons of

In forms covalent bonds but the remaining 1 (one) valence electron of In atom contributes to the conduction process. Zn has a smaller atomic diameter than In [atomic radius Zn: 1.38 Å, In: 1.66Å[16]]. So doping efficiency should not be very good and saturation may take place as discussed below.

The saturation of n occurs at a dopant concentration above 3 at% of In probably because at a constant substrate temperature ($T_s \approx 360^{\circ}C$) and limited doping efficiency. The energies that are acquired by the dopant atom from this substrate temperature limit to enter further In in the ZnO lattice and gives the saturation of n. When the films are heat treated in vacuum the trap stats localized at the grain boundaries are annihilated.As a result both n and μ are increased in their magnitudes but saturations of them till remained. Besides this μ may also be increased due to the increase of grain size.

5.14 OPTICAL TRANSMISSION, REFRACTIVE INDEX AND BAND GAP

Figure 5.15 shows the optical transmission spectra of undoped ZnO films of various thicknesses. Measurements have been taken in the wavelength range 3000 Å to 9000 Å on both as-deposited and vacuum heat treated films. No detectable change was found in the optical transmission due to heat treatment. In the case of doped films the optical transmission remained unaltered within the present doping concentration range.

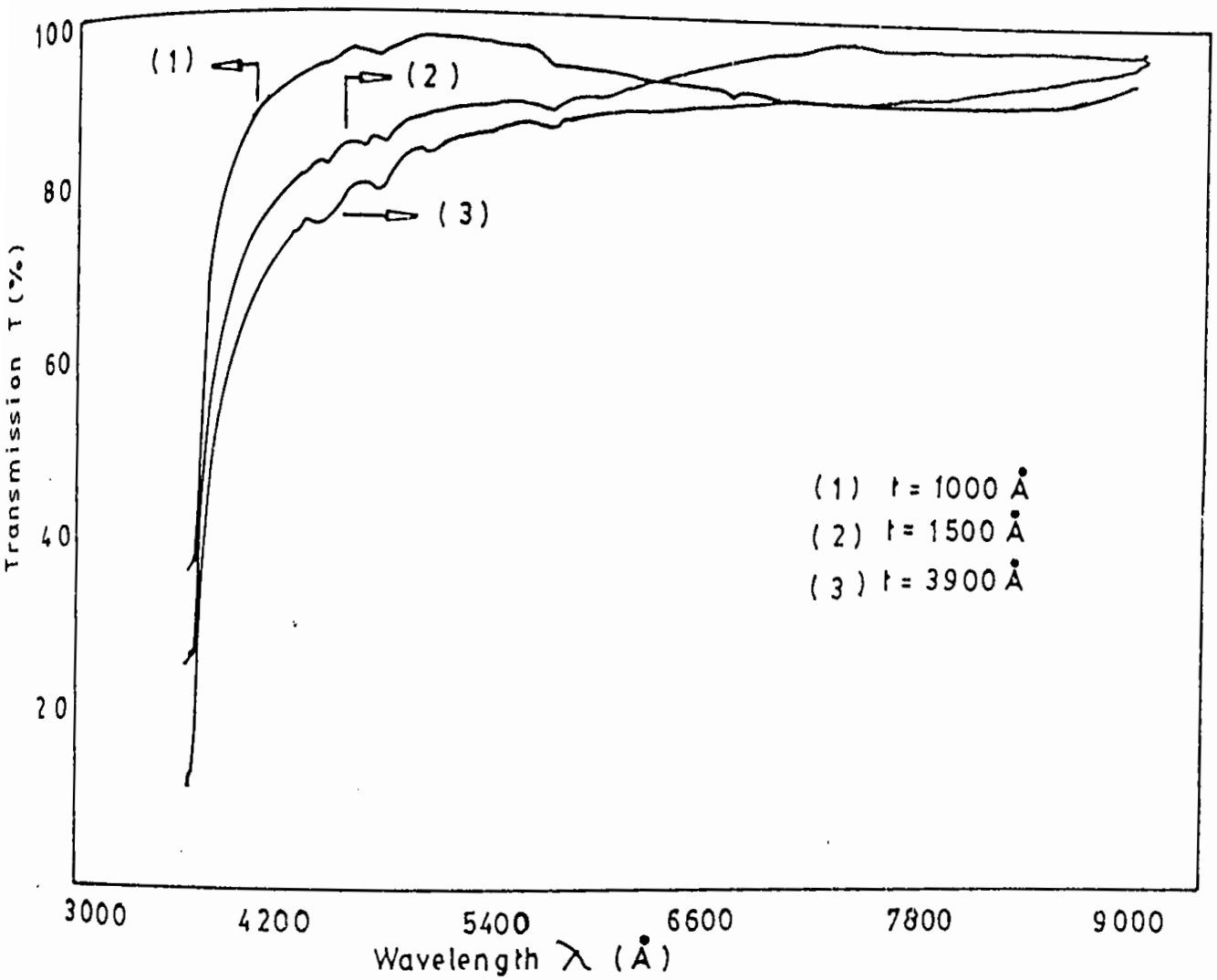

Figure 5.15: The plot of transmission T(%) vs. wavelength λ (Å) of ZnO films.

The transmission co-efficient T(%) is found about 96% for undoped films at wavelength around 5400 Å for the films of thickness below 2000 Å. At higher thiickness a decrease in transmission is obviously observed. All the samples were found to show a sharp UV cut off at about 3700 Å.

The refractive index was calculated from the transmission data. The values of refractive index lie between 1.57 and 2.05 at about 4600 Å in the visible range of the optical spectra. Higher values of refractive indices were also obtained in the films of higher thickness. The obtained value agreed with the reported value of 2 for ZnO crystal[17]. Since the ZnO films are found highly transparent between visible to near infrared region, the reflection co-efficient R has been neglected in calculating the absorption co-efficient in this region. The absorption co-efficient α can be directly determined from the transmission spectra using the relation

$$\alpha = \frac{In\frac{1}{T}}{t} \quad \ldots\ldots\ldots\ldots \quad 5.1$$

where t is the film thickness and T is the transmittance. Assuming that the transition probability becomes constant near the absorption edge, the absorption co-efficient α for direct allowed transition for a simple parabolic band scheme can be described as a function of incident photon energy $h\nu$ as

$$\alpha \propto \frac{(h\nu - E_g)^{\frac{1}{2}}}{h\nu} \quad \ldots\ldots\ldots\ldots \quad 5.2$$

where E_g is the optical band gap. Figure 5.16 shows the plot of $(\alpha h\nu)^2$ against $h\nu$ for a few samples with different carrier concentrations having same thickness. The films of different carrier concentrations were obtained by mere addition of different amounts of dopant in the working solution. One of the samples of figure 5.16 is undoped and the rest of them are In-doped. The values of E_g have been determined by extrapolating the linear portion of the curves to zero absorption line.

It is observed from the figure that fundamental absorption edge shifts gradually towards higher energies (shorter wavelength) with increasing carrier concentration. This effect of widening of the band-gap is attributed primarily to the Burstein-Moss shift in semiconductor,[18] but more detailed analysis has been presented elsewhere[19]. It is noticed from this figure 5.16 that the values of E_g = 3.21 eV at a carrier concentration of 6.5 X 10^{17} cm^{-3} increases upto 3.37 eV for a sample with carrier concentration of 2.4 X 10^{20} cm^{-3}. These values are in good agreement with the reported values [2,6,20]. The variation of Eg with film thickness was not noticeable. No remarkable aging effect on E_g was obtained.

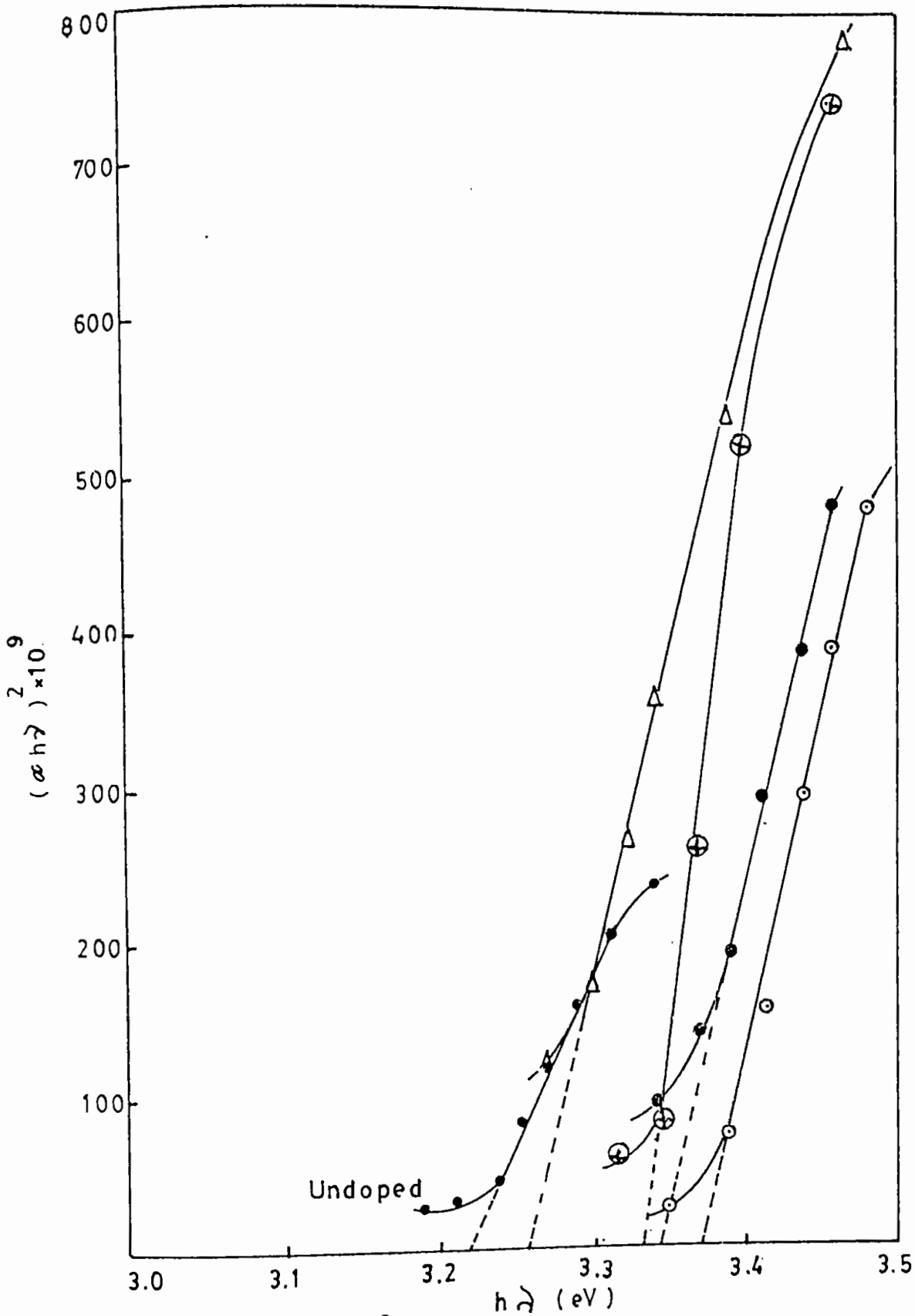

Figure 5.16 : Plot of $(\alpha h\nu)^2$ vs. $h\nu$ showing the shift of absorption edge with respect to the carrier concentration n cm^{-3} of ZnO films.

5.15 FIGURE OF MERIT OF THE LAYER

The figure of merit ϕ_{TC} [where $\phi_{TC} = T^{10}/R_{\square}$] as presented by Haacke for a transparent conductor has been calculated for these films. Highest ϕ_{TC} was obtained to be $0.64 \times 10^{-4}\ \Omega^{-1}$ for an undoped film of thickness 1742Å but it has been found to be $116.9 \times 10^{-4}\ \Omega^{-1}$ in the case of In-doped film having the same thickness. The variation of optical transmission T with the sheet resistance $R_{\square}$ at three different wavelengths in the visible region has been presented in figure 5.17 for undoped films. This implies no significant variation of optical transmission with sheet resistance except in lower wavelength side.

5.16 POST DEPOSITION HEAT TREATMENT OF ZnO FILM

The temperature dependence of resistivity ρ, Hall mobility μ and carrier concentration n of some as-deposited films of ZnO with thickness of about 1730Å have been studied between 30° and 200°C. The films were of various substrate temperatures viz. 300, 330, 360 and 390°C.

Due to heat treatment, several mechanisms may take part in bringing about the following changes in the film.

(i) Recrystallization of the amorphous part of the film

(ii) Reorientation of the existing crystallites.

(iii) Changes of frozen-in stresses and generation of internal stresses in the films and

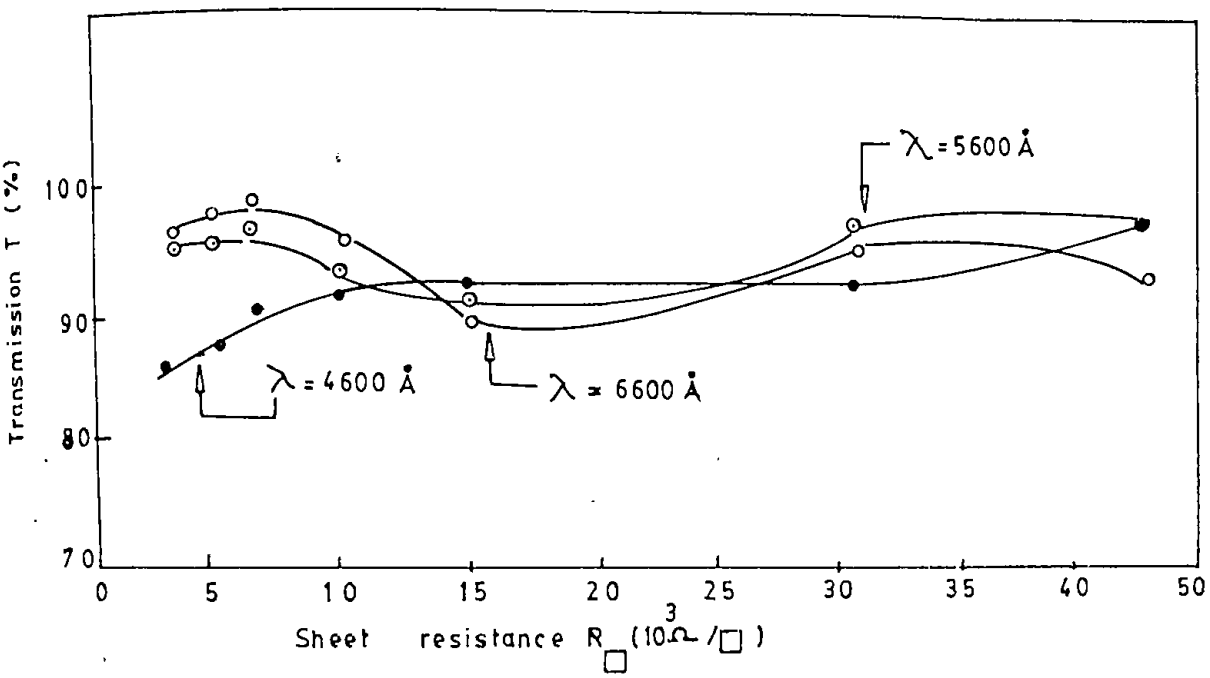

Figure 5.17: The plot of Transmission T (%) vs. sheet resistance at three different wavelengths. (a) $\lambda = 4600$ Å, (b) $\lambda = 5600$ Å, (c) $\lambda = 6600$ Å.

(iv) Oxygen chemisorption/desorption mechanism at the grain boundaries of the film.

All the above mechanisms may not be equally important for the present case. The deposition temperature of the films was 360°C which is much greater than the post-deposited heat treatment temperature, 200°C, and therefore it is quite likely that mechanism (i) may not take place. The mechanisms (ii) and (iii) are somewhat inter-related. Just et. al. [21] have pointed out that when the elastic stresses on a film decreases during the heat treatment the resistivity decreases simultaneously. These frozen-in stresses and the random orientation of the crystallites were produced in the film during their initial period of nucleation and this probably depends on the cooling rate of the film after the completion of deposition.

It may be mentioned here that the linear co-efficient of thermal expansion of semiconducting ZnO crystalline material is $\approx 4 \times 10^{-6}/°C$ in the direction perpendicular to the c-axis, whereas that of the glass substrate is $\approx 9 \times 10^{-6}/°C$. Therefore during the initial period of cooling of the film there is some possibility of stresses to be locked-in. In the subsequent heat treatment these stresses may be minimized. Mechanism (iv) is considered to be the most important here because of the polycrystalline nature of the oxide films and it is discussed later in article 5.16 (ii).

The experimental curves of figure 5.18 as obtained in this study have now been analysed in the light of the above discussion. The variation of resistivity with temperature for a typical undoped ZnO sample is shown in this figure. [The sample is undoped in the sense that no intentional dopant was used during deposition. But various crystal defects and impurities from the starting material may be present in the film]. It can be observed in this figure that the heating and cooling cycles are almost irreversible in the investigated range of temperature. During the first step of heat treatment, a virgin sample shows a sharp decrease of its resistivity when a temperature of about 100°C is reached. From room temperature to 100°C the variation of the resistivity with temperature is not very significant. This type of behaviour was observed for all the studied samples irrespective of their deposition temperature.

In this figure, BC represents the fall of the resistivity in one hour at a temperature of 200°C. In the reverse cycle of cooling i.e. CD, the resistivity does not change remarkably. In the second step of heat treatment, as represented by DE, the resistivity continues to go down gradually until a temperature of 130°C is reached then it remained stable upto 200°C. The cooling cycle EF is similar to CD. FG represents the fall of the resistivity when the sample is heat treated in vacuum at 200°C for an hour. The third step heat treatment on this vacuum annealed film was subsequently carried out in air. GH shows that the variation of resistivity. It

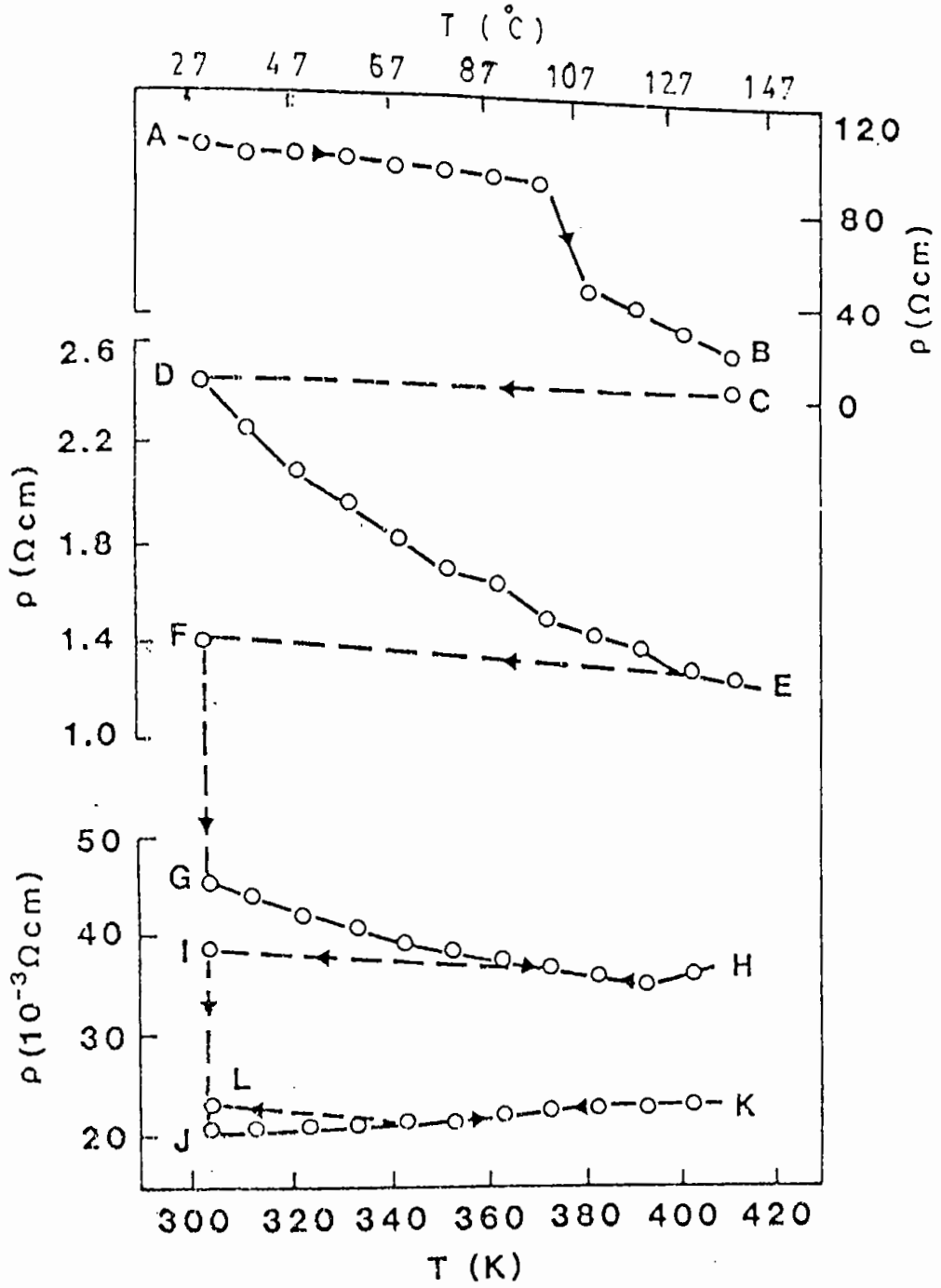

Figure 5.18: Resistivity ρ vs. temperature T for a typical ZnO sample deposited at a substrate temperature of 360°C, Data for successive heatings and coolings are shown, with arrows indicating temperature scan direction. FG and IJ represent drops of the sesistivity during the first and second vacuum heat treatment respectively.

still decreases slowly with temperature up to 117°C and then tends to increase slightly but noticeably. The cooling cycle HI at the beginning follows partially the heating cycle GH. This cycle is thus somewhat reversible. The drop of the resistivity in GH is relatively smaller than that 2nd cycle in DE. "IJ" shows the drop of resistivity due to second vacuum heat treatment. Finally, JK shows the results of the fourth heating cycle in air, and this time the resistivity displays a weak increase with increasing temperature. The reverse cycle of cooling, KL, mostly follows the heating cycle except in the last portion. Thus this cycle is also partially reversible. During the variation of resistivity ρ the carrier concentration n and the Hall mobility μ were also found to very with temperature. All of the samples exhibit n-type conductivity.

It is known that pyrolytically deposited ZnO films with deposition temperature >250°C are polycrystalline in structure[22,23]. Our samples were of small-grain structure uniformly distributed over the substrate surface [article, 5.1]. During the film deposition, and since air was used as a carrir gas, it is likely that a large number of oxygen molecules are chemisorbed in the film, both at the grain boundaries and on the surfaces; these molecules are unable to come out at the end of the deposition due to the rapid rate of cooling of the film. It seems that, in the virgin state of the film, these molecules have an empirical binding energy of about 0.032 eV (≈ 100°C). When this energy is supplied to

the sample in a post deposited heat treatment (i.e. during the first heating cycle), the molecules come out of the sample, and the resistivity drops down.

A detail explanation for the nature of the chemisorption on ZnO films has been given by Fujita et. al.[5], whose predictions were experimentally confirmed by Chang[24]. It was pointed out that the principal chemisorption species in ZnO is O^-_2 at low temperatures, and as the temperature of the sample rises the chemisorbed O^-_2 is desorbed from the sample surface donating an electron to ZnO [$O^-_2 \rightarrow O_2 + e$], and hence the conductivity goes up rapidly. The initial sharp fall of the resistivity above 100°C may thus be mainly a surface effect.

The second step of heat treatment is the most significant one, and we can apply conventional semiconductor theory to calculate various energy band parameters.

5.16(i) DONOR IONIZATION ENERGY

Although the samples are undoped, they are extrinsic and polycrystalline in structure. The electrical conductivity in such a film is mainly controlled by the impurity level. The carrier concentration n shows a temperature dependence, which can be represented by a conventional expression[25]

$$N = (n_c N_d)^{\frac{1}{2}} \exp(-E_d/2k_B T), \qquad (5.3)$$

where E_d is the donor ionization energy, N_d is the donor density, and

$$n_c = 2\left(\frac{2\pi m_e^* K_B T}{h^2}\right)^{\frac{3}{2}}$$

By plotting $\ln(nT^{-3/4})$ against $1/T$, one can calculate E_d. Figure 5.19 shows such plots, and the calculated values are given in table 5.1. The donor levels are shallow and are mainly due to the native defects such as interstitial Zn and oxygen vacancies.

Considering a hydrogenic model for the system, the effective electron mass m_e^* can be calculated using the relation,[25]

$$E_d = e^4 m_e^* / (2\epsilon^2 \hbar^2) \quad . \quad . \quad . \quad . \quad . \quad . \quad . \quad . \quad . \quad (5.4)$$

The value of ϵ involbed in this calculation is ϵ=8.5 taken from ref (26). Calculated values of m_e^* are given in table 5.1.

The position of the Fermi level E_F can be obtained from[25]

$$E_F = -\frac{1}{2}E_d + \frac{1}{2}(K_B T)\ln[N_d h^3/2(2\pi m_e^* K_B T)^{3/2} \quad . \quad . \quad . \quad (5.5)$$

Calculated values of E_F, with reference to the conduction band edge, are given in table 5.1. It can be observed that the Fermi levels in samples 2-4 lie near to but just above the donor levels E_d. In sample 1, E_F lies just below E_d. N_d is greater than n in samples 2-4, which is characteristic for an uncompensated

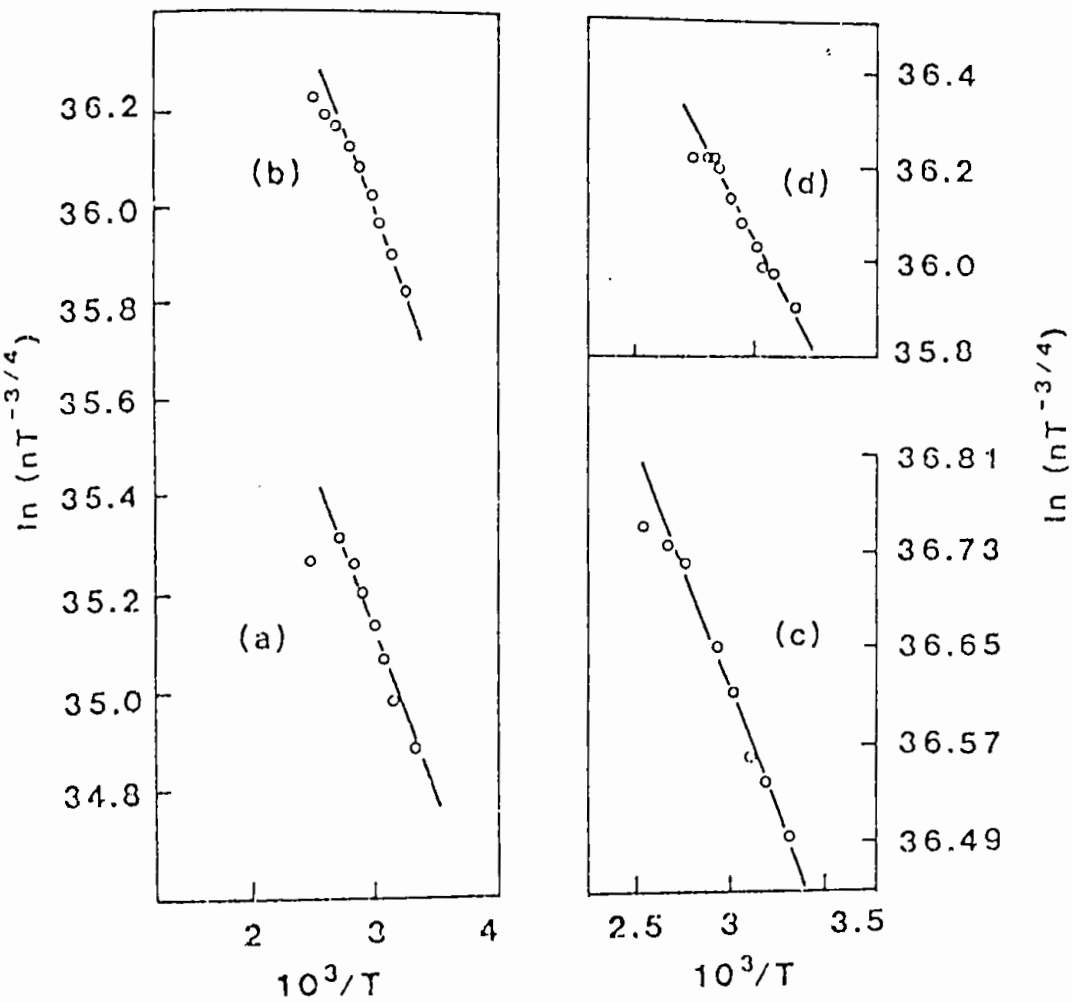

Figure 5.19 : $\ln(nT^{-3/4})$ vs. T^{-1} for samples deposited at substrate temperatures, 300°C(a), 330°C(b), 360°C(c) and 390°C(d), n is carrier concentration and T is temperature.

semiconductor. In sample 1, with a lower deposition temperature, probably a larger number of acceptor states is present[27], which reduce the donor density and also pulls the Fermi level to an energy just below the donor level. Barnes et. al.[28] pointed out that some acceptor states in ZnO may arise due to the presence of chemisorbed oxygen at the grain boundary region, and they may also come from point defects such as interstitial oxygen and Zn vacancies[2] and from the departures from stoichiometry. In polycrystalline thin film samples the carrier concentration may be reduced significantly due to trapping of carriers at the grain boundaries. This behaviour, as was observed in sample 1, has been termed auto-compensation by Amick[29]. It has been modeled by Bernarczyk et. al.[30].

TABLE 5.1: Parameters for ZnO films deposited at substrates temperature T_s. [m_e is the free-electron mass and temperature co-efficient of resistance is TCR]

Sample NO	T_s (°C)	ρ (Ω-cm)	n ($10^{17}cm^{-3}$)	E_d (eV)	E_F (eV)	N_d ($10^{17}cm^{-3}$)	m_e^*/m_e	TCR (10^{-3}/deg.)
1	300	14.5	1.1	0.112	0.12	0.92	0.59	-5.1
2	330	11.0	2.7	0.113	0.10	4.3	0.60	-4.0
3	360	2.44	5.1	0.069	0.061	7.5	0.36	-4.4
4	390	3.13	2.9	0.079	0.075	4.6	0.42	-4.7

5.16(ii) GRAIN BOUNDARY PARAMETERS

In polycrystalline samples, the electrical properties are largely controlled by grain boundary effects. Grain boundary trapping models[13,31] indicate that when the trapp states in the grain boundary region are occupied, they create a depletion region in the grain and a potential barrier at the interface. Under these conditions, and if the grain size l is larger than twice the Debye Screening length L_D the measured mobility μ is thermally activated with activation energy ϕ_b which is the barrier height at the grain boundary[13]. In extrinsic nondegenrate samples, thermally activated mobility can be accounted for by[31]

$$\mu = \mu_o T^{-1/2} \exp(-\phi_b / K_B T) \quad . \quad . \quad . \quad . \quad . \quad . \quad . \quad (5.6)$$

Here

$$\mu_o = el/(8\pi m^*_e K_B)^{1/2} \quad . \quad . \quad . \quad . \quad . \quad . \quad . \quad . \quad (5.7)$$

This μ_0 is a constant that depends on the grain size l. In our samples, the carrier concentrations are of the order of $\approx 10^{17}$ cm^{-3}, and the position of the Fermi level indicates that the samples are nondegenerate. Plotting $\ln(\mu T^{1/2})$ as a function of 1/T, ϕ_0 can be determined. Figure 5.20 shows such plots, from which it can be seen that the mobility is thermally activated in the investigated temperature range. Calculated values of ϕ_0 are given in Table 5.2.

The grain size might be estimated from equation (5.7) if one uses measured values of μ and ϕ_0 at room temperature. This procedure would not be entirely correct, since equation (5.6) is strictly valid when the mobility is limited mainly by the grain boundaries. An improved value of μ_0 can be obtained by using μ_g in place of μ in equation (5.6) where the approximation is based on Mattiessen's rule.

$$\frac{1}{\mu} = \frac{1}{\mu_g} + \frac{1}{\mu_s} \quad . \quad . \quad . \quad . \quad . \quad . \quad . \quad . \quad . \quad (5.8)$$

Here μ_g is the grain boundary limited mobility, and μ_s is the corresponding mobility if the sample were a single crystal and had the same structure as the film. s an approximation, the bulk value of μ can be taken for μ_s. We have obtained μ_s from the intercept in

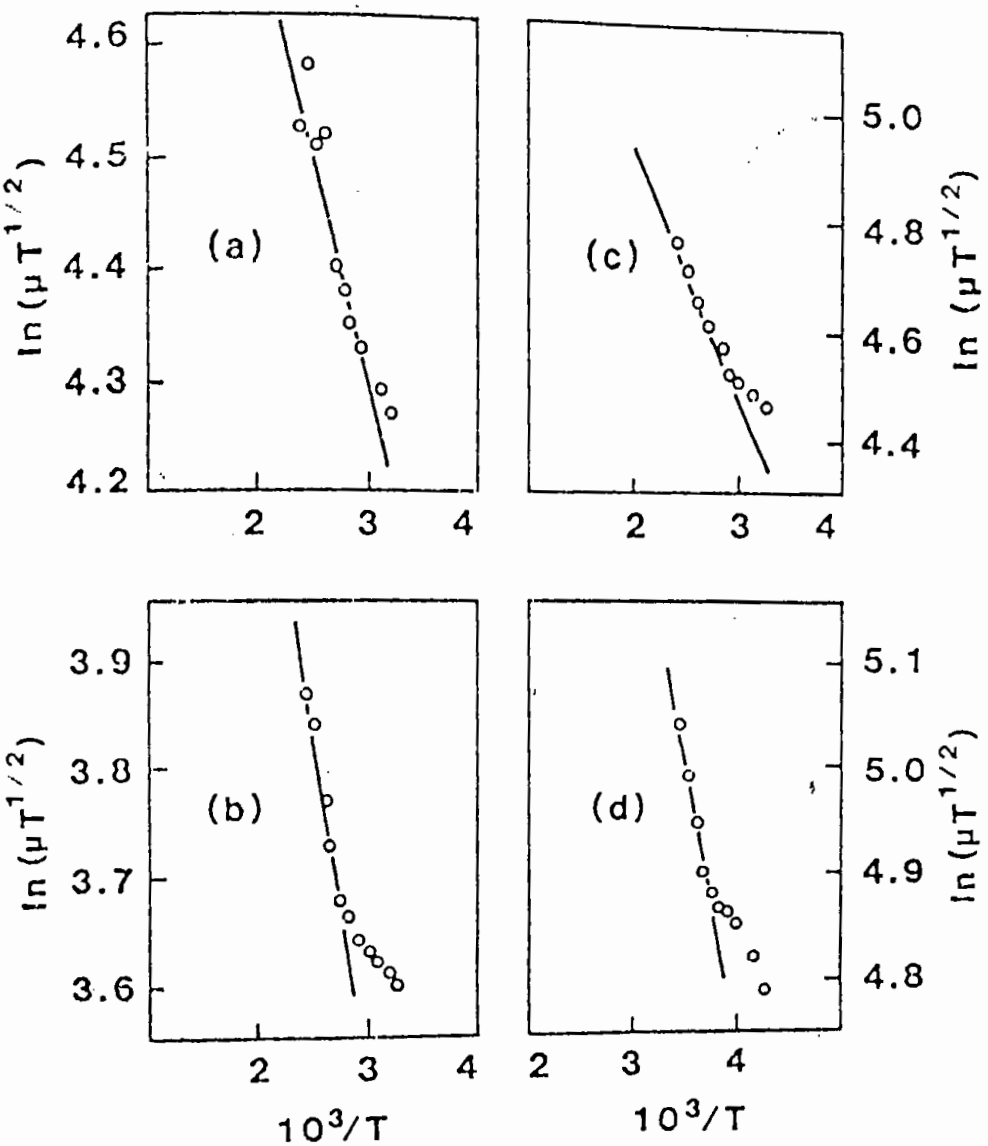

Figure 5.20: $\ln(\mu T^{1/2})$ vs. T^{-1} for samples deposited at substrate temperatures 300°C(a), 330°C,(b) 360°C and 390°C(d), μ is mobility and T temperature.

an μ versus 1/t plot, where t is the film thickness. Such a plot is given in Figure 5.21. Calculated values of grain size are shown in the table 5.2; they are of expeted magnitude. The analysis shows that a higher deposition temperature favours the formation of larger grains, which agrees well with our electron microscope observations as stated earlier.

TABLE 5.2: The grain boundary parameters for ZnO films [Hall mobility μ, grain boundary barrier height ϕ_b interface trap density N_t, carrier concentration in the barrier region n_b, grain size l, Debye screening length L_D, and mean free path L.]

Sample No.	T_s (°C)	μ (cm^2/VS)	ϕ_b (eV)	N_t ($10^{11} cm^{-3}$)	n_b ($10^{16} cm^{-3}$)	l (Å)	L_D (Å)	L (Å)
1	300	4.14	0.036	3.8	2.6	36	14	3.0
2	330	2.12	0.051	7.2	3.5	29	12	1.3
3	360	4.96	0.040	8.8	10.0	43	16	3.0
4	390	6.95	0.045	7.0	4.7	100	15	5.8

The Debye screening length can be calculated from a hydrogenic model of the possible donor centres. The pertinent expression[25]

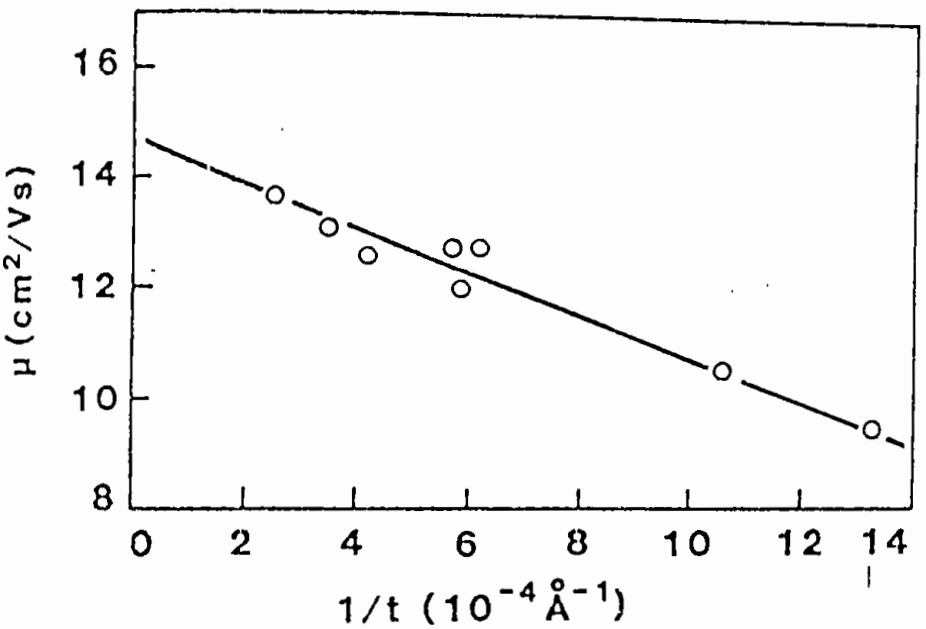

Figure 5.21: Hall mobility μ vs. inverse film thickness t^{-1} for heat treated samples.

$$\frac{1}{L_D^2} = 4n^{\frac{1}{3}}/a_o \quad \ldots\ldots\ldots\ldots \quad (5.9)$$

where a_0 is the Bohr radius for the donor centres. It is given by

$$a_o = \epsilon\hbar^2/m_o^* e^2 \quad \ldots\ldots\ldots\ldots \quad (5.10)$$

From equations. (4.9) and (4.10) we obtain

$$L_D = (\hbar/2e)\,(m_e^* n^{\frac{1}{3}}/\epsilon)^{-\frac{1}{2}} \quad \ldots\ldots\ldots\ldots \quad (4.11)$$

Calculated values of L_D, obtained from equation (5.9), are given in table 5.2. It can be noticed that the condition $2L_D < 1$ appropriate for a grain boundary trapping model is obeyed here. Thus our approach of analysing the data, using the grain boundary trapping model for the thermal activation of mobility, is valid.

The effect of successive heat treatments on the samples is briefly given in table 5.3. Heat treatment is seen to lower the resistivity drastically. The Hall mobility in the virgin samples was relatively difficult to measure, and the values given in table 5.3 are the results of several observations but may still be approximate.

TABLE 5.3: Effect of heat treatment on resistivity, Hall mobility, and carrier concentration.

Sample No.	Resistivity		Hall mobility		Carrier concentration	
	Virgin (Ω-cm)	Min (Ω cm)	Virgin (cm^2/VS)	Max (cm^2/VS)	Virgin (10^{15} cm^{-3})	Max (10^{18} cm^{-3})
1	97	0.22	4.1	16	2.6	1.8
2	99	0.086	4.4	11	13	6.3
3	101	0.02	4.8	13	8.8	29
4	30	0.058	6.9	12	4.0	3.7

Large changes in the Hall mobility occur in the films deposited at lower substrate temperature. In all cases, the mobility was found to increase due to heat treatment. The carrier concentration also increased by several orders of magnitude, although in the virgin film it was hard to measure. In the fourth step of heat treatment, the resistivity, Hall mobility and carrier concentration were almost independent of temperature, which indicates that the desorbable oxygen was exhausted so that the films were relatively stable towards further heat treatment.

In a polycrystalline oxide semiconductor, both oxygen chemisorption and desorption may occur at all temperatures upon heat treatment in air. The domination of a particular process is governed by the respective rates, which are functions of the ambient temperature and of the relative concentrations of the chemisorption species available in the ambient and in the

chemisorption site[32]. Thus upto the third step of heat treatment, the gross decrease of resistivity in the film is due to oxygen desorption processes that lower the grain boundary barrier heights and enhance the Hall mobility and carrier concentration. It seems that at the fourth step, chemisorption starts to dominate.

5.17 ACTIVATION ENERGY OF ZnO FILMS

The carrier activation energy E_a of ZnO films has been determined from the temperature dependence of electrical conductivity σ. Calculation has been carried out using the formula for extrinsic uncompensated semiconductor. For this purpose curves of ln σ versus 1/T for four samples were plotted in the temperature range 30° to 130°C Figures 5.22 and 5.23 show these plots. The samples were prepared at various substrate temperature as shown in the figure. It was observed that due to vacuum heat treatment, the values of the activation energy was reduced to about 50 -- 60% of its value for the as-deposited sample. The calculated values of E_a in the above temperature range is shown in table 5.4. In both cases films of higher substrate temperature possess lower values of activation energy. This is probably due to increase in stoichiometry of the film with the increase of substrate temperature. The reduction of activation energies in their values for the case of vacuum heat treated films can be interpreted in such a way that major number of impurity atoms have been completed their ionization process during vacuum heat treatment.

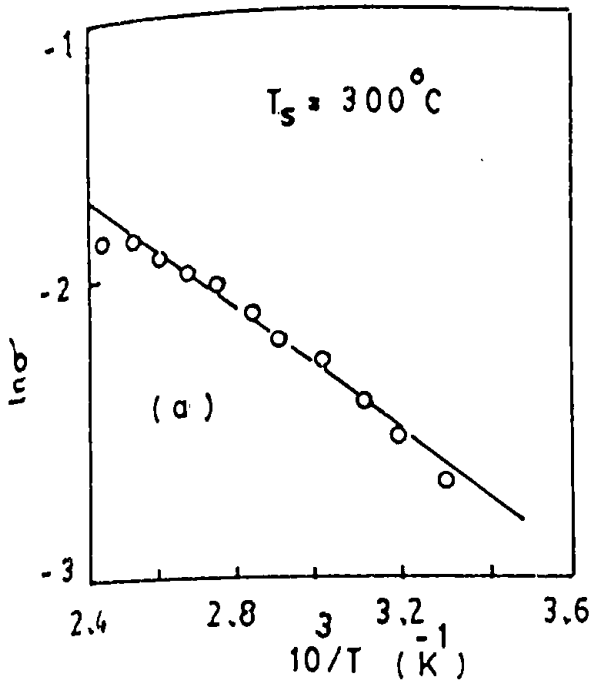

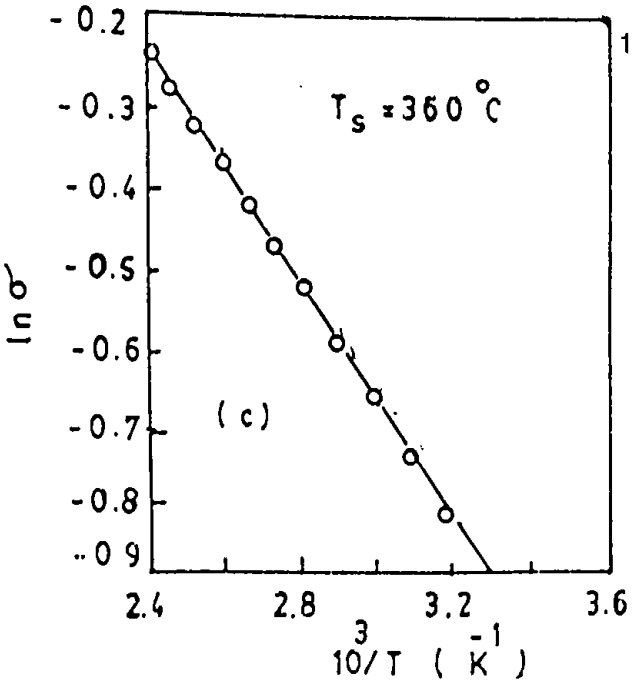

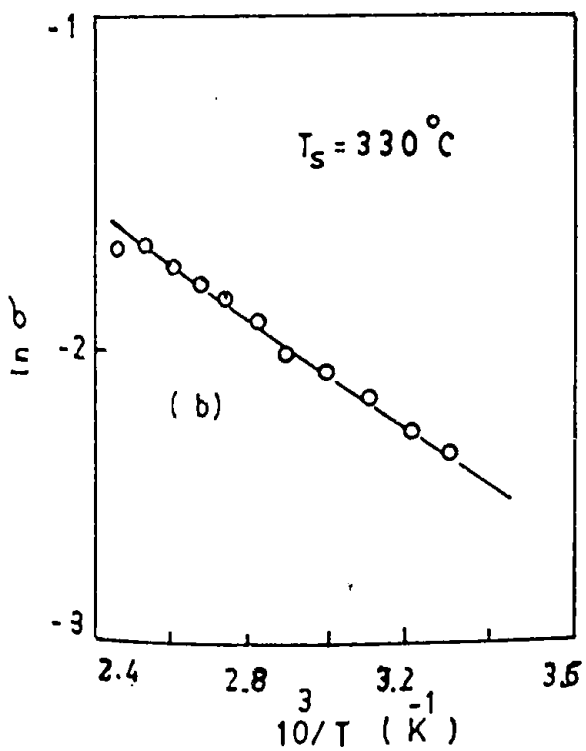

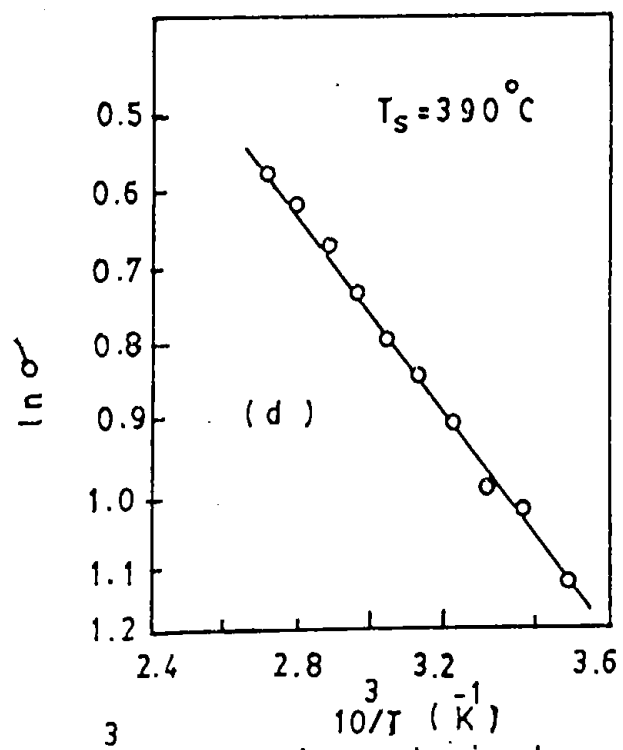

Figure 5.2 2: Plot of $\ln \sigma$ vs. $10^3/T$ for four typical as-deposited ZnO; In films.

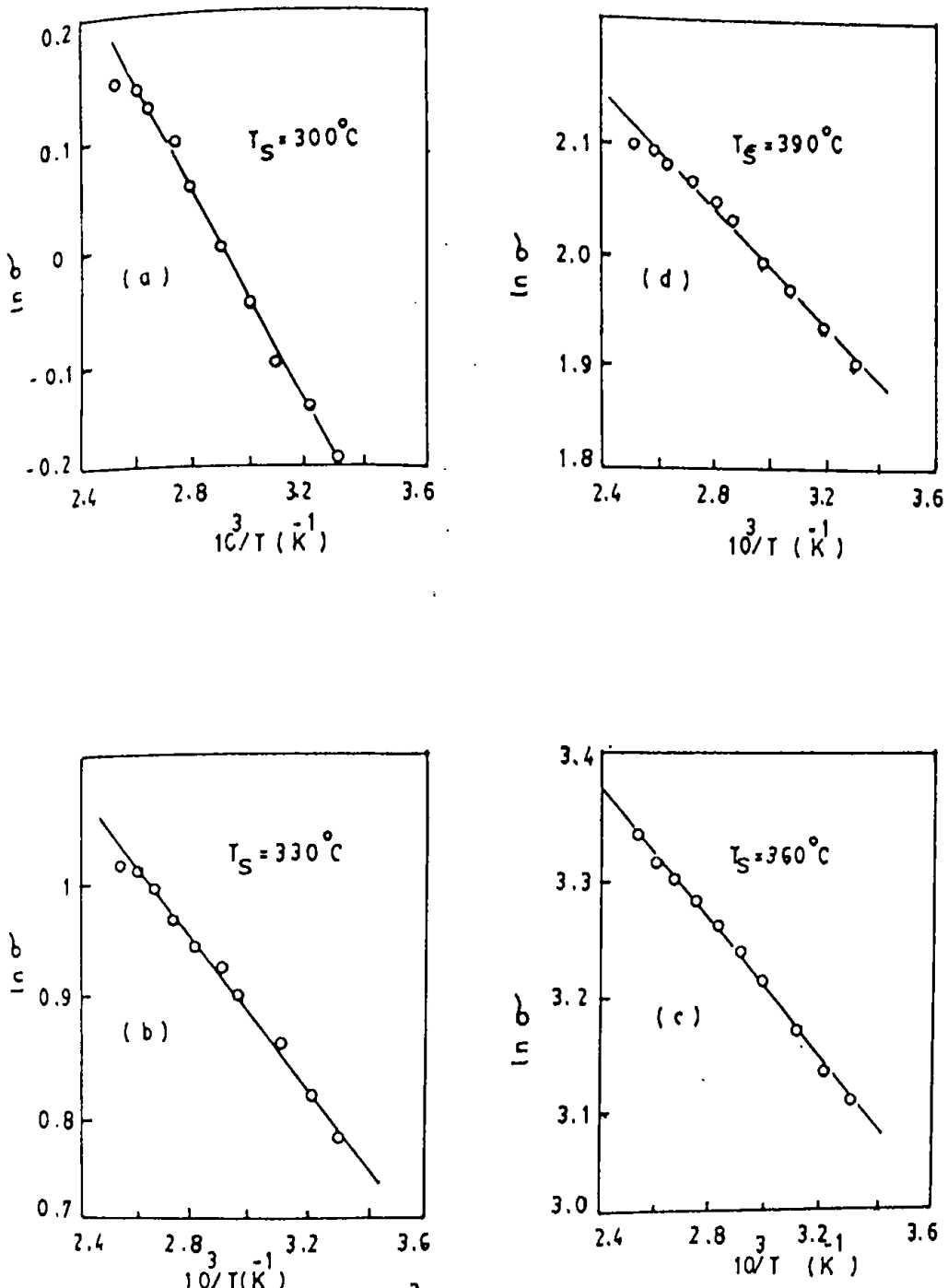

Figure 5.23: Plot of $\ln \sigma$ vs. $10^3/T$ for four typical vacuum annealed ZnO:In films.

TABLE 5.4: Activation energy of ZnO films before and after vacuum heat treatment.

Sample No.	Substrate Temperature (°C)	Activation energy for as-diposited film E_a eV	Activation energy for vacuum heat treated films Ev eV
1	300	0.161	0.082
2	330	0.150	0.058
3	360	0.126	0.043
4	390	0.115	0.051

5.18 THERMOELECTRIC POWER

The thermoelectric power (TEP) of some undoped vacuum heat treated samples of ZnO having different thicknesses were measured with reference to pure metallic lead (Pb). During the period of measurement the cold junction of the experimental sample was kept at 0°C and the temperature of the hot junction was varied upto 200°C. The detail experimental procedure has been described in chapter-4. The aim of the experiment is to study the nature of variation of Fermi level with film thickness and carrier concentration.

The measured values of thermo e.m.f at different temperatures are shown in figure 5.24. It was observed that the thermo e.m.f is positive with respect to lead. Figure 5.25 shows the variation of the corresponding thermoelectric power, Q, with inverse of temperature. It is observed from this figure that the thermopower decreases continuously with increasing temperature and saturates in the higher temperature region. The rate of change of Q with temperature is greater for films of higher thickness than for lower thickness. The saturation of Q with temperature also occures at relatively higher temperature in the thicker films than in thinner films. At a fixed temperature the variation of thermopower with film thickness is shown in figure 5.26.

Because Hall measurements on these samples show n-type conductivity, the thermopower should be negative. However, our present measurements on the vacuum annealed samples show a positive thermopower indicating a P-type behaviour. This is however, unusual, but there are many situations when an n-type material can show P-type thermopower. Mott and Davis[33] and Geballe and Hull[34] have pointed that in semiconducting samples when the carrier compensation ratio K (= N_A/N_D) for n-type material is less than 0.5 the sample may show this type of anomalous thermopower.

It is an established fact[13,35,36] that in polycrystalline semiconducting samples, oxygen chemisorption/desorption mechanism plays an important role in controlling the concentrations of

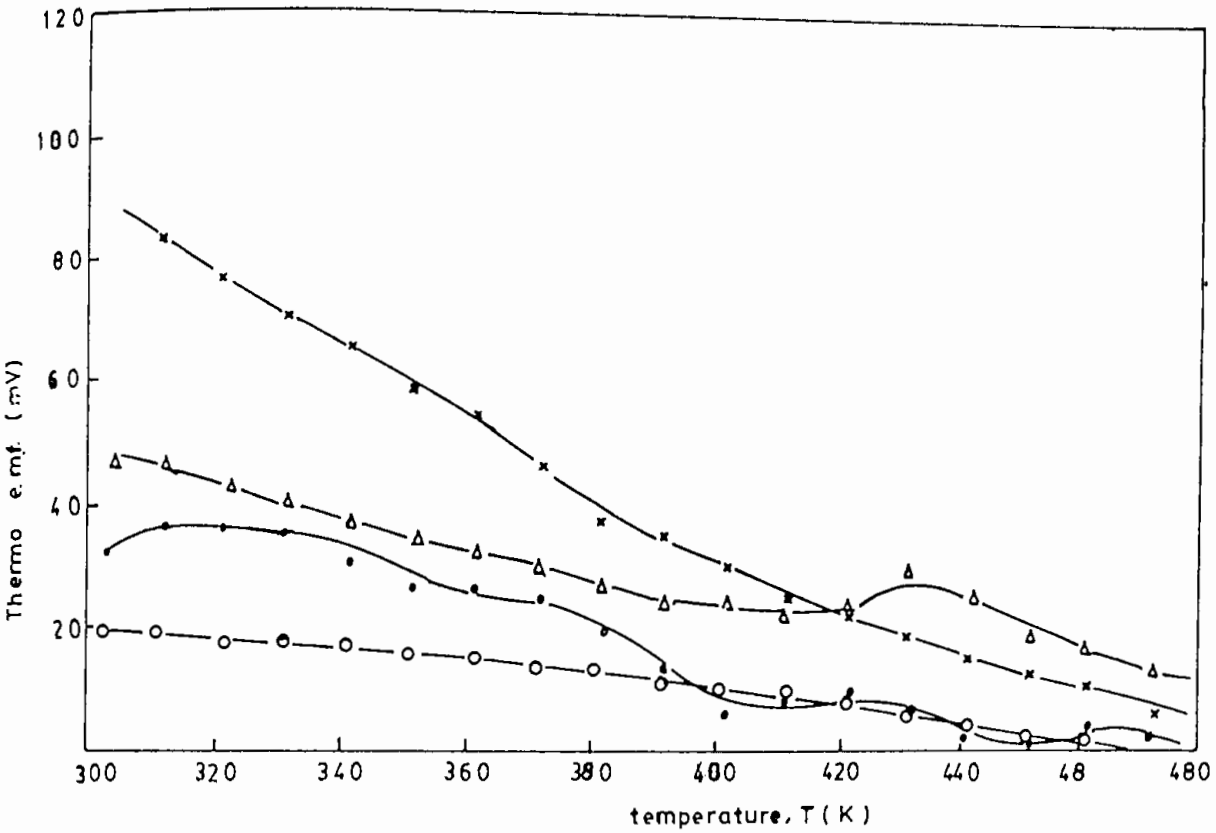

Figure 5.24: Variation of thermo e.m.f. with temperature of ZnO films of different thickness; (×) 2058 Å, (Δ) 1491 Å, (•) 1313 Å, (○) 953 Å .

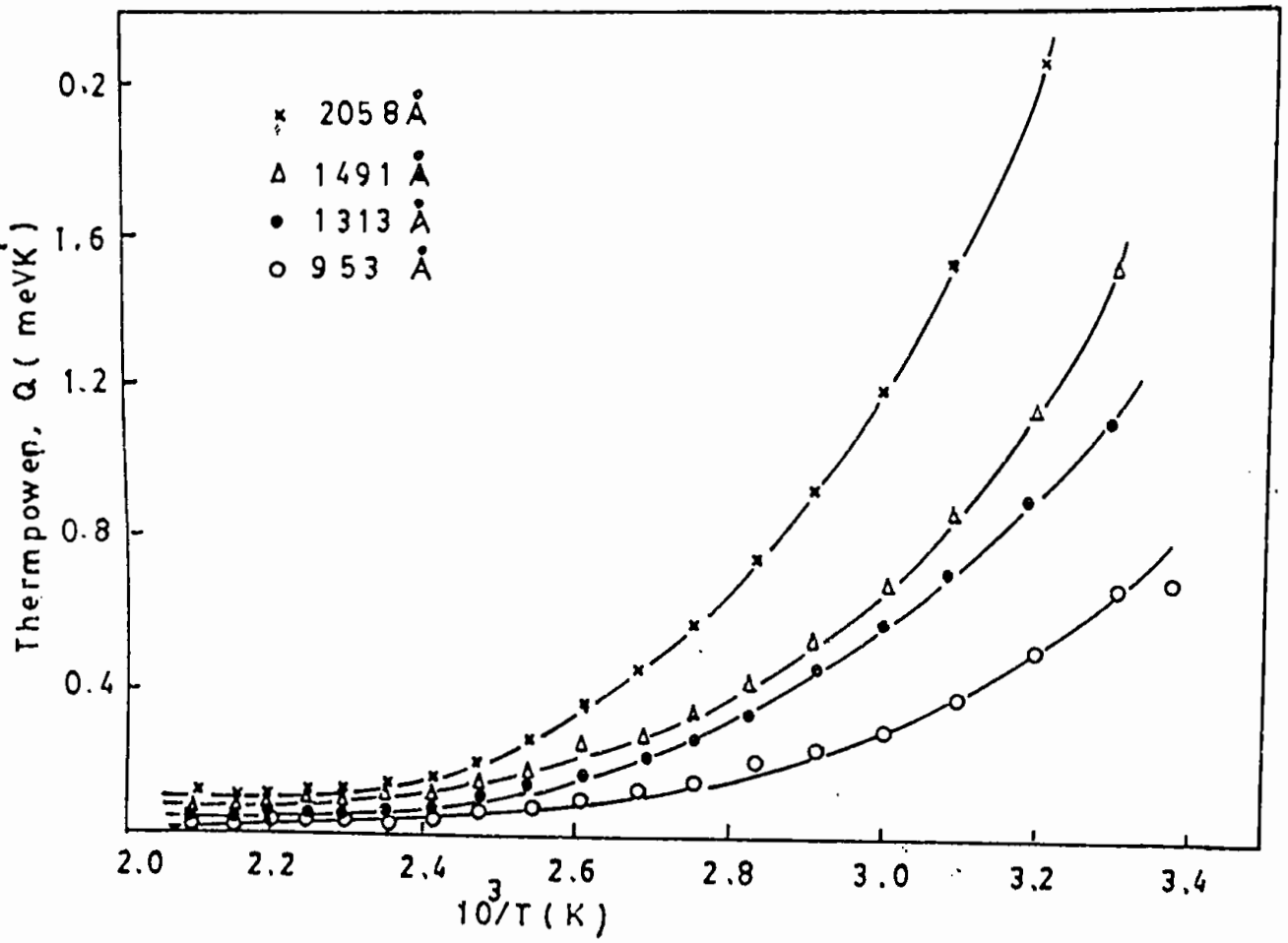

Figure 5.25: The plot of thermopower, Q, against inverse of temperature of ZnO films of various thickness.

acceptor and donor states, N_A and N_D, respectively. In the as-deposited ZnO film an excess of oxygen is trapped at the surface and at the grain boundaries of the film during the process of their pyrolysis in air. These excess oxygen trap states are known to give rise to surface acceptor states that contribute to the possible acceptor concentration, N_A[27]. In the as-deposited film, therefore, the carrier compensation ratio is relatively high and probably greater than 0.5. However, in a vacuum heat treated film, these so called surface acceptor states, as well as other similar states from the grain boundary region, are desorbed and these in turn raise the donor concentration, N_D. Thus the compensation ratio, K is lowered. During this process the chemisorbed O^-_2 ion donates one electron to ZnO [$O^-_2 \rightarrow O_2 + e$ or $2O^{-} \rightarrow O_2 + 2e$][24] which may either stabilize N_A at the surface, or may neutralize the interstitial Z^{++} ions which then can contribute their share to N_D[6]. Thus it is not unlikely that the compensation ratio k may be less than 0.5 in the vacuum annealed film and the sample may show anomalous thermopower. Reports on TEP measurement on as-deposited ZnO film has been published previously[1].

The carrier concentration, n, of the samples as obtained from the Hall effect is of the order of 3×10^{17} to 10^{18} cm^{-3}, and we feel it logical to employ a nondegenerate model to analyse the thermopower data. For a nondegenerate n-type crystalline semiconductor with spherical energy surface under thermal equilibrium the thermoelectric power is given by[33]

$$Q = -\frac{K_B}{e}\left(\frac{E_c - E_F}{K_B T} + A\right) \quad \ldots\ldots\ldots \quad (5.12)$$

where K_B is Boltzmann constant and E_c is the energy of the conduction band edge; A is a constant that depends on the nature of the scattering process. Normally, for a material like a Fermi glass, A runs between 2 and 4. If energy is measured with respect to the bottom of the conduction band then Equation (5.12) reduces to

$$Q = -\frac{K_B}{e}\left(A + \frac{E_F}{K_B T}\right) \quad \ldots\ldots\ldots \quad (5.13)$$

Harry et. al.[37] have pointed out that A = (5/2)-r, where r corresponds to the scattering index, and is equal to -0.5 for piezoelectric scattering and -1.5 for ionized impurity scattering. Thus A = 3 for piezoelectric scattering and 4 for ionized impurity scattering. from equation (5.12) it is clear that A corresponds to the value of the thermopower at infinite temperature limit.

From figure 5.25 the extrapolated tangent at the higher temperature region of the curves approximately gives a common intercept at the ordinate from which the value of A has been obtained as 3.01. This value corresponds to the scattering index ≈ -0.5 and is an indication of piezoelectric scattering dominant in these ZnO films. This is also in agreement with the fact that ZnO is a piezoelectric crystal[2].

In all our samples it has been found that (E_C-E_F) varies with temperature, T, and it can be assumed that for a limited temperature range[33]

$$E_C - E_F = E_o - \gamma T \quad \ldots\ldots\ldots \quad (5.14)$$

where E_0 is the low-temperature limit of (E_C-E_F) and corresponds to the activation energy equivalent to the bandgap, and γ is the temperature co-efficient of activation energy. Using equation (5.14) in equation (5.12).

$$Q = -\frac{E_o}{eT} + \left(\frac{\gamma}{e} - \frac{AK_B}{e}\right) \quad \ldots\ldots\ldots \quad (5.15)$$

Now the peltier co-efficient, π=QT, is given by

$$\pi = -\frac{E_o}{e} + \left(\frac{\gamma}{e} - \frac{AK_B}{e}\right)T \quad \ldots\ldots\ldots \quad (5.16)$$

This equation shows that π versus T plot should yield a straight line and the value of γ can be obtained from its slope. Figure 5.27 shows such plots and it is observed that the slopes at room temperature and high temperature regions are different. Both the slopes have been determined and using A=3 various values of γ were calculated for films of different thicknesses. These values of γ are plotted as a function of thickness in figure 5.28. It shows that at high temperatures, γ is almost thickness independent, while in the room temperature limit it shows a strong thickness dependence.

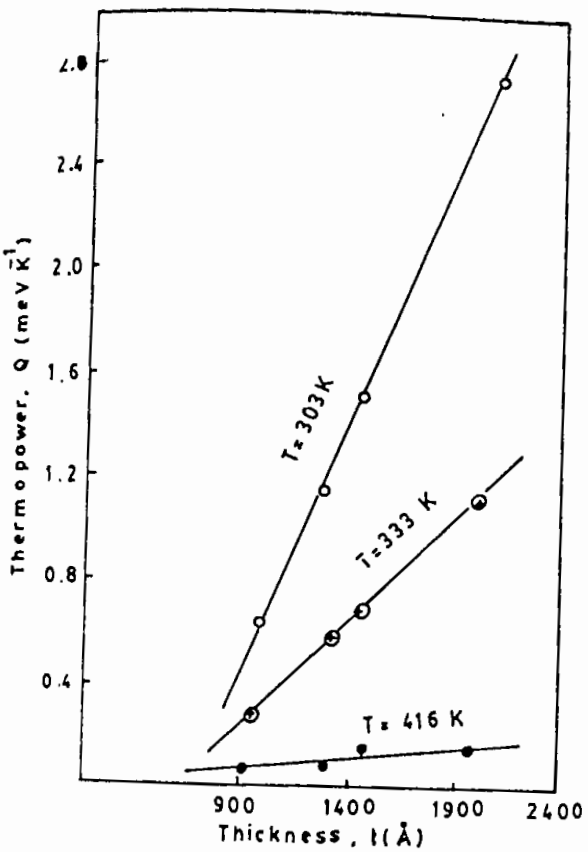

Figure 5.26:The variation of thermpower of ZnO film as a function of thickness at three different temperature.

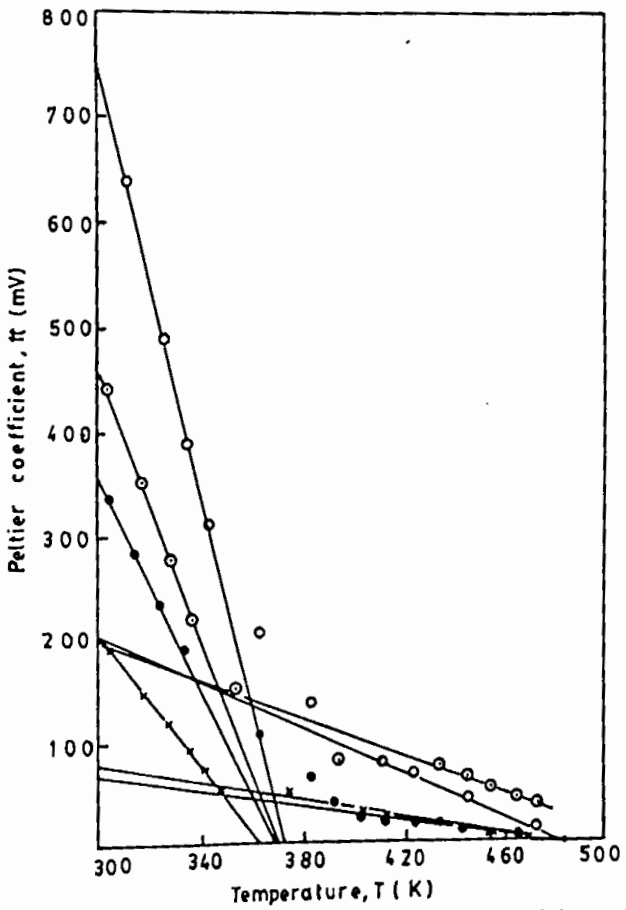

Figure 5.27:The plot of peltier coefficient, π, vs temperature, T, of ZnO films of various thicknesses. (o) 2058 Å, (⊙) 1491 Å, (•) 1313 Å, (×) 953 Å.

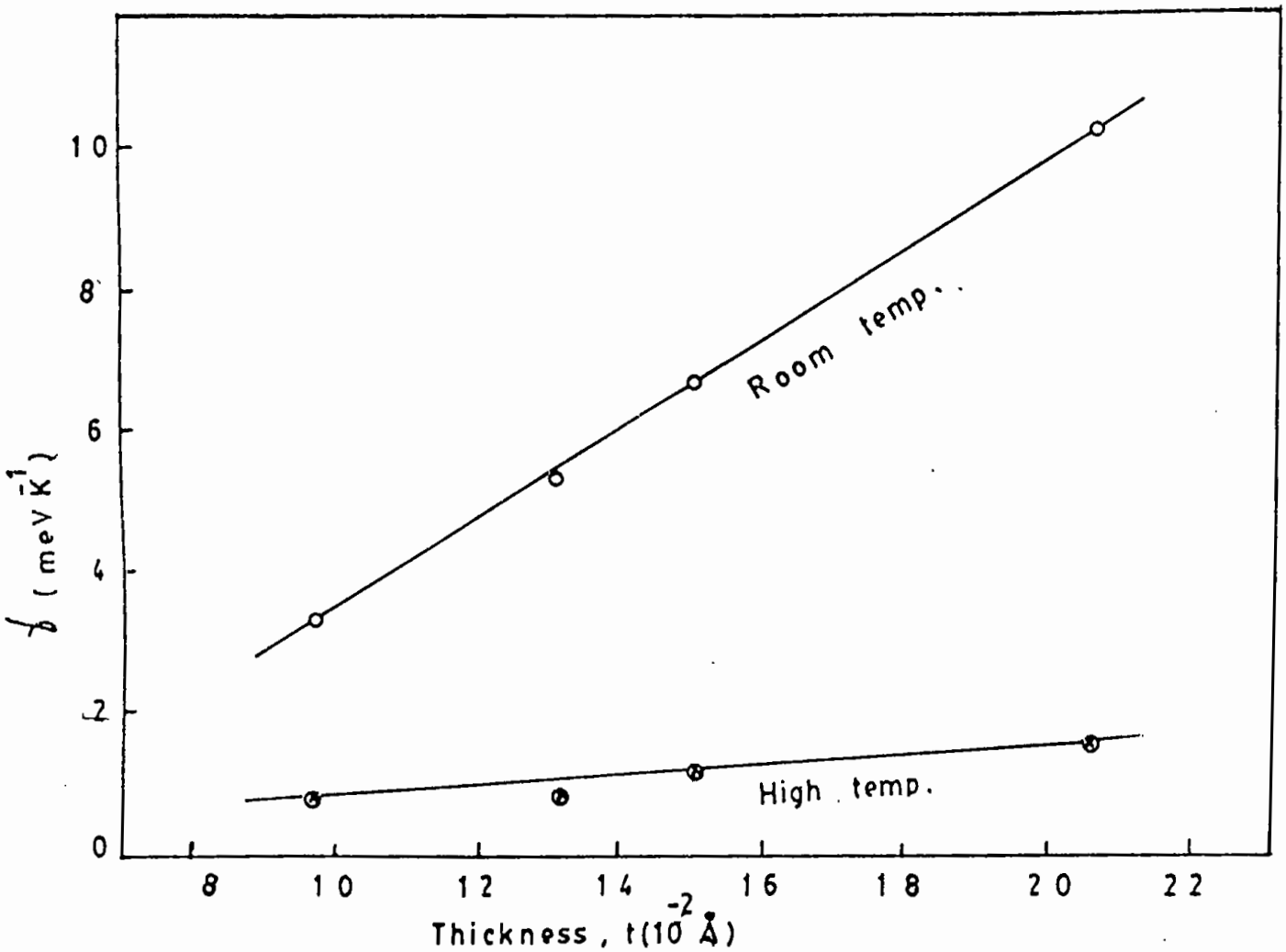

Figure 5.28:The variation of temperature coefficiet of activation energy, γ as a function of thickness, t, of ZnO thin films at room temperature and high temperature.

Using these values of γ at room temperature, the values of E_0 for different film thicknesses may be calculated from equation (5.16), and the values of (E_C-E_F) from equation (5.14). The variation of E_0 and of (E_C-E_F) at room temperature as a function of inverse film thickness, 1/t, is shown in figure 5.29. In this figure it is observed that E_0 has a fair thickness dependence and its bulk value corresponds to 1/t = 0, is 3.25 eV. This value agrees well with the band gap of ZnO crystal (3.2 and 3.3 eV, respectively) as reported previously[6,38]. This confirms the consistant nature of the analysis of our TEP data.

In extrinsic samples, the variation of E_0 with film thickness is obvious. E_0, which is calculated from Equation (5.14), is some type of thermal activation energy and depends on the detail variations of the pattern of conduction and valence band edges with the structure of the film, including verious defects. This energy does not necessarily correspond to vertical transition in the band picture . But the optical band gap, E_g corresponds to the optical absorption at some frequency and involves mostly vertical transition between the bands. Thus the variation of E_g with thickness is not so straightforward as for E_0. Of course, carrier concentration plays an important role in this case.

Because, in the high temperature region, the thermopower saturates for all the samples (Figure 5.25 and 5.26) it suggests that the Fermi levels in these films are pinned near the band edge

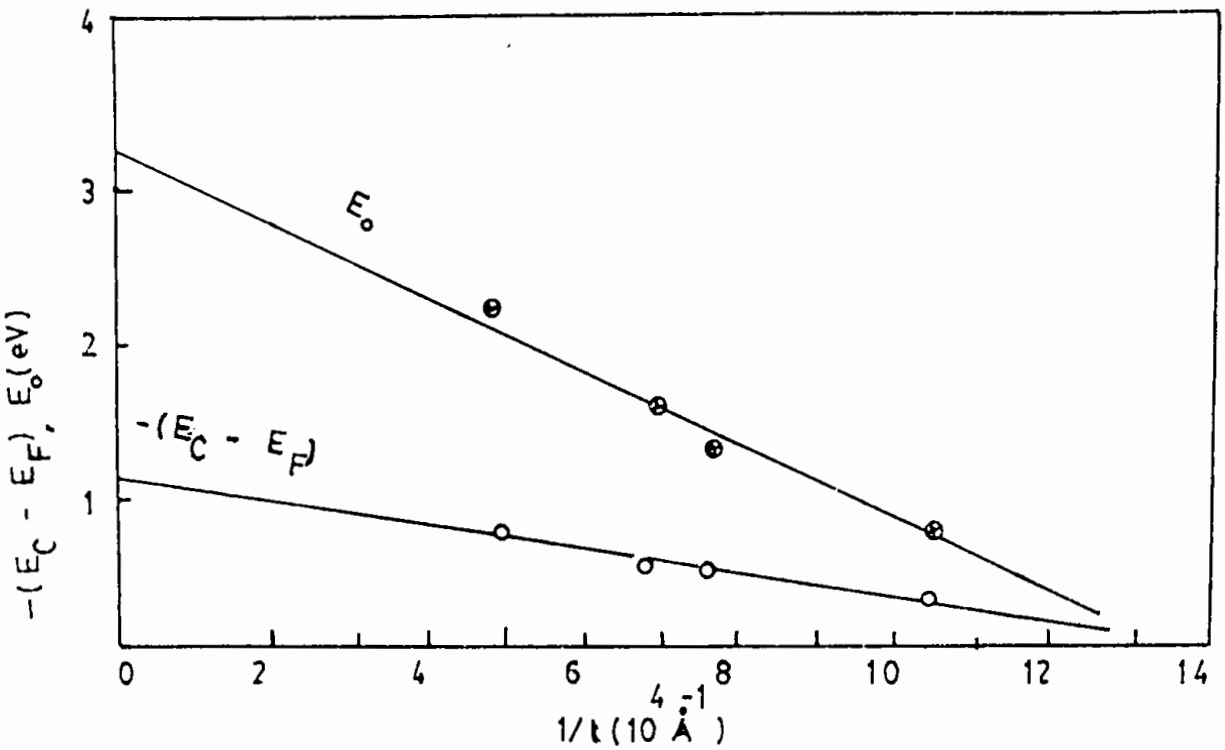

Figure 5.29: The variation of E_o and Fermi energy $-(E_C - E_F)$ with inverse of thickness.

at higher temperature. This is shown in figure 5.30 where this pinning can be clearly observed. The gradual decrease of thermopower with temperature as shown in figure 5.25, has also been reported by Hutson[39]. In thin film samples when the material be haves like a Fermi glass, this type of variation is usual[33]. We can obtain some idea about this variation by differentiating Equation (5.12) with respect to temperature, which yields.

$$\frac{dQ}{dT} = -\frac{K_B}{e}\left[\frac{d(E_c-E_F)}{K_BTdT} - \frac{(E_c-F_F)}{K_BT^2} + \frac{dA}{dT}\right] \quad . \quad . \quad . \quad . \quad (5.17)$$

From Figure 5.30 it is observed that since (E_C-E_f) is negative and it decreases with temperature so that in the brackets the 1st term of equation (5.17) is positive. The second term is also positive because (E_c-E_F) is negative and we have already ignored any possible temperature variation of A as it corresponds to the high temperature limit of the thermopower. Thus the whole terms in the bracket is positive and hence dQ/dT is negative, which suggests a decrease of thermopower with temperature. The minimum value of $-(E_c-E_F)$ as obtained from figure 5.30 is 0.12 eV and is almost five times that of K_BT at room temperature. Thus our previous consideration of a nondegenerate model is justified.

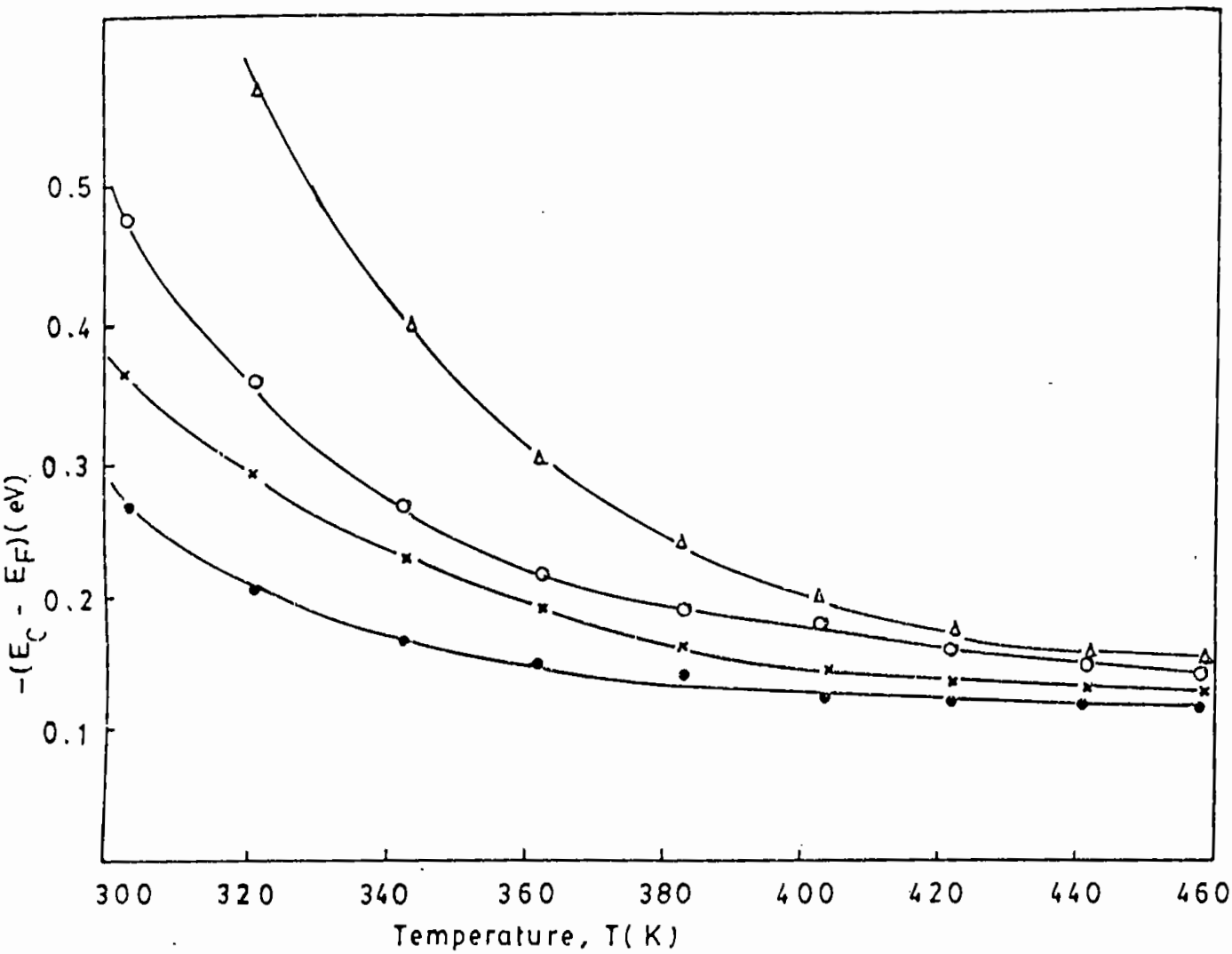

Figure 5.30: The plot of Fermi level as a function of temperature of ZnO films of different thickness; (Δ) 2058 Å, (○) 1491 Å, (×) 1313 Å, (●) 951 Å.

5.19 ELECTROMECHANICAL PROPERTIES OF ZnO FILMS

ZnO is a particularly attractive material for thin film piezoelectric transducers because of its comparatively high electromechanical coupling and great stability of the hexagonal phase.

Current transducer technology makes extensive use of element with pronounced and clear cut electromechanical properties in strain gauges, pressure gauges, displacement transducers, load cells, flow meters, torque indicators accelerometers etc.[40] Commonly used gauges are based on strained foil on continuous films of metals. They are characterized by a gauge factor γ, defined by

$$\gamma = \frac{\Delta R/R_o}{\Delta L/L_o} \quad \ldots\ldots\ldots\ldots \quad (5.18)$$

where ΔR is the strain induced change in electrical resistance from its unstrained value R_0, and ΔL and L_0 are the corresponding quantities for the length. The aim of this study is to point out the utility of ZnO films in sensitive strain gauges and related transducer elements.

The strain expressing relation can be easily derived from the formulae in reference (41) and was used in reference (42).

$$\frac{\Delta L}{L_o} = \frac{6wl}{Ybd^2} \quad \ldots\ldots\ldots\ldots \quad (5.19)$$

where w is the load, l is the length between the center of the

sample and the point of load suspension to the free end. Y is the Young's modulus of the steel bar used as cantilever, b is the width and d is the thickness of the bar. In this experiment we had l = 75 cm, b = 2.3 and d= 0.6 cm. Depending on the placement of the sample we could apply either a longitudinal tensile strain or a lonitudinal compressive strain. All the experimental data have been taken at room temperature.

Figure 5.31 shows the resistivity ρ vs. tensile strain of undoped ZnO film on glass substrate. It is seen that the longitudinal tensile strain lowers the resistivity approximately 1-2% in load increasing cycle whereas on the load dereaseing cycle an increase in resistance was noticed and the cycles are reversible. Compressive strain on the film slightly changes the resistence but was not very significant. Similar behavior has been observed in other samples but the relative magnitude of the variation of ρ differ from sample to sample.

Apparently it is found that the strain could not induce a remarkable change in electrical resistance for ZnO films. This is unlike the other non piezoelectric material, e.g. SnO_2, VO_2 etc. In these materials a converse effect was reported[43], i.e. the applied strain caused to increase the electrical resistance due to the increase of inter-grain separation distances when longitudinal tensile strain was applied on the sample. In that case the carrier transport occurs through electron tunneling between the adjacent

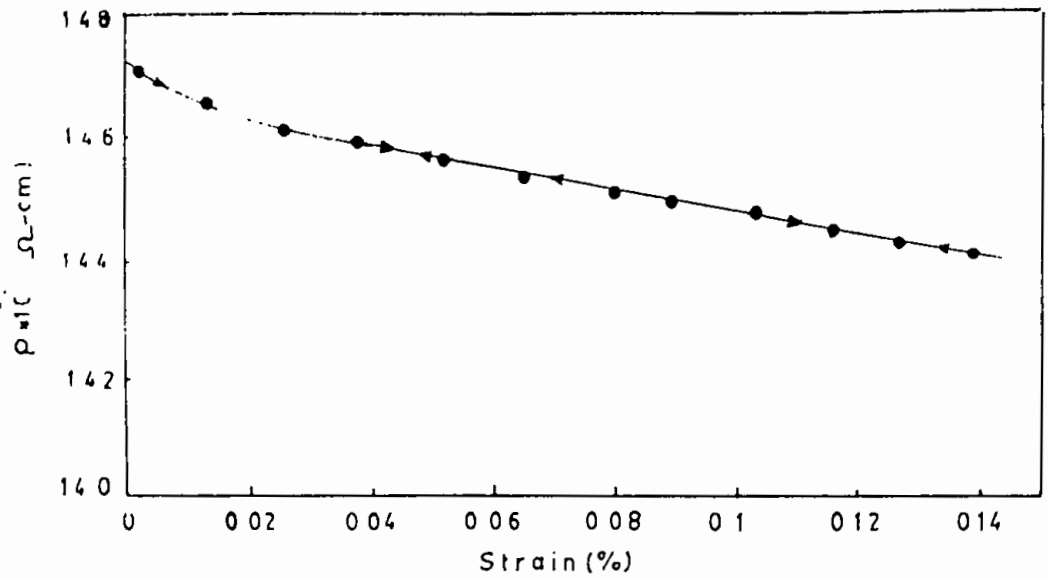

Figure 5 31 Resistivity vs. tensile strain for ZnO film.

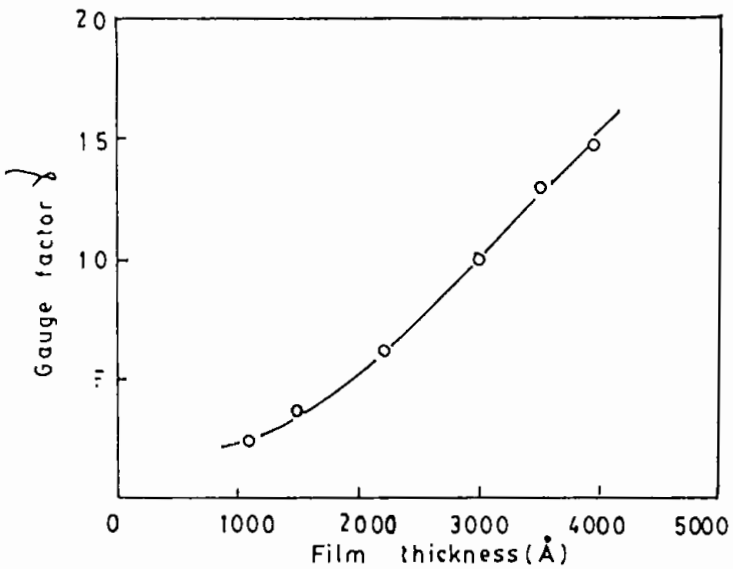

Figure 5.32: Gauge factor vs. thickness for ZnO film on glass.

grains.[44,45] It is well known that ZnO crystal is a piezoelectric material and a large change in electrical resistence due to strain was expected. But only a small effect was observed. The small reduction of electrical resistance by the application of longitudinal extensive strain is probably due to the piezoelectric effect. The strain may produce additional electric field in the direction of applied field which subdues the rise of electrical resistance due to the increase of inter-grains separation distance.

The crystals which have low symmetry or anisotropic crystallographic structures exhibit piezoelectricity than those which have high symmetry or isotropic crystallographic structure[46]. In these materials the electrical resistivity and piezoresistive co-efficients will also be anisotropic. This effect arises because the shape of the Brillouin zone reflects the crystallographic symmetry. The relative energies of the Fermi surface and Brillouin Zone boundaries are therefore direction-dependent. This in turn makes the number and the mobility of the conduction electrons direction dependent. In an unstrained condition, equivalent crystallographic directions will exhibit equal resistivities, giving rise to the multivalley model proposed by Herring[47]. Straining an anisotropic material, however, distorts the Brillouin Zone and destroys the equivalence between the valley. The resistance even in equivalent crystallographic directions therefore becomes unequal to an extent dependent upon the magnitude and nature of the applied field[48]. Any of the above mentioned causes

may occur in ZnO films and the actual mechanism is yet to be investigated.

For the case of In-doped ZnO films similar results were displayed with reduced magnitude of sample resistance. No contribution was observed to the strain induced change in electrical resistance due to doping concentration. Figure 5.32 shows the plots of gauge factor vs. film thickness. It is observed that the gauge factor γ increases with the increase of film thickness t. The gauge factor is not very high in these samples.

REFERENCES

1. M.N Islam, M.O. Hakim and H. Rahman, Journal of materials science, 22 (1987) 1379.
2. A.P Roth and D.F Williams. J. Appl. Phys. 52 (11) (1981) 6686.
3. H.H.V. Baumbach and C. Wagner, Z. Physik. chem. 22B (1933) 199.
4. M.G Ambia, M.N. Islam and M.O. Hakim, Solar energy materials and solar cells 28 (1992) 103.
5. Y. Fujita and T. Kwan. J. Res. Inst. catal 7 (1959) 24.
6. Leonid V. Azaroff, James J. Brophy. Electronic process in materails. (McGraw Hill book company 1963).
7. Julio Aranovich, Armando Ortiz and Richard H. Bube. J. Vac. Sci Technol. 16(4) (1979) 994.
8. S. Major, A. Banerjee and K.L. Chopra. Thin solid films 108 (1983) 333.
9. M.N. Islam and M.O. Hakim. J.phys. chem. solids vol. 46(3) (1985) 339.
10. S Major. A. Banerjee and K.L Chopra. Thin solid films. 125 (1984) 179.
11. L. Bahadur, M. Hamdani, J.F. Koenig and P. Chartier, Solar energy matrials. 14. (1986) 107.
12. C.X. Qiu and I. Shih, Solar energy mater. 13(1986) 75.
13. J.W. Orton and M.J. Powel, Rep. Prog., Phys., 43(1263).

14. K.L. Chopra and V. Dutta, proc. Int. symp. on polycrystelline semiconductors, perpignan, September 1982 in J. Phys. (paris) colloq C1, 43 (10 suppl.) (1966) 141.

15. J.Y.W. Seto. J. Appl. phys. 46(1966) 247.

16. H.C. Weller, R.H. Mauch and G.H. Bauer, Solar energy Materials and solar cells 27(1992) 217.

17. Mollwo. E. photoconducting conference (1956), Willey N.Y.

18. E. Burstein Phys. Rev. 93(1954) 632. T.S. Moss Proc. Phys. Soc. London B67(1954) 775.

19. I. Hamberg and C.G. Granquist, K-F Berggren, B.E. Sernelius and L. Engstrom. Solar energy materials 12(1985) 479.

20. A. Ortiz. C. Falcony, M. Garcin and A. Sanchez, J. Phys. D. Appl. Phys. 20(1987) 670.

21. M. Just, N. Maintzer and I. Blech, Thin Solid Films, 48(1978) L19.

22. K.L. Chopra, S. Major and D.K. Pandya, Thin Solid Films 102(1983) 1.

23. S.K. Ghandhi, R.J. Field and J.R. Shealy, Appl. Phys. Lett. 37(1987) 1379.

24. S-C. Chang. J. Vac. Sci, Technol. 17(1980) 366.

25. C. Kittel, Introduction to Solid State Physics, 4th Ed. (Wiley, New York, 1971).

26. A.R. Hutson. Phy. Rev. 198 (1957) 222.

27. M.G. Ambia, M.N. Islam and M.O. Hakim. Journal of Materials Science 27(1992) 5169.

28. J.O. Barnes, D.J. Leary and A.G. Jordan, J. Electrochem. Soc. 127(1980) 1636.

29. J.A. Amick, RCA Rev. 20(1959) 753.

30. D. Barnarczyk and J. Bernarczyk. Thin Solid Films 44(1977) 137.

31. L.L Kazmerski. Polycrystalline and Amorphous Thin Film and Devices, (Academic Press, New York, 1980).

32. M.N. Islam and M.O. Hakim, J. Phys. D 19(1986) 615.

33. N.F. Mott and E-A. Davis, "Electronic Procession in non crystalline materials" 2nd Edn (Clarendon Press. Oxford. 1979).

34. T.H. Geballe and G.W. Hull. Phys Rev. 98(1955) 940.

35. S. Major. A Banerjee and K.L. Chopra. Thin Solid Films 122(1984) 31.

36. J.P. Legre and S. Martinuzzi Phys. Status Solidi A1(1970) 689.

37. H. Harry, B. Kwok and R.H. Bube. J. Appl. Phys. 44(1973) 138.

38. R.A. Smith, "Semiconductors" (Cambridge University Press, Cambridge, 1986) 439.

39. A.R. Hutson, ibid. 8(1959) 467.

40. G.R. Witt. Thin Solid Films, 22(1974) 133.

41. B.L. Worsnop and M.T. Flint, Advanced practical Physics, Methuen, London, 1951, 9th edn. 73.

42. S. Sampath and K.V. Ramanaiah, Thin Solid Films; 137(1986) 199.

43. M.O. Hakim, S.M. Babulanam and C.G. Granqvist. Thin Solid Films, 158(1988) L249.

44. R.L. Parker and A. Krinsky, J. Appl. Phys. 34(1963) 2700.

45. St. Trapp. H. Fuchs and H. Gleiter, Thin Solid Films. 137(1980) L43.

46. Charles A. Wert and Robb M. Thomson. Material science and Engineering series (McGraw-Hill book company 1970) 405.

47. Herring C. Bell system Tech. J., 34, (1955) 237.

48. Pfann. W.G. and R.N. Thurston. J. Appl. Phys. 32, (1961) 2008.

CHAPTER 6

6.1 CONCLUSIONS AND SUGGESTIONS FOR FUTURE WORK

In the light of the electrical, optical and structural investigations in ZnO thin films the following conclusions may be drawn. It is evident from structural study that spray deposited ZnO thin films are polycrystalline and are n-type semiconductors.

The study of undoped and doped ZnO thin films indicates that films' properties are strongly dependent on deposition conditions. Electrical conductivity of as-deposited undoped films is poor whilst vacuum heat treated films are good condutors. Short period aging effect has been observed in the electrical conductivity of the films, but is limited to within the first two weeks of the deposition. Then it becomes stable.

The carrier concentrations of the sample were found in the range 10^{17} cm^{-3} to 2.38 X 10^{19} cm^{-3}. Normally the samples possess nondegenerate states. The optical band gap for direct allowed transition is around 3.3 eV. The magnitude of the band gap is similar to that of the pure bulk crystal although these films were impure and full of structural defects. The band gaps are undoubtedly wide. The high transparency and high conductivity of the films may be ascribed to the deviation from stoichiometry and/or to the presence of excess impurity atoms. In the undoped samples, the possible donor levels are shallow and are situated at

various depths in the band gap. Fermi levels lie near the donor levels and are at 2.4 to 4.8 K_BT below the conduction band edge at room temperature. It may be stated from the optical study that these films are defect semiconductors.

Indium was used as dopant in ZnO films. Doping increases the film's conductivity by 1 to 2 order of magnitude. The carrier concentration increases upto 5 X 10^{20} cm^{-3} due to the doping effect. Burstein-Moss shift is present with fundamental absorption edges of ZnO films. The optical band gap widens upto 3.38 eV for ZnO:In films. This may be due to many body effects or Burstien shift. The effective mass of electrons in the conduction band lie in the range of 0.36 to 0.60 of free electron rest mass.

The refractive indices of these films in the visible range of wavelengths are found between 1.57 and 2.05 for ZnO films. The higher value of refractive index is found in the film of higher thickness. The transparency were similar for both undoped and doped ZnO films. The Hall mobility in the film of ZnO is substantially lower than that of single crystal.

Oxygen chemisorption-desorption process in polycrystalline ZnO thin film are important for their power to control the electronic transport properties. When these films are deposited by spray pyrolysis process in air, a lot of oxygen molecules from the atmosphere are chemisorbed at the grain boundaries and also on the surface of the film during the deposition. The chemisorption of

oxygen produces a very high resistivity in the virgin state of undoped films. When these films were heat treated in vacuum or in normal atmosphere, desorption took place from the films, which drastically increases their electrical conductivity, Hall mobility and carrier concentration. The Hall mobility is controlled by the grain boundary potential barrier heights, which are modulated by the heat treatment. It has been observed that for obtaining a low resistivity device, successive heat treatment operations can performed without any marked deterioration of the film structure.

Thermopower in spray-deposited nonstoichiometric ZnO thin film shows a thickness as well as temperature dependence. The Fermi levels are found to show a gradual pinning mode near the band edge with increasing temperature. Carrier compensation due to the chemisorption-desorption process in these films on annealing in vacuum may create an anomaly in the nature of variation of the thermopower values. An annealed sample may show a p-type thermopower while Hall effect shows n-type behaviour on the same film. In general the transport properties of these samples are controlled mainly by the piezoelectric scattering of index -0.5 obtained from thermopower data. Film thickness also have remarkable effect on the temperature coefficient of activation energy, γ . In the room temperature region γ has a strong thickness dependence while in the high temperature region it is almost thickness independent.

FUTURE STUDY

To have better understanding of ZnO material research work may be extended in the following areas.

(i) Making MIM device either in planer or sandwich form electron emission and switching study may be carried out.

(ii) To obtain precise information about trapping levels in the band gap of the material thermally stimulated current study may be carried out.

(iii) Electroluminescence may be explored in these materials

(iv) Photoconductivity is an interesting area for investigation.

(v) Finally to obtain significant information about the electronic energy band diagram studies in low temperature rigion is necessary.

PUBLICATIONS

1. M.G., Ambia, M.N. Islam and M.O. Hakim, "Studies on the effects of Deposition variables on the Spray pyrolysis of ZnO thin film" "Journal of Materials Science". U.K. (1994) (in press).

2. M.G. Ambia, M.N. Islam and M.O. Hakim. Solar Energy Materials and Solar cells. 28(1992) 103.

3. M.G. Ambia, M.N. Islam and M.O. Hakim. Journal of Materials Science. 27(1992) 5169.